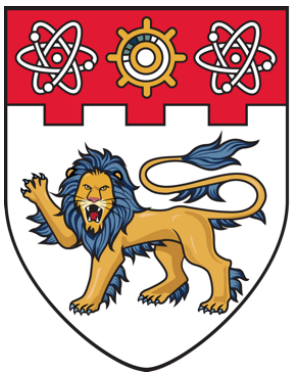

NANYANG TECHNOLOGICAL UNIVERSITY
SINGAPORE

# DEVELOPMENT OF IMMUNE-MODULATORY RNAS TO REGULATE RIG-I-LIKE RECEPTORS MEDIATED ANTIVIRAL IMMUNE RESPONSE FOR THERAPY AND VACCINATION

YONG HUI YEE

SCHOOL OF BIOLOGICAL SCIENCES

2019

# DEVELOPMENT OF IMMUNE-MODULATORY RNAS TO REGULATE RIG-I-LIKE RECEPTORS MEDIATED ANTIVIRAL IMMUNE RESPONSE FOR THERAPY AND VACCINATION

**YONG HUI YEE**

**SCHOOL OF BIOLOGICAL SCIENCES**

A thesis submitted to the Nanyang Technological University in partial fulfilment of the requirement for the degree of Doctor of Philosophy

2019

## Statement of Originality

I hereby certify that the work embodied in this thesis is the result of original research done by me except where otherwise stated in this thesis. The thesis work has not been submitted for a degree or professional qualification to any other university or institution. I declare that this thesis is written by myself and is free of plagiarism and of sufficient grammatical clarity to be examined. I confirm that the investigations were conducted in accord with the ethics policies and integrity standards of Nanyang Technological University and that the research data are presented honestly and without prejudice.

9/1/2019

. . . . . .

Date

. . . . . .

Yong Hui Yee

**Supervisor Declaration Statement**

I have reviewed the content and presentation style of this thesis and declare it of sufficient grammatical clarity to be examined. To the best of my knowledge, the thesis is free of plagiarism and the research and writing are those of the candidate's except as acknowledged in the Author Attribution Statement. I confirm that the investigations were conducted in accord with the ethics policies and integrity standards of Nanyang Technological University and that the research data are presented honestly and without prejudice.

9/1/2019

. . . . . .
Date

. . . . . .
Assistant Prof. Luo Dahai

# Authorship Attribution Statement

This thesis contains material from 2 papers published in the following peer-reviewed journals where I was the first author.

Part of the materials in Chapter 1 is published as:

1) **Yong HY**, Luo D (2018) RIG-I-Like Receptors as Novel Targets for Pan-Antivirals and Vaccine Adjuvants Against Emerging and Re-Emerging Viral Infections. *Front Immunol* **9:** 1379
2) Yong HY, Luo D. RIG-I-Like Receptors . eLS: **Encyclopedia of Life Sciences**; 2015 www.els.net/WileyCDA/ElsArticle/refId-a0026237.html

The contributions of the co-authors are as follows:

- A/Prof Luo Dahai provided the initial project direction and edited the manuscript drafts.
- I prepared the manuscript drafts.

9/1/2019

. . . . . .

Date

. . . . . .

Yong Hui Yee

**ACKNOWLEDGEMENTS**

Firstly, I would like to express my sincere gratitude to my supervisor, Asst Prof. Luo Dahai for providing me with an opportunity to do my PhD. He is always available for scientific discussion and to provide directions in my project. Without his help and guidance, my graduate studies would not have been possible. I would also like to take this opportunity to thank my co-supervisor and thesis advisory committee Assoc Prof. Liu Chuan Fa, Dr. Katja Fink and Asst Prof. Wu Bin for their support, patience and guidance.

My sincere thanks also go to my fellow lab mates, Ms. Wint Wint Phoo, Ms. Li Kuohan, Dr. Zhao Yongqian, Dr. Chen Ming Wei, Mr. Tan Yaw Bia, Ms. Zhang Zhenzhen and Dr. Melissa Wirawan for help with experiments, scientific discussion and friendship. I would also like to thank Mr. Victor Ho and Dr. Zheng Jie whom I work closely with, in a collaboration project.

Finally, I would like to take this opportunity to thank my parents and family for their unwavering support in all my life's endeavour

**TABLE OF CONTENTS**

**LIST OF FIGURES**

**LIST OF TABLES**

**TABLE OF ABBREVIATIONS**

| Abbreviations | Full Name |
|---|---|
| 5’pp | 5 prime diphosphate |
| 5’ppp | 5 prime trphosphate |
| ADP | Adenosine Diphosphate |
| ASC | apoptosis-associated speck-like protein containing a CARD |
| ATP | Adenosine triphosphate |
| ATPase | Adenosine triphosphatase |
| β-ME | β-mercaptoethanol |
| CARDs | Caspase Activation and Recruitment Domain |
| CCP4 | The collaborative computational project number 4 |
| CLRs | C-type Lectin Receptors |
| CpG ODN | CpG Oligodeoxynucleotide |
| CTD | C-terminal Domain |
| DAAs | Direct Acting Antivirals |
| DAMPs | Damage Associated Molecular Patterns |
| ds | Double stranded |
| DTT | Dithiothreitol |
| Hel | Helicase |
| HDX-MS | Hydrogen Deutrerium Exchange-Mass Spectrometery |
| IAV | Influenza A virus |
| IFN | Interferon |
| IL-1 | Interleukin-1 |
| ImmRNA | innate immune modulatory RNA |
| IPTG | Isopropyl-β-D-thiogalactopyranoside |
| IRF3/7 | Interferon Regulatory Factors 3/7 |
| ISGs | Interferon stimulated genes |
| IVT | *In vitro* transcription |
| JAK-STAT | Janus tyrosine Kinase Signal Transducer and Activator of Transcription |
| $K_{cat}$ | Turnover number |

| | |
|---|---|
| $K_M$ | MIchaelis constant |
| kDa | Kilo Dalton |
| LGP2 | laboratory of genetics and physiology 2 |
| lncRNA | Long non-coding RNA |
| LRR | Leucine rich repeat |
| MAVS | Mitochondrial antiviral-signalling protein |
| MDA5 | melanoma differentiation associated gene 5 |
| Mg | Magnesium |
| NADH | Reduced Nicotinamide adenine dinucleotide |
| NLR | NOD-like receptors |
| NTP | Nucleotide triphosphate |
| NF-κB | Nuclear Factor Kappa B |
| PAMPs | Pathogen Associated Molecular Patterns |
| PEG | Polytethylene glycol |
| PCR | Polymerase chain reaction |
| PDB | Protein Data Bank |
| PRRs | pattern recognition receptors |
| RC | Replication complex |
| RIG-I | Retinoic Acid-Inducible Gene I |
| RLRs | RIG-I like receptors |
| RNA | Ribonucleic Acid |
| SDS-PAGE | Sodium dodecyl sulphate-polyacrylamide gel electrophoresis |
| TLRs | Toll like receptors |
| TAMPs | Tumour Associated Moelcular Patterns |
| TIR | Toll/interleukin-1 (IL-1) receptor |
| TRIM | tripartite motif-containing proteins |
| UTR | Untranslated Region |
| VLP | Virus-like particle |

**Summary**

Retinoic Acid-Inducible Gene I (RIG-I) is a cytosolic pattern recognition receptor (PRR) involved in initiating host defence response against viruses. RIG-I distinguishes between self and foreign nucleic acids by recognising chemical features not found in endogenous cytoplasmic RNA. RIG-I exhibits a high affinity binding for blunt ended duplex RNA terminus containing a 5' triphosphate moiety. In this thesis, the development of potent innate immune modulatory RNA (ImmRNA), capable of triggering a robust type I interferon signalling in human cells is reported. Several short hairpin RNAs terminated at one end with a stable UUCG tetraloop and the other with 5' triphosphate were designed. From these hairpin dsRNAs, the shortest hairpin required to activate type I interferon signalling is the RNA with 10 perfectly base paired stem RNA (3p10L). From these findings, mismatch along the stem of the RNA was introduced to create a guanosine insertion along the stem of the 3p10L RNA and enhanced type I interferon signalling in both HEK-Lucia™ RIG-I cells and THP1-Dual™ with the guanosine insertion at the position 9 of 3p10L (3p10LG9) were observed. Conformational dynamics studies via HDX-MS of human RIG-I bound to 3p10LG9 revealed that the overall binding of CTD and HEL1 domain was tighter to 3p10LG9 as compared to 3p10L.

Next, the encapsulation of ImmRNAs into virus-like particles (VLP) was carried out. The coat protein for two different RNA bacteriophage, MS2 and Q beta were cloned and recombinantly expressed in *E.coli*. A spontaneously formed VLP from both MS2 and Q beta were obtained after several purification steps and was confirmed via negative staining Electron microscopy. Furthermore, coat protein for Q beta was also purified and assembled with the immRNA into Q beta VLP. Altogether, the work in this thesis provides insights into the development of robust innate immune modulatory RNAs as agonists of RIG-I and the development of potential delivery tools for ImmRNAs.

## Chapter 1: Introduction

### 1.1 Viral recognition by innate immune sensors

The innate immune sensors form the early line of detection and act as sentinels against viral infection. The activation of the innate immune sensors drives the expression of type 1 interferon and pro-inflammatory cytokines genes (Iwasaki & Medzhitov, 2010). These innate immune sensors are collectively named as pathogen recognition receptors (PRRs). The host immune surveillance by the PRRs are activated by a group of pathogen related molecules known as pathogen associated molecular pattern (PAMPs)(Roers et al, 2016). The activation of the production of interferon subsequently results in the activation and expression of ISGs (Interferon stimulated genes) under the JAK-STAT signalling pathway (Haller et al, 2006). ISGs inhibit virus replication by several different mechanisms including degradation of viral nucleic acid and inhibition of viral gene expression (Schoggins & Rice, 2011).

The engagement of PRRs could also result in the activation of caspase-1 via the inflammasome formation (Franchi et al, 2009). The formation of inflammasomes causes the activation of caspase-1. Activated caspase-1 activates the pro-interleukin (IL)-1β and pro-IL-18 via cleavage to its active form which causes the molecule to be secreted to the extracellular milieu (Denes et al, 2012). Caspase-1 activation via the inflammasome pathway could also trigger programmed cell death by pyroptosis and apoptosis. This will, in turn, prevent the spread of viruses to the adjacent cells (Miao et al, 2011).

### 1.2 Classes of PRRs

As described in the previous section, each different cell compartments are equipped with different pathogen recognition receptors which are responsible to hinder the progression of viral infection at various stages of infection. In this section, the various different classes of PRRs are being discussed including the Toll like receptor, C-type lectin receptors, NOD-like receptors and RIG-I like receptors.

#### 1.2.1 Toll like receptors (TLRs)

The toll like receptors (TLRs) were first reported in *Drosophila melanogaster* as proteins involved in the early development dorsoventral axis of the embryo (Hashimoto et al, 1988). The toll-like receptors were later determined to be an essential factor protecting flies from fungal infection (Lemaitre et al, 1996). There are 12 different TLRs in mice and 10 in human which have been identified and possesses a distinct or overlapping function in pathogen recognition (Akira & Takeda, 2004). Toll like receptors 1, 2 and 6 recognise the cell wall lipid in bacteria and fungus (Chau et al, 2009; Talreja et al, 2003). Whereas, Toll like receptors 3, 7, 8 and 9 have been reported to recognise of viral nucleic acids (Alexopoulou et al, 2001; Helminen et al, 2016; Pohar et al, 2018). Other Toll like receptors such as TLR 4 and 5 recognise the envelope proteins and polysaccharides in bacterial and fungal cell walls (such as lipopolysaccharide, mannan and flagellin) (Akira & Takeda, 2004; Poltorak et al, 2000).

Toll like receptors are membrane glycoproteins with a tripartite structure. The N-terminal domain contains the leucine rich repeats (LRRs) that fold into horse-shoe

like structure. The N-terminal domains of TLR are involved in PAMP recognition. A transmembrane domain exists in the middle region of the protein. The C terminal domain has a Toll/interleukin-1 (IL-1) receptor (TIR) and this domain is responsible for signalling (Kang & Lee, 2011). The TIR domains are similar in both TLRs and IL-1 family receptors and are known to trigger similar signalling cascade when activated (Ve et al, 2015).

In most cases, the activation of TLRs is due to the interaction with ligands which results in the dimerisation of the receptors (Gay et al, 2006). Some TLRs pre-exist in a dimer form such as TLR7, 8 and 9 (Latz et al, 2007; Tanji et al, 2013). The interactions of the N-terminal domain with ligand result in the stabilisation of receptor-complex dimer and conformational changes of TIR domain. The TIR domain stabilises and binds to other protein with TIR domain such as MyD88. Most TLRs interact with MyD88 except TLR3. The activated MyD88 then interacts with IL-1R associated kinase (IRAK)-4 via its death domain. This triggers the downstream signalling events and the activation of mitogen activated protein kinase (MAPK), dimerisation of nuclear factor κB (NF- κB) and interferon regulatory factor 3 (IRF3) (Akira & Takeda, 2004). The activation of MAPK, NF- κB and IRF3 results in the secretion of pro-inflammatory cytokines and type 1 interferon (Pasare & Medzhitov, 2005).

### 1.2.2 C-type lectin receptor (CLRs)

C-type lectin receptors (CLRs) are proteins that binds carbohydrate by C-type lectin-like domain (CTLD) (Zelensky & Gready, 2005). Several motifs were identified in CLRs which can recognise different ligands. The EPN motif recognises mannose, N-acetylglucosamine, L-fucose and glucose while QPD motif recognises galactose and N-acetylgalactosamine (Dambuza & Brown, 2015; Drickamer & Fadden, 2002). While CLRs include protein with at least 1 carbohydrate binding domain, they might not always bind to carbohydrate. The CLRs are expressed as soluble or transmembrane proteins in myeloid cells and recognised pathogen-associated molecular patterns (PAMPs) as well as some tumour related molecular signature (Dambuza & Brown, 2015). The CLRs can be classified into two different groups; namely protein with mannose asialoglycoprotein receptors (Geijtenbeek & Gringhuis, 2009).

The activation of C-type lectin receptors triggers many different immune responses with cross talk with other PRR signalling pathway. There are generally two different CLR signalling pathways. Several different CLRs such as macrophage-inducible C-type lectin, dectin 2, blood DC antigen 2 protein and C-type lectin domain family 5 are associated with adaptor protein with ITAM motifs (Bakker et al, 1999; Cao et al, 2007; Sato et al, 2006; Yamasaki et al, 2008). Another signalling pathway involves CLRs with immunoreceptor tyrosine-based inhibition (ITIM)-motif and is activated by protein kinases and phosphatases interacting with their cytoplasmic domain. Activation the CLRs with ITIM-motifs lead to the activation and signalling of Syk-dependent or independent pathways.

### 1.2.3 NOD like receptors (NLRs)

The NOD-like receptor (NLRs) recognises PAMPs from bacteria, viruses and parasite. To date, there are more than 20 known NLRs identified in human (Schroder & Tschopp, 2010). The N-terminal of NOD-like receptors consists of a protein-protein interaction domain. This is followed by a central NOD-domain and at the C-terminal there is a leucine rich repeat (LRR) domain. The defining feature of the NLRs is the NOD also known as NACHT domain, whose name derived from NAIP, CIITA, HET-E and TP1 protein. The NACHT domain has 7 conserved motifs and includes ATP/GTPase loop and $Mg^{2+}$ binding site (Koonin & Aravind, 2000; Martinon et al, 2002). The NLRs are further divided into 4 different subfamilies; NLRA, NLRB, NLRP and NLRC. The subfamilies are divided based on the N-terminal domain, Caspase activation and recruitment domain (CARDs), baculovirus IAP repeat (BIR), pyrin domain (PYD), and the acidic transactivation domain (TA)(Schroder & Tschopp, 2010; Ting et al, 2008).

The activation of NLRs by PAMPs leads to four different events including signalosome, autophagosome, Inflammasome and enhanceosome. Most NLRs can form inflammasome when activated by PAMPs or DAMPs, these NLRs binds to ASC an apoptotic protein via the pyrin-pyrin domain interaction (Chae et al, 2006). Pro-caspase 1 then binds to the ASC via the CARDs domain. This form the complete inflammasome complex. The inflammasome functions to mediate caspase 1 activation and secretion of proinflammatory cytokines such as interleukin 1β (IL-1β) and IL-18 (Elinav et al, 2011; Keller et al, 2008; Kobayashi et al, 2002; Martinon et al, 2002). Some activated NLRs interact with downstream adaptor protein such as RIP2 to activate the NF-κB. The NF-κB then acts as a transcription activator for pro-

inflammatory cytokines (Kobayashi et al, 2002). Other NLRs such as CIITA activates the MHC class II whereas NLRC5 activates MHC class I. NLRC5 for example, mediate the expression of MHC class I gene by recruiting the transcription activator such as RFX (regulatory factor X), CREB1 (cAMP-responsive-element-binding protein 1), ATF1 (activating transcription factor 1), and NFY (nuclear transcription factor Y) at MHC I promoter (Kobayashi & van den Elsen, 2012). Another mechanism of activation of NLR is autophagy. NOD1 and NOD2 trigger autophagy on by interacting with autophagy related protein (ATG) such as ATG5–ATG 12 (Deretic, 2011; Lei et al, 2012; Travassos et al, 2010).

### 1.2.4 RIG-I like receptors (RLRs)

The RIG-I-like receptors (RLRs) are a group of protein that is localised in the cytoplasm. RLRs are known to initiate inflammatory signalling when triggered by viral infections. The RLRs has a C-terminal domain that recognises nucleic acid ligands, a central DExH helicase domain and an N-terminal domain, CARDs which interacts with adaptor protein and triggers the downstream signalling events (Jiang et al, 2012a; Kowalinski et al, 2011; Luo et al, 2011). The RLRs can be found expressed in many cells including immune and non-immune cells. Cells that are uninfected expressed a low basal level of RLRs and the expression increases during viral infection (Yoneyama & Fujita, 2004). Cells primed with interferon or with the ectopic expression of RLRs enhances the PAMP recognition and signalling activation suggesting that the RLRs' function is related to the expression (Yoneyama & Fujita, 2004; Yoneyama et al, 2005b).

There are three members in RLR family of proteins; RIG-I MDA and LGP2 (Yoneyama & Fujita, 2004). RLRs are activated by the binding of foreign RNA which triggers ATP-dependent domain rearrangement to evict the CARDs domain. The exposed CARDs domain then interacts with the adaptor protein MAVS via its CARD domain (Kawai et al, 2005; Meylan et al, 2005; Seth et al, 2005; Xu et al, 2005). RLR activation and signalling results in the activation of two adaptor proteins, the NF-κB and the IRF-3. The activation of NF-κB and IRF-3 will eventually triggers the expression and secretion of pro-inflammatory cytokines and interferon (Liu et al, 2013; Paz et al, 2011; Vallabhapurapu & Karin, 2009; Yoneyama et al, 1998).

### 1.2.5 RIG-I-like receptor activation and signalling

In uninfected cells, RIG-I exists in the cytoplasm in the autoinhibited conformation (Kohlway et al, 2013; Luo et al, 2011; Ramanathan et al, 2016; Saito et al, 2007b). The RIG-I CARD domain interacts with the HEL2i domain on the helicases. MDA5 however, is more elongated with no interaction of the CARD-HEL2i domain (Zheng et al, 2015). The ligand induced activation of RIG-I releases the CARDs and allows the RIG-I to engage with the downstream signalling adaptor protein MAVS (also known as IPS-1, VISA and Cardif) to induce the expression of host antiviral genes. MAVS is a 62 kDa protein with a CARD domain in the N-terminus, a proline-rich motif, and a transmembrane domain (Kawai et al, 2005; Meylan et al, 2005; Seth et al, 2005; Xu et al, 2005).

The MAVS protein is localised in the outer layer of mitochondria. The aggregation of CARDs on the surface of mitochondria was reported to occur

concomitantly with the activation of RIG-I and MDA5 (Seth et al, 2005; Tang & Wang, 2009). The formation of filaments by the CARD domain of MAVS is essential for the recruitment of the downstream signalling proteins such as TRAF. Mutagenesis carried out on MAVS also showed that the filament formation correlates with signalling in cells (Peisley et al, 2014; Peisley et al, 2013; Xu et al, 2014). For the efficient interaction of RIG-I with MAVS, the CARD domain of RIG-I is linked by ubiquitin chain at lysine-63 (Oshiumi et al, 2012). The MAVS oligomer then recruits downstream protein to form complexes. The example of downstream protein includes TRADD (tumour necrosis factor receptor type-1-associated death domain), RIP1 (receptor interacting serine/threonine-protein kinase 1), FADD (Fas-associated protein with death domain), NF-κB essential modulator (NEMO)/inhibitor of NF-κB kinase subunit γ(Ikkγ) and many other signalling proteins (Shu et al, 1996; Zhang et al, 2010).

MAVS recruit TBK1 and IKKε via TRAF and causes its oligomerisation and phosphorylation(Fang et al, 2017). IRF3 and IRF7 function as transcription factors and are activated by phosphorylation from IκB kinases IKKε or TBK1. The activated IRF3 and IRF7 then form dimers and enter into the nucleus to activates the expression of type 1 interferon (Figure 1.1) (Jensen & Niewold, 2015; Zhao et al, 2015). NF-κB is activated due to the degradation of IκB protein. The activation of protein IKK(IκB kinase) results in the phosphorylation and degradation of IκB protein (Chen, 2005). The degradation of IκB protein frees the NF-κB and allows the transcription factor to translocate into the nucleus. The activated IRF3, IRF7 and NF-κB form complex with ATF2, c-Jun and CBP-300 and form enhanceosome to drive the transcription of IFN-β (Panne, 2008).

The IFNβ secretion due to the RLR activation is then released to bind to IFN receptors. This events subsequently activates the JAK-STAT (Janus activated kinase-signal transducer and activator of transcription) signalling pathway and stimulates the expression of interferon stimulated genes (ISGs) (Howell et al, 2018; Schneider et al, 2014). This signalling pathway amplifies the IFN response and triggers the enhanced expression of IFN-α and some ISGs such as IFIT family of proteins, OAS, MX1, IRF7, TLRs, viperin, tetherin, PKR and many others (Munir & Berg, 2013; Schoggins et al, 2011). The expression of these ISGs leads to the establishment of an antiviral state in the surrounding cells which control infection from spreading.

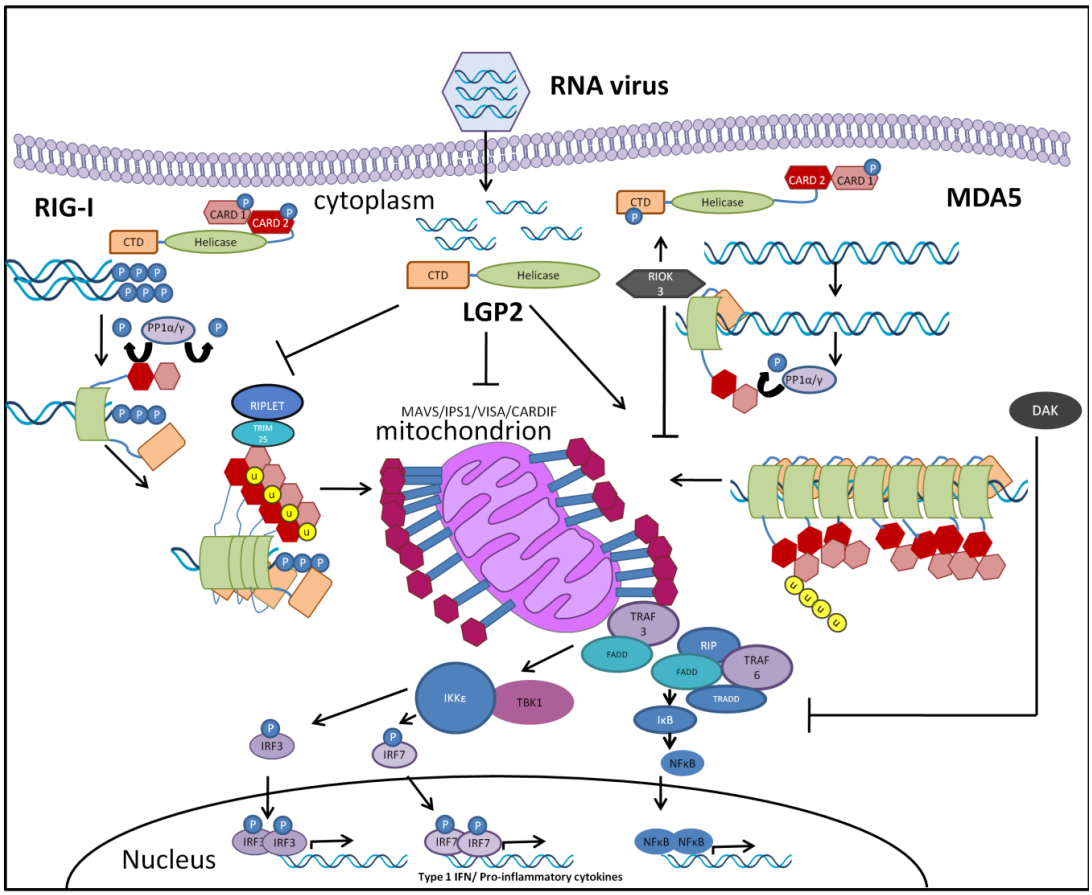


**Figure 1.1 Signalling cascade activated by RIG-I-like receptor signalling.** RIG-I-like receptors (RLRs), RIG-I, MDA5 and LGP2 recognises the viral RNA ligands. RIG-I and MDA5 recognise different foreign cytosolic dsRNA species. LGP2 plays a regulatory role in the signalling of RIG-I and MDA5. Both RIG-I and MDA5 are phosphorylated in the inactive state at some residues to repress it from unwanted activation. The phosphatases PP1$\alpha$ and PP1$\gamma$ are responsible for the dephosphorylation of the activated RLRs when bound to viral RNA. The activated RIG-I tetramerises and the MDA5 forms oligomers. Both RLRs are then polyubiquitinated at the K-63 and triggers the CARD-CARD domain interaction with MAVS. Activated MAVS then recruits its interaction partners such as of TRAF3, TRAF6, TRADD, RIP1, FADD and other signalling molecules. TRAF3 activates TBK1 and IKK$\varepsilon$ which activates IRF3 and IRF7 via phosphorylation. The dimerised IRF3 and 7 then enter the nucleus to drive the expression of type 1 interferon genes. MAVS also forms interactions with RIP, FADD, TRAF6 and TRADD and activates I$\kappa$B kinase. The activated I$\kappa$B kinase phosphorylates the IκB protein to release NF-$\kappa$B. NF-$\kappa$B then translocate into the nucleus and drives the expression of type 1 interferon and pro-inflammatory cytokines genes. The released IFN then induces the expression of hundreds of interferon stimulated genes (ISGs) via the JAK-STAT pathway (Adapted from Yong & Luo 2015, www.els.net/WileyCDA/ElsArticle/refId-a0026237.html) .

### 1.2.6 RLR recognises the different family of viruses

RIG-I-like receptors recognise different classes of viruses including viruses from the single-stranded negative-sense RNA viruses, positive-sense RNA viruses and the double stranded RNA viruses (Schlee, 2013). In the negative stranded ssRNA viruses, RIG-I recognises viruses from the family of filoviridae, paramyxoviridae, rhabdoviridae, arteriviridae, arenaviridae, bunyaviridae and orthomyxoviridae.

Marburg and Ebola viruses (EBOV) from the family filoviridae are examples of negative stranded ssRNA that are detected by RIG-I in cells. The priming of cells with RIG-I agonist protects the cells from EBOV infection in cells indicating that the RIG-I is the main PRR which recognises EBOV infections (Spiropoulou et al, 2009). On the other hand, EBOV also develops a mechanism to evade RIG-I detection by utilising RIG-I antagonist, VP 35 (Basler et al, 2000). The protein VP35 binds to the RNA and sequester the PAMPs from detection by RIG-I (Cardenas et al, 2006). Besides that, VP35 also inhibits the phosphorylation of IRF 3 and IRF 7 (Hartman et al, 2008; Prins et al, 2009). In another study by Luthra et al, the VP35 protein also interacts directly with RIG-I and suppresses RIG-I signalling activity (Luthra et al, 2013).

RIG-I and MDA5 were identified as the PRRs activated in the infections of several paramyxoviridae including measles viruses, parainfluenza and Sendai viruses. The leader RNA sequence from paramyxoviruses is a potent PAMP of RIG-I (Plumet et al, 2007). In contrast, the V protein from paramyxoviruses is recognised as the antagonist of RLRs. The V protein of paramyxovirus inhibits MDA5 and in parainfluenza binds to LGP2 to modulate RIG-I's activities (Childs et al, 2012; Childs et al, 2007; Childs et al, 2009; Motz et al, 2013). Sendai virus is a paramyxovirus and a

model virus widely studied for activating RIG-I mediated IFN response. The defective interfering (DI) RNA that is produced during Sendai virus infection has been identified as the RIG-I specific PAMPs. The DI RNA contains complementary ends forming a hairpin RNA with the 5'ppp ends (Baum et al, 2010).

In the bunyaviridae family, the viral RNA from the N-gene serves as the ligand for RIG-I. Lee et al showed that the transfection of the N-gene from bunyaviruses could activate RIG-I signalling. However, the co-transfection of the N-gene and the E3 gene from vaccinia viruses which binds to dsRNA inhibits the innate immune activation. Therefore, it is possible that the N-gene mRNA is a RIG-I specific ligand that activates RIG-I during the Hantavirus infection (Lee et al, 2011). In contrast, the expression of NY-1V G1 cytoplasmic tail of pathogenic hantaviruses inhibits IFN expression by binding to cellular protein kinases and preventing the phosphorylation of TBK1 (Alff et al, 2006). Therefore, in the case of Hantaviruses, different genes are shown to be the agonist and antagonist for RLR signalling pathway activation.

In the family orthomyxoviridae, the Influenza viruses develop different mechanisms to evade the host detection. This is accomplished by blocking host gene expression, hijacking the cap of host, regulation of transcription and inhibition of RIG-I activation (Schmolke & Garcia-Sastre, 2010). During Influenza A virus (IAV) infection, the presence of 5'ppp genomic single stranded RNA is detected by RIG-I. Specifically, the 3' UTR of the viral genome with lariat structures were identified as the ligand responsible for RIG-I activation even in the absence of 5' triphosphate moiety (Davis et al, 2012). One of the non-structural protein, NS1 from Influenza virus, on the other hand, suppresses the RIG-I by forming a complex that blocks the signal activation of

RIG-I by preventing TRIM 25 from ubiquitinating RIG-I (Rajsbaum et al, 2012). A study by Malur et al also showed that NS1 from IAV inhibits RIG-I activation via LGP2 (Malur et al, 2012).

RIG-I and MDA5 also recognise some coronaviruses. However, the genomic RNA of the 5' is capped and it is likely that the genomic RNA of coronaviruses will not be recognised directly by RIG-I. Therefore, it is postulated that some replication intermediate or subgenomic RNAs may act as the substrate for RIG-I or MDA5 (Kell & Gale, 2015). Some corona viruses encode protease which blocks the ubiquitination of signalling component in the innate immune system. For example, a protease encoded by Severe Acute Respiratory Syndrome (SARS) coronavirus inhibits IFN expression by blocking the ubiquitination of RIG-I, STING, TRAF and TBK1 (Chen et al, 2014; Sun et al, 2012). The M protein of SARS also prevents RIG-I activation by interacting with TRAF and TBK1 to prevent TRAF from binding to other downstream signalling proteins (Siu et al, 2014).

Besides that, flaviviridae is another positive strand single stranded RNA virus that is recognised by RLRs. In the example of West Nile viruses (WNV), both RIG-I and MDA5 are PRRs which recognise the viruses with RIG-I and MDA5 recognising WNV infection during early and late stages respectively (Errett et al, 2013). The genomic RNAs of WNV has a 5' cap structure to protect it from RIG-I recognition. Hence, the replication intermediate which has the 5'ppp moiety or the non-coding subgenomic RNAs generated during the infection could act as RIG-I PAMPs (Roby et al, 2014). In Dengue viruses (DENV) the innate immune activation is triggered by RIG-I, MDA5 and TLR3 (Loo et al, 2008; Nasirudeen et al, 2011). The knockdown of all three PRRs

completely abrogates the immune signalling during the viral infection (Nasirudeen et al, 2011). DENV inhibits RIG-I activation via NS4A and NS2B-NS3 proteins. The NS4A has been shown to associate with MAVS making it unavailable for RIG-I binding and thus inhibiting the IRF3 activation. Whereas the NS2B3 bind to 14-3-3ε, a protein responsible for RNA-bound RIG-I translocation to mitochondria thereby preventing RIG-I-MAVS interactions for downstream signalling (Chan & Gack, 2016; He et al, 2016; Liu et al, 2012).

Another member of flaviviridae, the hepaciviruses are also recognised by RLRs. RIG- I was shown to be the main activator of innate immunity during the hepacivirus infection, for example, the Hepatitis C virus (HCV). The region of genomic RNA specifically recognised by RIG-I is the 3' UTR region with a long tract of poly U/UC motif (Saito et al, 2008; Schnell et al, 2012). The introduction of poly U/UC RNA into cells trigger RIG-I signalling which suppresses the HCV infection (Saito et al, 2008). On the other hand, the non-structural protein NS3/4A protease suppresses RIG-I signalling by cleaving MAVS and this has been linked to chronic HCV infection (Foy et al, 2003; Horner et al, 2012; Loo et al, 2006).

As a member of the dsRNA viruses, reoviruses have segmented genomic RNA which forms blunt end hairpin structures. The genome of reoviruses encodes protein which has two different functions; the helicase and phosphohydrolase activity (Bisaillon et al, 1997). The phosphohydrolase converts the 5'ppp to 5'pp in the RNA. In a recent study by Goubau et al, 5'pp RNA was shown to activate the IFN-I expression via RIG-I. The response to the 5'ppRNA was lower than that of 5'pppRNA

(Goubau et al, 2014). Hence, 5'pppRNA to 5'ppRNA by phosphohydrolase I may function to reduce the innate immune activation during reovirus infection.

All viral factors involved in activation or inhibition of RIG-I signalling are summarized in table 1.1

**Table 1.1**: The regulatory factors of viruses governing the activation or inhibition of RIG-I signalling and their mechanisms

| Regulatory Factors | Mechanism | Upregulation/ Downregulation of IFN | References |
|---|---|---|---|
| VP35 (EBOV) | Binds to RNA to prevent RIG-I detection<br>Inhibit phosphorylation of IRF3 and IRF7<br>Interacts with RIG-I prevents RIG-I activation | Downregulation | (Cardenas et al, 2006) (Luthra et al, 2013) |
| V protein | Inhibit MDA5<br>Binds to LGP2 and inhibit RIG-I | Downregulation | (Childs et al, 2012; Childs et al, 2007; Childs et al, 2009; Motz et al, 2013) |
| DI RNA (Sendai virus) | RIG-I PAMP | Upregulation | (Baum et al, 2010) |
| Leader RNA sequence | RIG-I PAMP | Upregulation | (Plumet et al, 2007) |

| | | | |
|---|---|---|---|
| N-gene | RIG-I PAMP | Upregulation | (Lee et al, 2011) |
| NY-1V G1 | RIG-I antagonist | Downregulation | (Alff et al, 2006) |
| 3’ UTR of the viral genome (Infleunza) | RIG-I PAMP | Upregulation | (Davis et al, 2012) |
| NS1 (Influenza) | Inhibit TRIM 25 from ubiquitinating RIG-I Activation of LGP2 to inhibit RIG-I | Downregulation | (Rajsbaum et al, 2012) (Malur et al, 2012) |
| Protease (SARS) | blocking the ubiquitination of RIG-I, STING, TRAF and TBK1 | Downregulation | (Chen et al, 2014; Sun et al, 2012) |
| M protein (SARS) | prevents RIG-I activation by interacting with TRAF and TBK1 | Downregulation | (Siu et al, 2014) |
| NS4A (DENV) | Associate with MAVS to prevent RIG-I binding | Downregulation | (He et al, 2016; Liu et al, 2012) |
| NS2B3 (DENV) | Bind to 14-3-3ε and prevent recruitment of RIG-I | Downregulation | Chan & Gack, 2016 |
| poly U/UC RNA (HCV) | RIG-I PAMP | Up regulation | (Saito et al, 2008; Schnell et al, 2012) |
| NS3/4A protease (HCV) | Cleave MAVS | Down regulation | (Foy et al, 2003; Horner |

| | | | |
|---|---|---|---|
| | | | et al, 2012; Loo et al, 2006) |
| Phosphohydrolase 1 (Reovirus) | Convert triphosphate to diphosphate RNA | Reduce activation | (Goubau et al, 2014) |

### 1.3 Structural Architecture of RLRs

#### 1.3.1 Overall structure of RIG-I

RLRs are a class of DExD/H box helicase that comprises 3 members: Retinoic acid inducible gene 1 (RIG-I), melanoma differentiation-associated gene 5 (MDA5) and laboratory of genetics and physiology 2 (LGP2) (Yoneyama et al, 2005b). RIG-I and MDA5 share similar domain architectural features: the N-terminal tandem caspase activation and recruitment domain (CARDs), a central helicase core and a C-terminal domain. LGP2, on the other hand, lacks the CARDs domain involved in downstream signalling processes (Figure1.2).

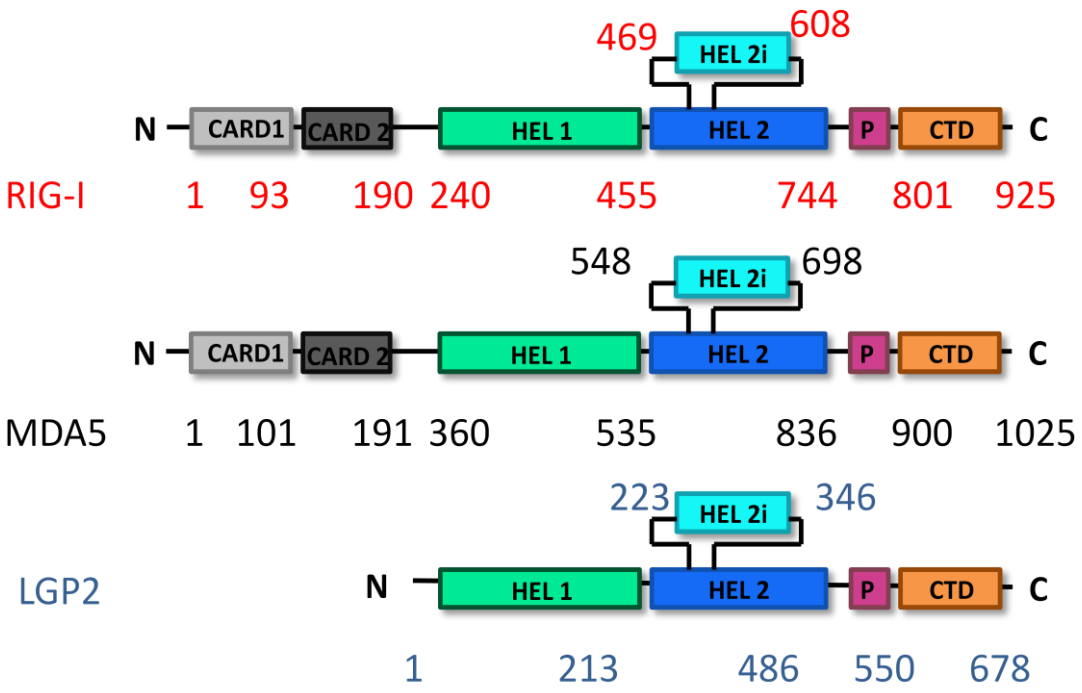


**Figure1.2: The domain organisation of RIG-I, MDA5 and LGP2.** The individual domains and the domain boundaries for all three proteins are given above.

The core structure of the helicase in RLRs has two functions: RNA binding and ATP hydrolysis. Two domains from the helicase core structure, HEL1 and HEL2, form a cleft for the binding of ATP while on the HEL2 domain, a unique insertion domain (HEL2i) is involved in RNA binding. This unique insertion domain, HEL2i also interacts with CARDs signalling domain in the inactive conformation of RIG-I. The C terminal domain of RLRs mediates specificity for RNA ligands (Jiang et al, 2012a; Kowalinski et al, 2011; Luo et al, 2011).

The C-terminal domain of RIG-I has a lysine-rich cleft and a phenylalanine that binds to and interacts with the 5'-PPP end of dsRNA to selectively binds to the blunt end triphosphate RNA (Lu et al, 2011; Wang et al, 2012b). Viral replications are known to produce triphosphorylated ends as intermediates with some viruses producing diphosphorylated ends (Goubau et al, 2014). This end features in RNA is an

important recognition factor for RIG-I activation. Using short dsRNA with hydroxyl moiety as end feature does not trigger the activation of signalling in RIG-I (Ramanathan et al, 2016; Rawling et al, 2015; Vela et al, 2012). Based on the structure of MDA5, the CTD interacts with the stem region of dsRNAs to form an open ring structure around the stem (Wu et al, 2013). The CTD of LGP2 binds to the end of the dsRNA with hydrophobic residues (Feng et al, 2012; Li et al, 2009a; Pippig et al, 2009). The feature of the CTDs explains the preference for the recognition of different and overlapping viral RNA species. Connecting the CTD to the helicase domain is a V shape long alpha-helical structure aptly named pincer, which coordinates the enzymatic and signalling activity of RIG-I (Figure 1.3) (Rawling et al, 2014).

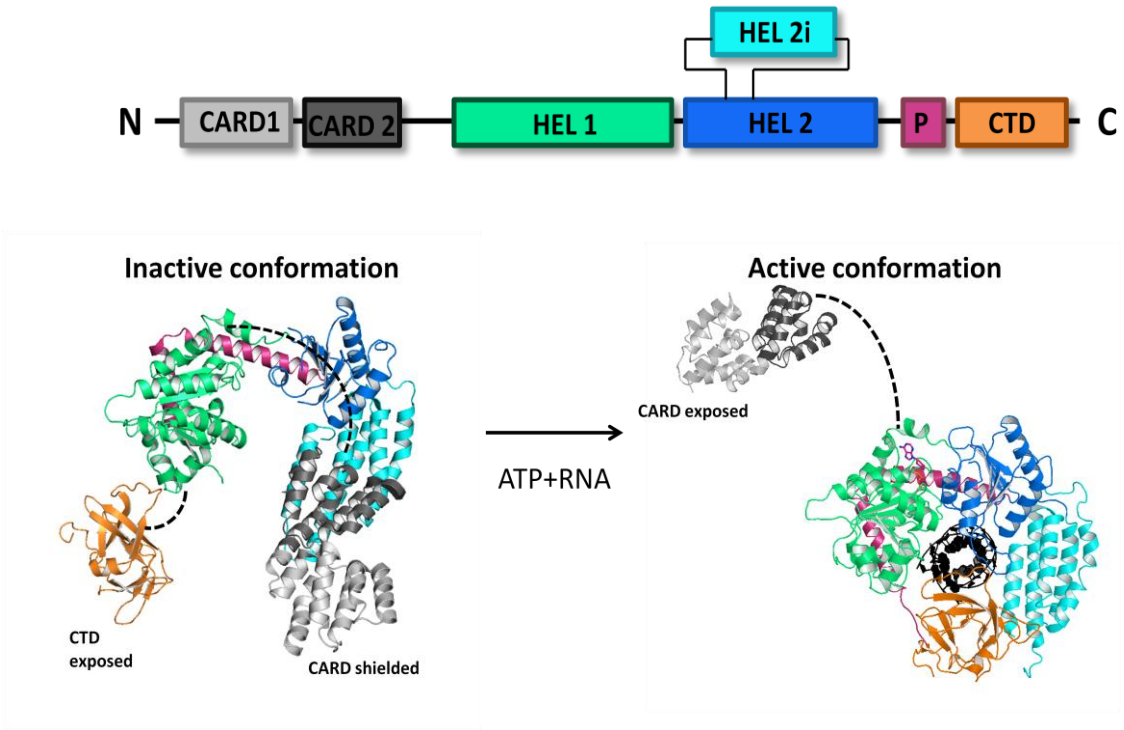


**Figure1.3: The conformation of RIG-I in the presence and absence of ligands.** RIG-I adopts an open conformation whereby the inactive CARD2 domain is bound to the HEL2i domain and the CTD is exposed to survey the cytoplasmic milieu for the presence of non-self RNA. Upon the binding of the foreign RNA, CTD presents the RNA to the helicase domain. ATP binding and hydrolysis triggers the formation of the active conformation whereby the CARDs domain

is exposed to transmit downstream signal. The colours of the individual domain are displayed in Figure 1.2. The dotted lines represent the flexible linker. The figure is based on human CTD (PDB id: 2QFB), helicase domain with the CARDs bound from duck (PDB id: 4A2Q), human RIG-I without CARDS bound to dsRNA (PDB id: 5E3H).

### 1.3.2 Ligand free conformation of RLRs

The structural studies carried out in duck RIG-I revealed that the helicase adopts an open elongated conformation. The helicase domain 2 and 2i are rigidly attached to each other (Civril et al, 2011; Jiang et al, 2012a; Kowalinski et al, 2011; Luo et al, 2011). The helicase domain 1 is loosely connected to the helicase domain 2 via the pincer domain. In the absence of RNA ligand, ATP can bind to the helicase 1 but is unable to hydrolyse as the domain 2 is rotated away from domain 1 (Civril et al, 2011). The CTD is linked to the HEL1 domain via a flexible linker (Kowalinski et al, 2011; Zheng et al, 2015).

In the inactive conformation, the CARD2 domain interacts with HEL2i and prevents CARDs of RIG-I from interacting with MAVS. The interaction site of RNA with HEL2i is not exposed due to CARD2-HEL2i interaction and this promotes RIG-I in the autorepressed conformation (Kowalinski et al, 2011; Zheng et al, 2015). In addition, some of the binding site of helicase 2i domain to CARD2 also overlaps with RNA binding sites. The helicase domain 2i and CARD 2 interface acts as a checkpoint for RNA selectivity which can only be disrupted by compatible RNA (Ramanathan et al, 2016; Zheng et al, 2015).

In the ligand free state, MDA5 adopts an open elongated conformation with flexible CTD. In contrast to RIG-I, MDA5 has longer flexible linker between CARD2 and

HEL1. In a study using HDX-MS, the region of CARD2 of MDA5 corresponding to the RIG-I CARD2-HEL2i interaction interface was shown to be open and therefore the MDA5 does not have a similar autoinhibitory conformation as RIG-I (Zheng et al, 2015). A critical phenylananine residue, P540 in helicase2i domain of RIG-I which is involved in the CARD2 binding to helicase is also not conserved in MDA5 (Berke & Modis, 2012). Hence, MDA5 is believed exist in two states in the cells a compact and extended conformation, with the compact conformation favoured in the absence of ligand. Due to the lack of the autorepressed conformation, there is a higher background activity of MDA5 activity as compared to RIG-I (Berke & Modis, 2012).

### 1.3.3 Ligand induce conformational changes and the RLRs activation

The binding of RNA ligand triggers the domains rearrangement of RIG-I which allows the CTD and the helicase domain to wrap around the dsRNA. The conformational changes of RIG-I creates the ATP binding pocket that is formed between HEL1 and HEL2 domain. The binding of RNA without the binding of ATP is thought to destabilise the CARD and HEL2i interface and resulting in the partial release of CARDs (Zheng et al, 2015). The binding of ATP in the mature ATP binding pocket induces the compaction of helicase domains especially the domain 1 and 2. This binding and the compaction of helicase are sufficient to cause the clash of the CTD with the CARDs domain and the release of CARDs due to HEL2i movement on the RNA strand (Kohlway et al, 2013). Several structures were captured with different ligand showing different conformation induced upon ligand binding. The most compact structure is the structure with ATP analogues and RNA (Figure 1.4).

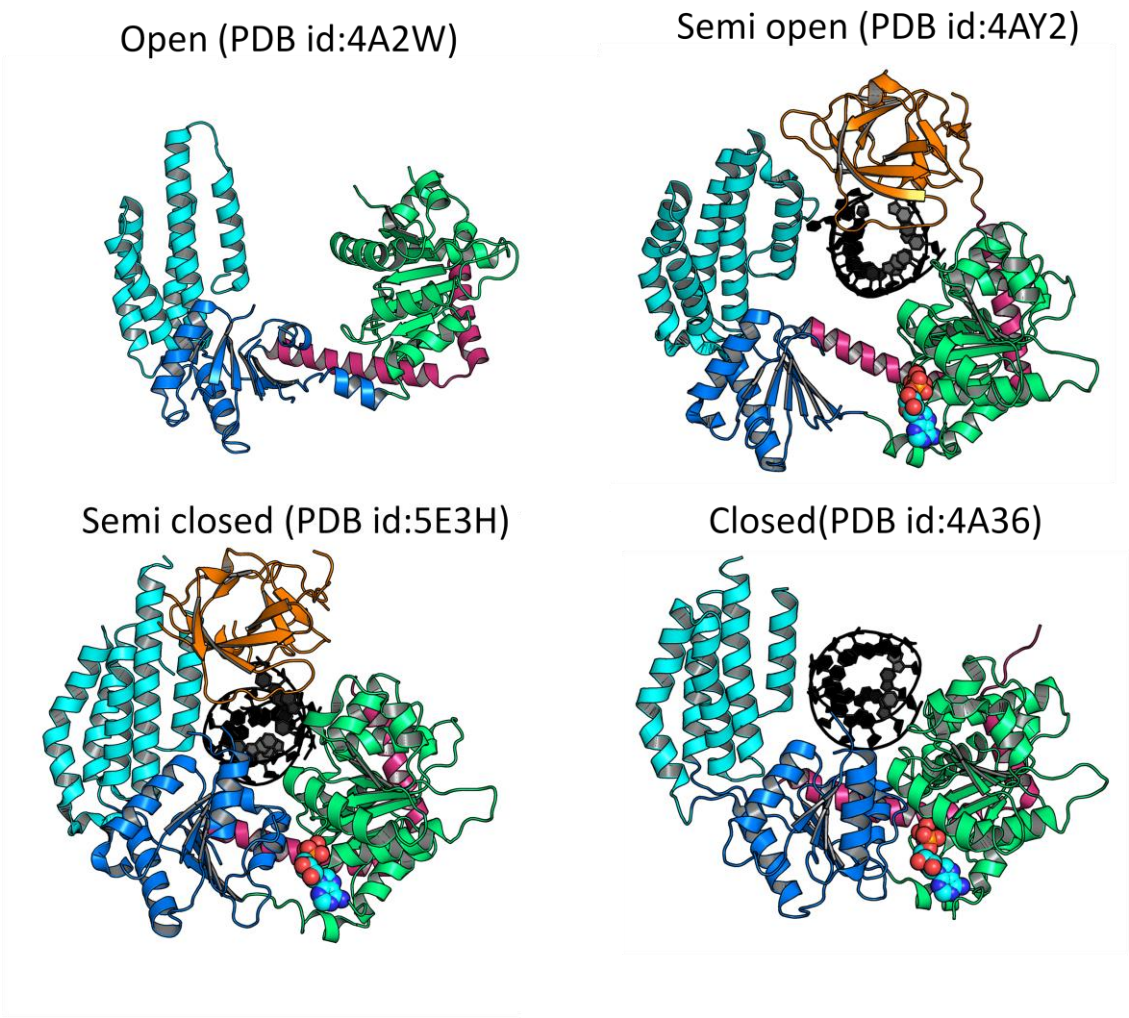


**Figure 1.4 The different conformation arrangements of domains.** The ligand-free open conformation was captured for the duck RIG-I without the CTD (PDB id: 4A2W), the semi-open conformation was captured in the human RIG-I without the CARDs with ADP occupying the ATP pocket (PDB id: 4AY2), the semi-closed conformation was captured in the human RIG-I without the CARDs with ADP-$BeF_3$ occupying the ATP pocket (PDB id: 5E3H) and the closed conformation was captured in the duck RIG-I without the CTD and the CARDs with the ATP-$AlF_3$ occupying the ATP pocket (PDB id: 4A36).

The interaction with the dsRNA is provided mainly by the CTD, helicase 1 and helicase 2 domain. These three domains form a rigid hold on the RNA from the 5' end. The HEL2i domain interacts with both upper and lower strand and was captured in various conformations moving along the strands of dsRNA (Kohlway et al, 2013). The

Pincer forms contacts between domain 1, 2 and CTD. The pincer functions to exert allosteric control for the productive reorganisation of the domains for the efficient catalytic function of helicase domains (Rawling et al, 2014). As shown in the studies by Rawling et al. the mutation of domain 1 and pincer interface hampers the immune signalling due to the defect in RNA dissociation and ATP hydrolysis while the binding to the ligands remain intact (Rawling et al, 2014).

The CTD of RIG-I interacts with 5' triphosphorylated RNA end via a positively charged surface end of the capping loop. The capping loop has several lysine residues which interact with the phosphate backbone and the 5' triphosphate of the RNA (Cui et al, 2008; Lu et al, 2011; Wang et al, 2010). This positively charged surface capping loop is able to accommodate 5' triphosphate, 5' diphosphate and cap 0 dsRNA (Devarkar et al, 2016; Goubau et al, 2014; Hornung et al, 2006; Lu et al, 2011). The key residue in the CTD involved in the selectivity of the 5' moiety of the dsRNA as non-self RNA is the His830 residue. Mutation in the His830 residue to alanine of RIG-I resulted in the binding and activation of RIG-I by $N_1$-2' O-methylated RNA (Schuberth-Wagner et al, 2015). The H830 also contributes to the preference of RNA over DNA with the H830 forming hydrogen bond with the ribose hydroxyl group of the first base (Jiang et al, 2012a).

RIG-I binds dsRNA as a monomer by end-capping without forming protein-protein mediated oligomers (Kohlway et al, 2013). However, it was shown by Peisley et al that RIG-I can only form oligomers in the event of ATP hydrolysis (Peisley et al, 2013). The release of CARDs from its autoinhibitory conformation allows the engagement of RIG-I CARDs with the CARD of MAVS. Four CARDs domain from

different RIG-I oligomerise via the CARDs domain and form tetrameric complex (Figure 1.5A) (Jiang et al, 2012b; Peisley et al, 2014). In RIG-I, CARDs tetramer forms a left-handed helical 5Å rise per CARDs. Ubiquitin chain transiently wraps around the CARD tetramer to stabilise the complex. The CARD tetramer complex then forms a scaffold for MAVS–CARD filament assembly (Figure 1.5B) (Wu et al, 2014).

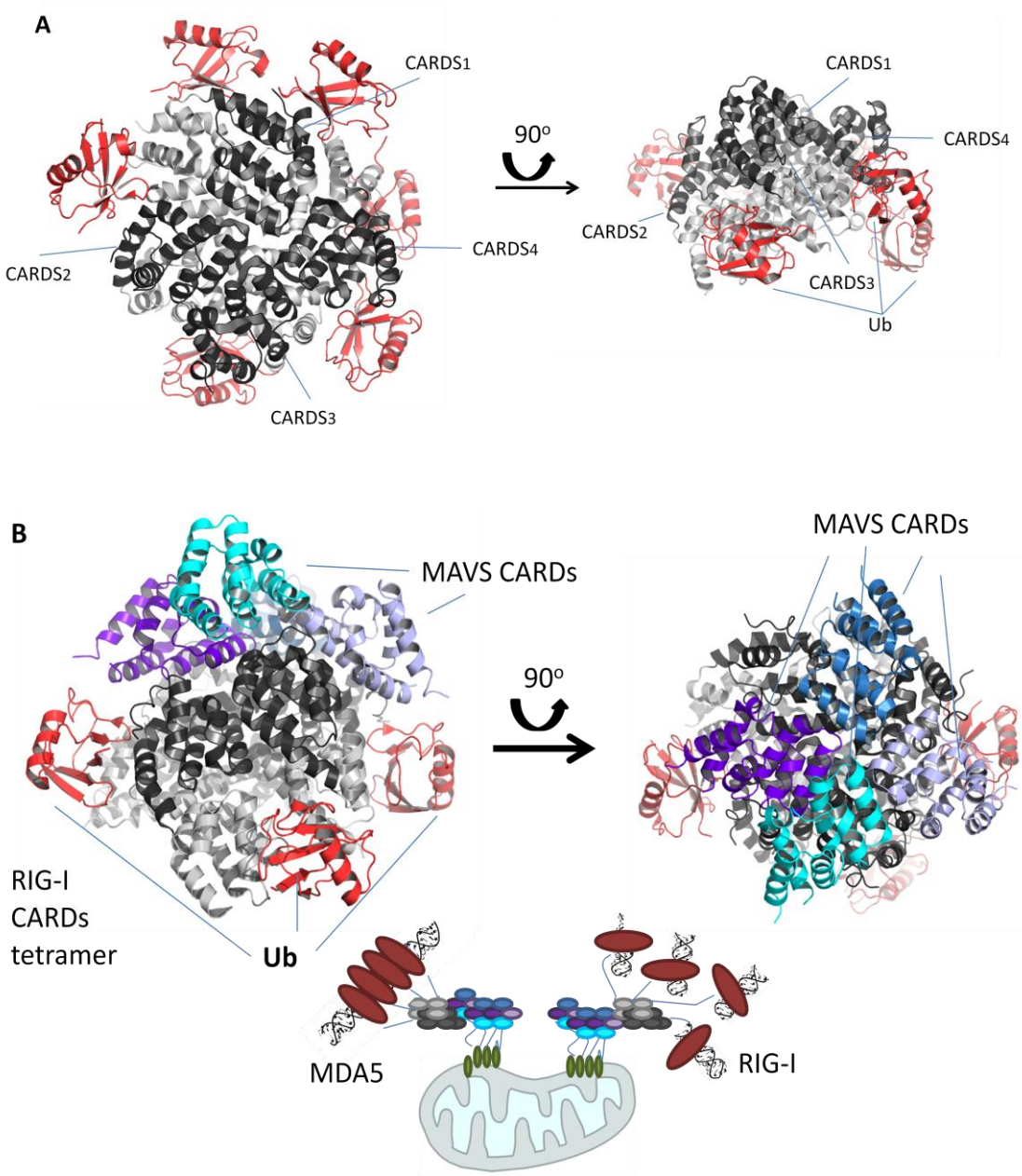


**Figure 1.5 The CARDs assembly and the interaction with MAVS CARD**. A) Four CARDs domain assemble to form CARDs tetramer (PDB id: 4NQK). B) These CARDs tetramer form the scaffold for MAVS CARD assembly into a larger filament. The structural stability of the CARDs tetramer is provided by ubiquitin chains forming around the complex. Also shown below is the model of RIG-I and MDA5 nucleating CARDs with the MAVS filament. MDA5 binds cooperatively onto longer dsRNA whereas several RIG-I comes together to form the CARDs tetramer and binds to MAVS filament.

### 1.3.4 Overall Structure of MDA5

MDA5 was captured bound to RNA by forming a partial circle around the stem of long dsRNA. The CTD of MDA5 is parallel to dsRNA axis. MDA5 coats along the dsRNA in a front to back protein conformation with a $70^{o}$ turn forming long filaments along the stem of dsRNA (Berke & Modis, 2012). The CTD of MDA5 is rotated compared to RIG-I CTD and is parallel to the dsRNA stem leaving a gap of approximately $30^{o}$. MDA5, therefore, form a more open C-shape structure with the MDA5 binding internally on the stem region of dsRNA (Wu et al, 2013). The crystal structure of MDA5 CTD with dsRNA also revealed that the CTD recognise the stem region of the dsRNA and the capping loop is unfolded (Figure 1.6)(Li et al, 2009b). The filament formation along the dsRNA brings the CARDs domain close together to each other and favours the formation of CARDs oligomer. CARDs oligomer subsequently triggers MAVS to form filament as well and this leads to the activation of antiviral signalling (Wu et al, 2013). The release of MDA5 CARDs are not strictly linked to ATPase activity as observed in RIG-I (Modis & Berke, 2012; Zheng et al, 2015).

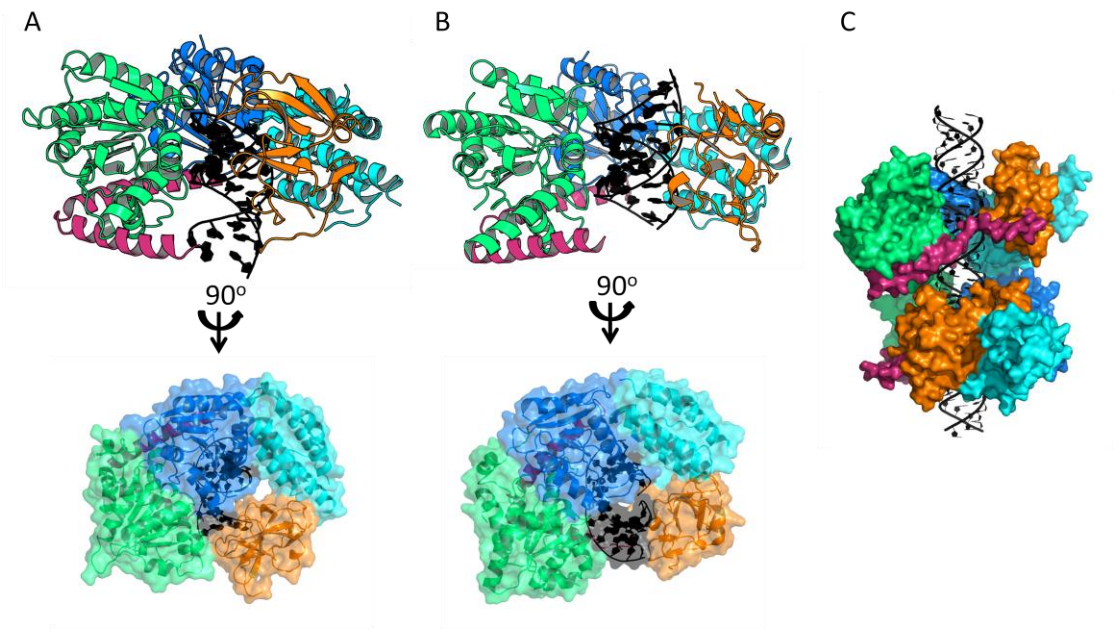


**Figure1.6: The filament formation of MDA5** A) Structure of RIG-I (B) MDA5 without CARDs domain bound to dsRNA. (A, PDB id: 5E3H) and (B,C PDB id: 4GL2) A) In RIG-I, the CTD capped the end of dsRNA and does bind to the stem making a characteristic 'O' circle around the dsRNA B) In MDA5, the CTD binds to the stem region of dsRNA forming a C-ring architecture along the dsRNA C) Model of cooperative binding of MDA5 filament with 70$^{o}$ angle turn per molecule (Wu et al, 2013). The colour scheme of each domain is based on the Figure1.2.

### 1.3.5 Overall Structure of LGP2

The domain architecture of LGP2 is similar to RIG-I and MDA5 but without the N-terminal CARDs domain and it is therefore, unable to transmit signal. The structure of LGP2 was determined for chicken LGP2 (chLGP2) with various RNAs and ATP analogues. The overall domain architecture revealed similar domain arrangement with HEL1, HEL2, HEL2i and CTD wrapping around dsRNA. The distinct difference of RIG-I and LGP2 is the pincer domain, whereby the second pincer domain of chLGP2 is longer and connects directly to the CTD whereas RIG-I has a shorter second pincer domain followed by a long proline connecting peptide. Hence, the LGP2 pincer is

more rigid and might not be as flexible in the RNA free conformation as compared to the RIG-I (Uchikawa et al, 2016).

The CTD domain of chLGP2 binds to dsRNA by capping the ends, similar to those observed in RIG-I. The CTD domain however, has a longer footprint and tolerate 3’ and 5’ overhang in RNA better than RIG-I CTD. The capping loop of CTD in chLGP2 contains the hydrophobic aromatic amino acids such as Phe595, Phe599, and Trp602 that form stacking interaction with the terminal base of the dsRNA (Figure 1.7B) (Li et al, 2009a; Uchikawa et al, 2016). The conformation of chLGP2 without the nucleotide but with dsRNA revealed a semi-closed conformation with the HEL2 domain disordered. The chLGP2 with dsRNA displayed a semi-closed conformation and chLGP2 with the dsRNA and ATP analog displayed a closed conformation. The overall structure revealed that the binding of ATP resulted in the co-operative tightening around the dsRNA and the ATP hydrolysis resulted in the loosening of grip on the dsRNA (Figure 1.7A) (Uchikawa et al, 2016).

The overall structure of chLGP2 is a cross between the structure of RIG-I CTD and helicase of MDA5. The LGP2 displays a similar longer HEL2i domain as that of MDA5 and a CTD with hydrophobic capping loop similar to that of RIG-I. Based on these structural features, LGP2 is thought to be the end binding protein similar to RIG-I and could possibly form filaments although with weaker binding to RNA than MDA5 (Uchikawa et al, 2016).

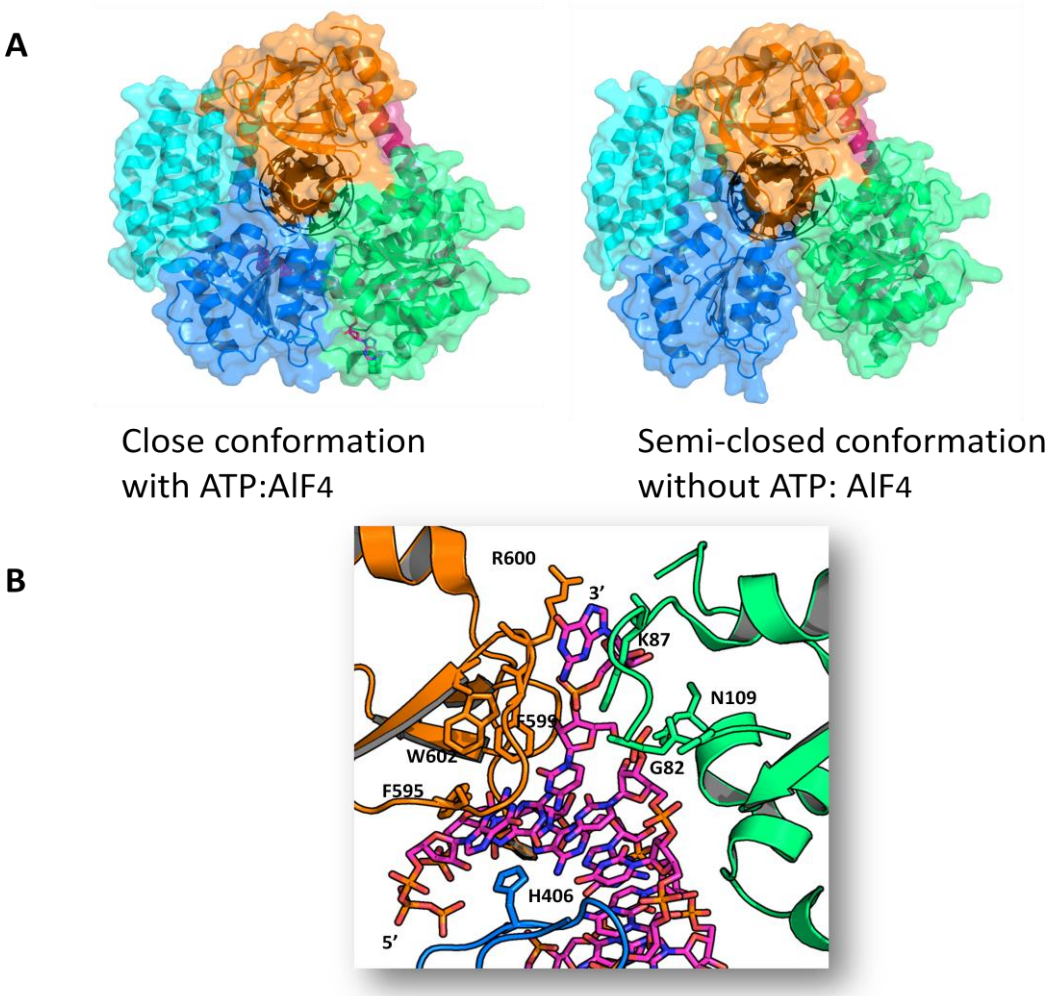


**Figure1.7 Structure of chLGP2**. A) The overall structure of chLGP2 with (PDB id: 5JB2) and without ATP analog (PDB id: 5JBJ). B) The CTD capping loop is able to accommodate the binding of RNA with 3' overhang better the movement form the HEL1 domain to allow the extrusion of the extra nucleotides (PDB id: 5JBG).

### 1.3.6 LGP2- role in innate immunity

LGP2 is unable to transmit signals because of the absence of CARDs at its N terminus. Several studies attempted to define the role of LGP2 in modulating RIG-I and MDA5. Overexpression of LGP2 was shown to interfere with the sensing of viral RNA by RIG-I and MDA5 (Rothenfusser et al, 2005; Yoneyama et al, 2005a). With LGP2 showing higher binding affinity to viral RNA compared to RIG-I or MDA5, sequestration is proposed as LGP2's role in the inhibitory mechanism (Rothenfusser et al, 2005). However, overexpression of mutant LGP2 defective in RNA binding was also unable to trigger IFN production(Bamming & Horvath, 2009). In another study, LGP2 is proposed to exert its inhibitory role by interacting with CTD of RIG-I and preventing RIG-I self-association (Saito et al, 2007a). LGP2 also inhibits antiviral signalling via interaction with MAVS and competes with the kinase IKKi/IKK$\varepsilon$ for the same interaction region on MAVS (Komuro & Horvath, 2006). In contrast, LGP2 knockout mice had impaired type I interferon production when infected with EMCV and polio virus, both of which are sensed by MDA5 implying LGP2 is a positive regulator of MDA5 (Kato et al, 2006; Satoh et al, 2010). The mechanism of synergistic activation of MDA5 and LGP2 was recently unravelled. LGP2 was shown to increase initial rates of filament formation and the stability of MDA5-dsRNA, generating a greater number and shorter lengths of filaments to optimise signalling output (Bruns et al, 2014). To reconcile the dual roles of LGP2, a model of activation was proposed whereby LGP2 acts as a positive regulator during the early stage of infection and a negative regulator during the resolution of RLR signalling (Rodriguez et al, 2014a). However, the molecular basis for this model requires further investigation (Figure 1.8).

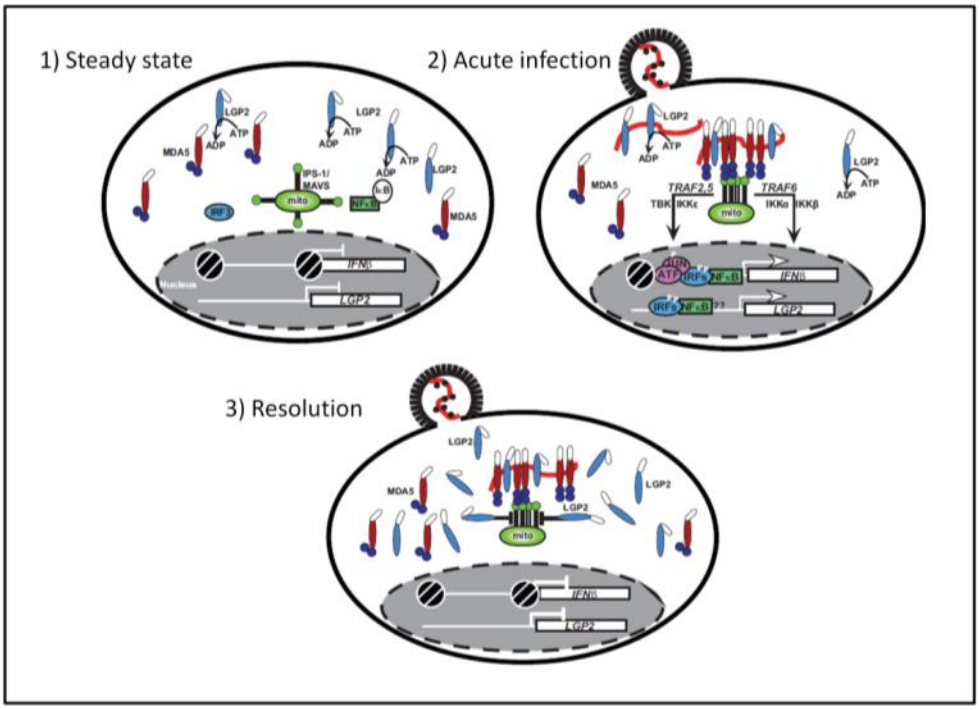


**Figure 1.8 :** A proposed model for LGP2 function in the cell as activator and inhibitor of signalling(Rodriguez et al, 2014b). 1) For clarity the model does not include RIG-I. In the uninfected cells, RLRs are present in a steady state. 2) After virus entry, the cell enters the acute stage of infection. LGP2 facilitates MDA5 recognition of foreign RNA by seeding filament formation, hence turning on the signal transduction pathway leading to IFN production. 3) During the resolution stage of infection higher level of RLRs including LGP2 negatively regulates the signalling by RIG-I and MDA5 to block uncontrolled activation and return the cells to its pre-infection steady state

### 1.3.7 The ATPase domain of RIG-I-like receptors

RIG-I-like receptors are also often referred to as RIG-I-like helicase as it is a class of SF2 helicase. The ATPase activities of RLRs are stimulated by the presence of nucleic acid binding. The RLRs are helicases that do not unwind the nucleic acid. The ATP hydrolysis still occurs at the ATP binding pocket between two RecA-like fold in the presence of RNA. Thus the term duplex-RNA activated ATPases (DRAs) was coined for the RLRs (Luo et al, 2013).

RLRs displayed a common sequence and structural arrangement of the conserved motifs for RNA binding and ATP hydrolysis and these conserved motifs are distributed between helicase domain 1 and helicase domain 2 of the helicase core. The motifs involved in ATP binding and hydrolysis includes the Q motif, motif I also known as Walker A motif and motif II also known as Walker B motifs in HEL1 domain and motif VI in HEL2 domain (Walker et al, 1982). The Q motifs and Walker A motif coordinate the NTP for hydrolysis and the Walker B motif binds a magnesium ion which helps to coordinate the β and γ phosphate and stabilises the ATP conformation for hydrolysis. Residue in Walker B motifs also serves as the catalytic base which activates the water molecule for the hydrolysis of ATP. Motif VI from the opposing site of ATP binding pocket stabilises the ATP hydrolysis transition state (Jankowsky, 2011; Luo et al, 2013).

Several conserved SF2 motifs in RLRs are involved in binding the RNA stands such as motif Ia, Ib, Ic, IV, 1Va, and motif V. Motif III and VI helps to couple the RNA binding and ATP hydrolysis (Jankowsky, 2011). In addition to the motifs mentioned, the RLRs has two other motif IIa and Vc which helps to recognise the top strand of RNA thus enabling the RLRs to bind to double stranded RNA (Luo et al, 2013) (Figure1.9).

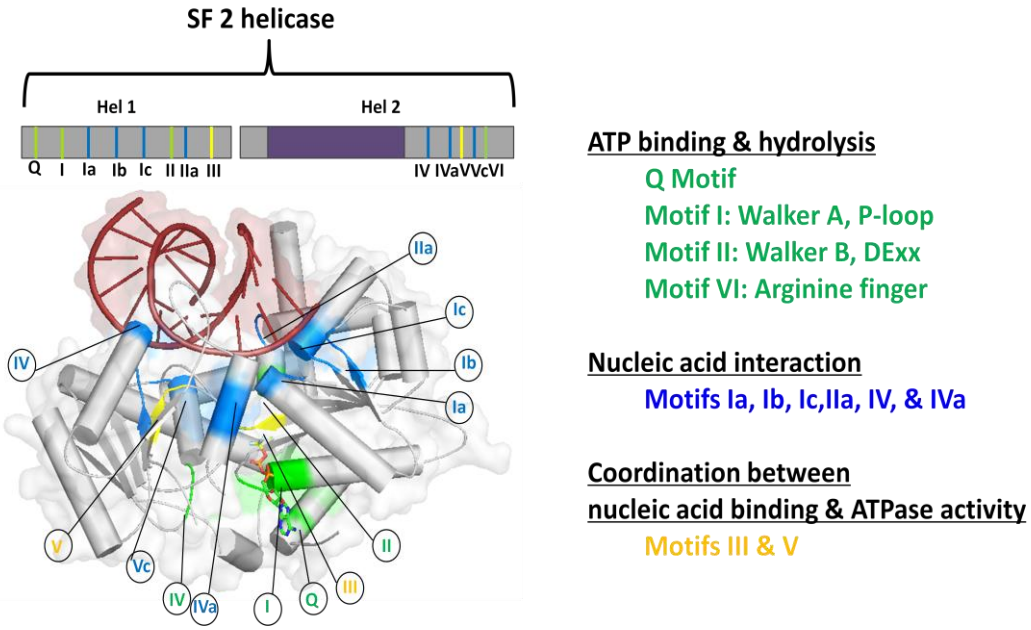


**Figure 1.9 RIG-I-like receptor helicase motif.** The motif localisation of the amino acid sequence and on the three-dimensional structure of RIG-I helicase domains 1 and 2. The function of the domains is highlighted according to the colour indicated. The domain shown here are from the structure of RIG-I (PDB id: 5E3H).

### 1.3.8 Function of ATP hydrolysis in RIG-I-like receptors

Despite extensive studies of the structure, ligand binding and activation of RLRs, a consolidated role for ATP hydrolysis by the helicase domain remains elusive. Several roles for ATP hydrolysis including translocation, oligomerisation, signalling activation and self-nonself RNA discrimination were suggested (Anchisi et al, 2015; Lassig et al, 2015; Louber et al, 2015; Myong et al, 2009; Patel et al, 2013; Ramanathan et al, 2016; Rawling et al, 2015; Wu et al, 2013).

Unlike the bonafide helicases, the helicase domain in RLR does not unwind the double-stranded RNA. Instead, it was suggested that ATP hydrolysis drives the reorientation of the helicase domain causing an allosteric clash and the

disengagement of CARDs from a autoinhibited conformation (Kohlway et al, 2013). The suggested mechanism of activation is based on the structures of RIG-I captured with ATP analogues and ADP. The ATP hydrolysis allows the temporarily available CARDs a window of time to be polyubiquitination (Jiang et al, 2012a; Kolakofsky et al, 2012; Kowalinski et al, 2011; Luo et al, 2011). However, the mutation on several key residues involved in ATPase activity resulted in only selective inhibition of signalling (Bamming & Horvath, 2009; Rawling et al, 2015; Yoneyama et al, 2004). Another suggested function of ATPase for this motor protein is the translocation of the protein along the double stranded RNA (Myong et al, 2009). However, this function is not an absolute requirement for signalling or activation as RIG-I can induce IFN production binding to short double stranded RNA with a footprint for a single protein (Kohlway et al, 2013).

Various biochemical studies have shown that RIG-I form filament on longer dsRNA. The RIG-I filament formation is ATP-dependent and correlates with the immune signal activation (Patel et al, 2013; Peisley et al, 2013). The RIG-I binds to the ends of the RNA then, translocate to the inner stem of RNA coupled by the hydrolysis of ATP and form a stack along the stem region. For this process to occur, RIG-I needs to change the conformation of CTD whereby the capping loop needs to adopt a different orientation resulting in loss of affinity to the end of the RNA. The RIG-I filament formation is formed based on very limited cooperativity and coats the long dsRNA inefficiently. This allows CARDs of RIG-I to come closer together which enhances the CARD domain tetramer formation which forms the scaffold for MAVS CARD filament formation. The RIG-I filaments are capable of signalling without the

binding of ubiquitin to further stabilise the CARDs (Peisley et al, 2013). However, ubiquitin could help stabilise the molecules along the stem and prevent RIG-I dissociation from long dsRNA.

In the case of MDA5, the addition of ATP *in vitro* was shown to destabilise the MDA5 RNA complex. MDA5 was thought to use the ATPase activity to disassemble protein bound to the ends of RNA and to affect the stability of shorter dsRNA–filament MDA5 complexes (Peisley et al, 2011). MDA5 is thought to use this mechanism to discriminate length and therefore have a preference for longer dsRNA. The cycles of ATPase activity can also improve the gap filling process during filament assembly and promote the coating of MDA5 along the stem of RNA. The formation of filament is dependent on the ATPase process since the addition of ADP or the non-hydrolysable analogues hinders the formation of filament in MDA5. MDA5 was also unable to transmit signal in the absence of filament on long dsRNA (Figure 1.10) (Modis & Berke, 2012; Peisley et al, 2011).

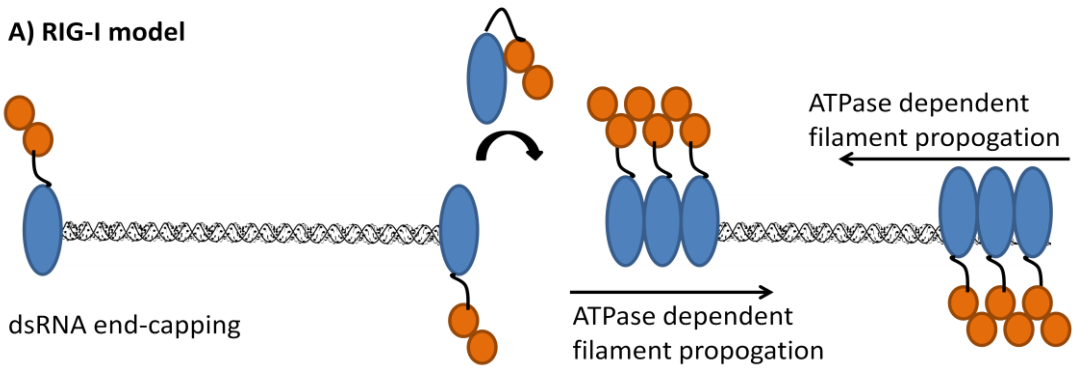

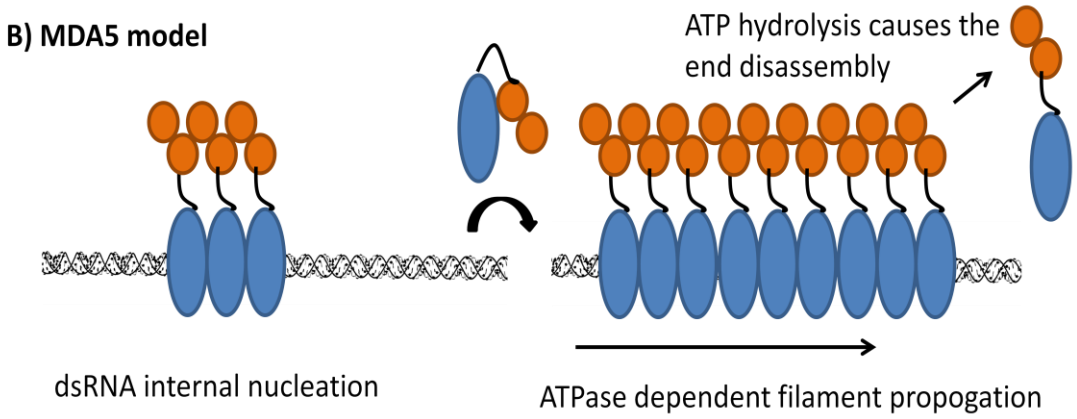


**Figure 1.10 Model of RLR ATPase driven oligomerisation** A) Model of RIG-I ATP-dependent filament formation. RIG-I prefers to bind to the ends of dsRNA due to the nature of the CTD. By hydrolyzing ATP, RIG-I translocates along the dsRNA to the stem region. The filament propagation is formed based on very limited cooperativity. B) Model of MDA5 ATP-dependent filament formation. MDA5 prefers to assemble as the stem of dsRNA and form cooperative filament. ATP hydrolysis increases the filament formation length but also helps to dissociate RNA that coats the end of dsRNA. This enhances the longer filament formation in MDA5. Figure adapted from (Peisley et al, 2013).

Another proposed function for ATP hydrolysis is to recycle RIG-I when it is bound to foreign RNA. The binding of non-self RNA enhances the allosteric effect of ATP binding. When a self RNA binds to RIG-I, the dsRNA is less stably anchored to the CTD and ATP hydrolysis weakens the interaction between helicase and dsRNA. ATP hydrolysis functions to opened up the helicase domain slightly and the weakly bound RNA is selectively removed thus discriminate self vs non-self RNA. Binding to favourable non-self RNA triggers a sustained level of ATP binding and hydrolysis per RIG-I and allows a longer exposure of CARDs for effective signalling (Lassig et al, 2015) (Anchisi et al, 2015; Louber et al, 2015; Rawling et al, 2015). In a study by Rawling et

al, it was shown using the mutant K270 that ATP binding and not hydrolysis plays an important role in activating RIG-I signalling (Figure 1.11)

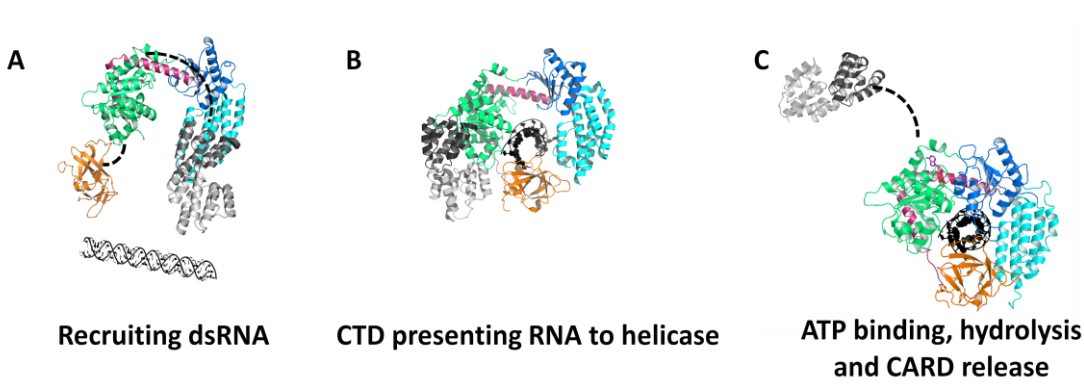


**Figure1.11: Model of ATP hydrolysis and CARD release from the helicase domain** A) The CTD of the RIG-I is surveying the cytoplasm for non-self RNA Figure is based on human CTD (PDB id: 2QFB), helicase domain with the CARDs bound from duck (PDB id: 4A2Q), B) The CTD presents the non-self RNA to the helicase domain (PDB id: 4AY2) and the CARDs of duck (PDB id: 4A2Q) C) The binding of ATP in the presence of non-self RNA causes an allosteric effect which weakens CARDs interaction to HEL2i domain. Binding of the non-self RNA increases the sustained level of ATP binding and hydrolysis and longer effective CARDs exposure (PDB id: 5E3H). The color scheme of each domain is based on the Figure1.2.

Using bulk and single molecule kinetic analysis, MDA5 was shown to undergo rapid cycles of assembly and disassembly at the ends of dsRNA due to weakened MDA5-RNA interaction (Peisley et al, 2012). In the longer dsRNA, a longer filament dissociates slower as compared to the dissociation of MDA5 from short filaments on the shorter dsRNA. The nucleation of MDA5 becomes the rate limiting factor and select against the short filaments.

### 1.3.9 RNA ligand recognition by RIG-I-like receptors

The different member of RLRs recognises distinct but overlapping classes of viruses. RIG-I recognises most of the negative-strand RNA viruses from the orthomyxoviridae, rhabdoviridae and bunyaviridae family. MDA5, on the other hand, recognises viruses from the family of picornaviridae and caliciviridae. Other viruses from the family of flaviviridae, paramyxoviridae and reoviridae are recognised by RIG-I and MDA5 (Schlee, 2013).

Several different *in vitro* experiments were carried out and the optimal ligand for RIG-I activation was determined to be dsRNA with 5'tri or diphosphate with the length of 10 bases in a Watson-Crick base-pairing (Goubau et al, 2014; Schlee et al, 2009; Schmidt et al, 2009; Schuberth-Wagner et al, 2015; Zheng et al, 2015). RIG-I displays a low nanomolar range binding affinity towards 5' triphosphorylated RNA (Ramanathan et al, 2016; Wang et al, 2010). Although the optimal ligand for RIG-I is the 5' triphosphorylated RNA, RIG-I was also shown to bind other blunt-ended dsRNA without phosphate and unmethylated cap 0 structure (Devarkar et al, 2016; Schuberth-Wagner et al, 2015). A study carried out by Anchisi et al. shows RIG-I also binds RNA: DNA hybrid to a certain extent. However, the presence of DNA at bottom strand was not too important for RIG-I signalling (Anchisi et al, 2015). RIG-I also showed to a certain extend higher tolerance for the overhang at the 3' end rather than the 5' end due to the binding specificity of the CTD to the 5' of the RNA(Schlee et al, 2009). The CTD of RIG-I displayed a positively charge lysine rich patch which binds with higher preference to the negatively charge 5' triphosphorylated moiety (Li et al, 2009b; Lu et al, 2011) (Figure 1.12). Besides that, several studies have also

shown that RIG-I can be activated by synthetic polyIC (Kohlway et al, 2013; Linehan et al, 2018; Yoneyama et al, 2004; Zheng et al, 2015). Besides that, RIG-I and MDA5 were shown to prefer U and AU rich RNA (Saito et al, 2008; Schnell et al, 2012; Takahasi et al, 2009).

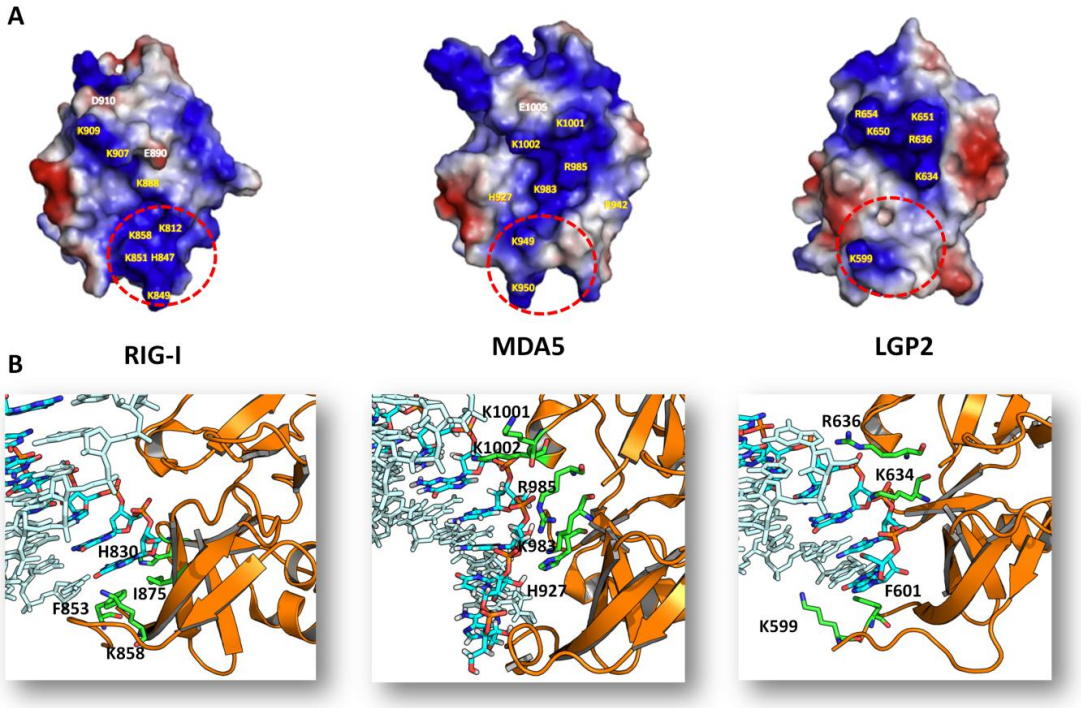


**Figure1.12: Comparison of CTD bound to RNA in RIG-I, MDA5 and LGP2** A) Surface electrostatic charge showing positively charge surface (blue) and negatively charge surface (red) of the C-terminal domain of RIG-I, MDA5 and LGP2. The RIG-I CTD binding site to the 5' triphosphate and counterparts in LGP2 and MDA5 are highlighted in a red circle. The important amino acid residues for RNA binding are labelled. B) Crystal structure of CTD of RLRs (RIG-I PDB id: 3OG8, MDA5 PDB id: 3GA3 and LGP2 PDB id: 3EQT). Residues in involved in the binding of RNA are labelled and shown as sticks in green.

Although there are several defining features that are recognised as the characteristics of RIG-I specific ligands *in vitro*, the nature of the *in vivo* ligand of RIG-I

is still controversial. The tri- and diphosphorylated dsRNAs with blunt end have been shown to activate RIG-I *in vivo* in cell transfection assay by many groups (Chiang et al, 2015; Linehan et al, 2018). However, the length of the dsRNA varies and depends on the stages of infection, amount of RIG-I induced and the RNA substrates. Several studies determined that short duplex RNA accommodating 1 RIG-I molecule per short dsRNA is sufficient to trigger the activation of RIG-I (Kohlway et al, 2013). Others have shown the importance of RIG-I CARDs tetramer in triggering the activation of RIG-I signalling events, although this could be postulated to involve different RIG-I molecule coming together binding to different short RNA ligands (Peisley et al, 2014; Peisley et al, 2013).

Several other unique RNAs features are also able to activate RIG-I signalling *in vivo* and these include the RNaseL cleavage product of viral RNA which possess unphosphorylated ends stem-loop structure from defective interfering RNA, viral nucleocapsid as well as short internal deletion defective Interfering particles(Baum et al, 2010; Liu et al, 2015a; Malathi et al, 2007; Malathi et al, 2010; Saito et al, 2008; Weber et al, 2013; Xu et al, 2015). Besides that, several recent studies also revealed that RIG-I is able to recognise and bind to unique RNA present in the cells such as circular RNA and 3' untranslated region (3' UTR) of some viruses (Cadena & Hur, 2017; Lee et al, 2011; Wang et al, 2017; Zhang et al, 2013). In another study published recently, Chazal et al. showed using riboproteomics approach that RIG-I recognises and is activated 5' UTR in flaviviruses of Dengue and Zika viruses (Chazal et al, 2018). Besides that, RIG- I also recognises some DNA present in the cytosol by interacting with RNA polymerase II and transcribing AT-rich DNA present in Epstein-

Barr virus, Herpes simplex 1 viruses and adenoviruses (Ablasser et al, 2009; Chiu et al, 2009; Minamitani et al, 2011).

MDA5 on the other hand, binds internally on duplex RNA stem region and have a preference for long RNA *in vitro* (Kato et al, 2008; Peisley et al, 2011; Pichlmair et al, 2009). MDA5 was shown to detect mainly picornaviruses including encephalomyelocarditis virus (EMCV), Mengo's virus, and Theiler's virus (Gitlin et al, 2006). It was shown that in particular, MDA5 recognises and is activated by the RNA replicative form and not the in-coming plus-strand genomic RNA of picornaviruses (Feng et al, 2012). MDA5 was also shown to bind to the positive strand RNA of the L gene measles virus (Runge et al, 2014).

### 1.3.10 Regulation of RLR signalling

The regulation of RLR signalling is mediated by several post-translational modification and the direct interactions of the RLR proteins with other regulatory proteins to modulate its function. These post-translational modifications include processes such as ubiquitination, phosphorylation, acetylation, deamidation and other mechanisms. Besides the regulation by the host machinery, RLRs signalling proteins are often regulated by the proteins involved in the viral evasion mechanisms. In this section, the focus of the discussion is on the host regulation of RIG-I signalling. The modulations of RIG-I signalling by viral proteins are discussed in the section 1.2.6 of this chapter.

**Ubiquitination**

The activation of RLR signalling is governed by several different mechanisms to avoid costly inflammatory response to uninfected cells. One of the most important regulatory mechanisms is the ubiquitination of RLR. Ubiquitination is a post-translational modification with the attachment of 8.6 kD ubiquitin protein covalently. There are 7 lysine residues within ubiquitin which are capable of forming the polyubiquitin chain (K6/K11/K27/K29/K33/K48/K63) (Heaton et al, 2016). In RIG-I, the activated protein exposes the CARDs domain and the lys 172 on the CARD domain will be polyubiquitinated by TRIM 25 which has the E3 ubiquitin ligase activity (Gack et al, 2007). Another TRIM protein, TRIM 4 also mediates the polyubiquitination of RIG-I at the CARDs domain at lys164 and lys 172 (Yan et al, 2014a). Besides TRIM 25 and TRIM 4, another E3 ubiquitin ligase Riplet (also known as RNF135/REUL) also promotes RIG-I activation by ubiquitinating the C-terminal domain. The role of Riplet in antiviral signalling is crucial and it is proposed to activate RIG-I by releasing CARDs from its autorepressed conformation (Figure 1.13) (Oshiumi et al, 2009; Oshiumi et al, 2010a; Oshiumi et al, 2013). In RIG-I, the CARDs domain polyubiquitinated either by K63-linked or unanchored polyubiquitin chain association causes the formation of tetramer that stabilise the activation of downstream signalling complex formation (Peisley et al, 2014).

Besides RIG-I, several downstream proteins such as TRAF and TBK1 are also activated by ubiquitination. TRAF 3 and TRAF6 are proteins involved in the downstream signalling of MAVS. TRAF3 and TRAF 6 is activated by K63-linked polyubiquitination by cIAP1/2 and RNF166 (Chen et al, 2015; Mao et al, 2010).

Besides that, TRIM 25 also enhances TRAF6 mediated NF-κB activation via MDA5 (Lee et al, 2015).

To diminish the RLR signal activation, RNF 125 is involved in covalently linking the K-48 polyubiquitin chain on the activated CARDs of RIG-I and MDA5. The polyubiquitin chain attachment signal leads to degradation of RIG-I and MDA5 receptors via proteasome and reduces the IFN signalling (Arimoto et al, 2007). Besides that, RIG-I is also ubiquitinated by c-CBL by linking the K48 polyubiquitin chain on CTD with the help of Siglec-G (Chen et al, 2013b). RNF 125 also ubiquitinates activated MAVS and mark it for degradation by the proteasome (Arimoto et al, 2007). RNF125 is regarded as a protein that destabilises proteins that are activated by CARD domains. Another protein complex LUBAC containing SHANK-associated RH domain-interacting protein (SHARPIN), heme-oxidised IRP2 ubiquitin ligase 1L (HOIL-1L) and HOIL-1 interaction protein (HOIP) also interferes with RLR mediated IFN expression. HOIL-1L competes with TRIM25 for the CARDs binding site on RIG-I. HOIP on the other hand, promotes TRIM25 mediated K48-linked polyubiquitination inducing proteasomal degradation on TRIM 25 (Inn et al, 2011). Besides that, protein such as tetraspanin-6 which is ubiquitinated can block RLR-MAVS interaction inhibiting downstream signalling event (Wang et al, 2012b).

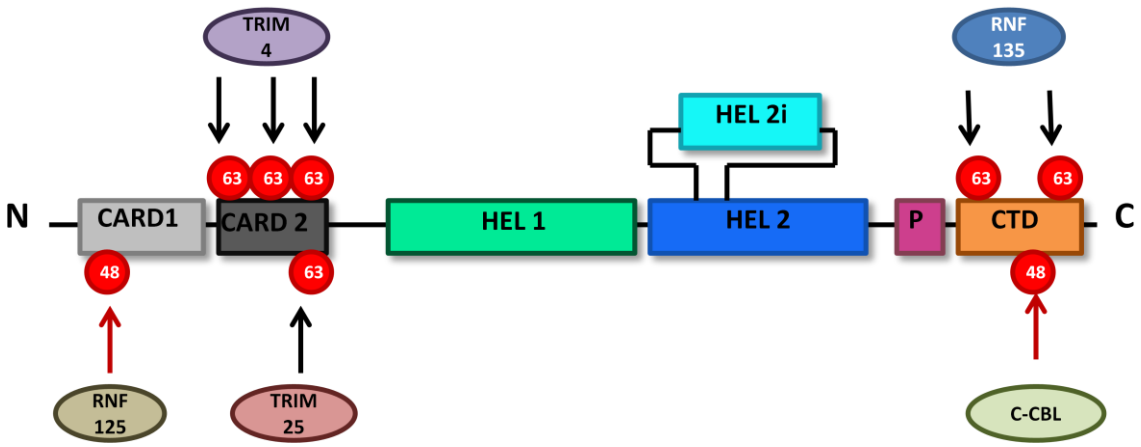

**Figure1.13. The ubiquitination site on RIG-I.** The addition of ubiquitin chain on RIG-I are shown in red circles. The linkages that are formed by the polyubiquitin chain are shown in the red circles. The K63 linked polyubiquitin chain activates RIG-I and the upregulation of IFN expression whereas the K48 linked polyubiquitin chain is a signal for the proteasome-mediated degradation. The red arrow indicates the down-regulation of IFN expression and black arrow indicates the up-regulation of IFN expression.

**Phosphorylation**

In the uninfected cells, RIG-I and MDA5 are kept in an inactive state by phosphorylation of serine/threonine residues on CARDs and CTD and thereby preventing CARD domains from forming filaments (Gack et al, 2010). In the inactive state of MDA5, two serine residues S88 and S104 in the CARDs domain and the residue S828 of the CTD are phosphorylated by RIO kinase 3 (Takashima et al, 2015). In the inactive state of RIG-I, the residues S8 and T170 on the CARDs are phosphorylated by PKC α/β. Another residue on the CTD domain of RIG-I, S788 is phosphorylated by casein kinase II (CKII) (Maharaj et al, 2012; Sun et al, 2011). Once the cells are infected with viruses, the cytoplasmic RIG-I and MDA5 interact with PP1α or PP1γ phosphatases to dephsphorylation the CARDs of RIG-I and MDA5 (Wies et al, 2013). The dephosphorylation of the CARDs of RIG-I and MDA5 increases the CARDs binding affinity to MAVS and improve the IFN secretion. When the phosphorylated residues of CARDs are mutated to nonphosphorylated residues, these residues bind better to TRIM25 and get ubiquitinated triggering stable MAVS CARD interaction.

**Deamidation**

Deamidation is a process chemical modification on amide group side chain in a protein. This process is mediated by amidotransferase. In the infection by

herpesvirus, a herpesviral glutamine amido-transferase (vGAT) was identified by mass spectrometry as the RIG-I interaction partner. vGAT from herpesvirus then induce deamidation of RIG-I at residues Q10, N245 and N445 with the help of phosphoribosylformylglycinamidine synthetase (PFAS) from the host cells. The deamidation of RIG-I residues leads to the activation of RIG-I through conformational changes due to changes in the electrostatic potential of glutamine and asparagines residues to the negatively charge glutamate and aspartate residues (He et al, 2015). Herpes simplex virus 1 (HSV-1) encodes a protein known as UL37, a deamidase that targets RIG-I. UL37 targets residue N495 and N549 of the HEL2i domain. The deamidation of N549 perturb the RNA binding capability of RIG-I and the RIG-I mutant of both N495 and N549 were unable to hydrolyse ATP *in vitro* (Zhao et al, 2016a).

**Acetylation**

During RNA virus infection, RIG-I is reversibly acetylated to modulate RIG-I antiviral signalling. The main site for acetylation was determined to be the K909 and acetylation at this site blocks the ability of RIG-I to form the signalling active form of oligomer with MAVS (Liu et al, 2016). Histone deacetylase 6 (HDAC6) deacetylates RIG-I during infection to promote RIG-I signalling. The acetylation of K909 was postulated to perturb the hydrogen bond formation between RIG-I and 5'triphosphate RNA and preventing RNA recognition by RIG-I (Choi et al, 2016). Studies were also carried out to determine the role of HDAC6 in RNA virus infection antiviral response. Cells with a low level of HDAC6 expression are more susceptible to hepatitis C (HCV) and Influenza virus infection. The knockout of HDAC6 in mice also

increases is susceptibility to West Nile Virus (WNV) and Vesicular Stomatitis Virus (VSV) (Choi et al, 2016).

**lncRNA**

In another recent study, a long noncoding RNA known as lnc-Lsm3b was identified to regulate RIG-I innate immune activation. The host lnc-Lsm3b was shown to compete with viral RNA for the RIG-I binding site during the late stages of immune response as a negative feedback mechanism. The binding of the RIG-I protein to lncRNA restricts RIG-I in an inactive conformation and prevent downstream signal activation and preventing continuous IFN induction. Lnc-Lsm3b contains multiple motifs on a long stem which can sequester many copies of RIG-I. This data is the first reported "self" RNA that acts by competing for the RIG-I binding site with foreign RNA and the induction of this RNA occurs at the late stage of viral infection reponse. This lncRNA is a first self RNA that is reported to act as the regulator for the homeostasis of RIG-I activation by competing with nonself RNA to prevent excessive inflammatory responses (Jiang et al, 2018).

**Other regulatory Mechanisms**

One of the processes involved in the regulation of RIG-I activity is SUMOylation. Sumoylation serves as a process to positively regulates RIG-I signalling by enhancing RIG-I binding to MAVS (Mi et al, 2010). SUMO 1 is responsible for the SUMOylation which enhances RIG-I signalling (Mi et al, 2010). Another protein, TRIM 38 also function as SUMO ligase for RIG-I and MDA5 enhancing the IFN responses triggered by RLRs. TRIM 38 catalyse the SUMOylation of RIG-I at K96/K889 and MDA5 at

K43/K865 during infection to facilitate PP1 dephoshorylation. The PP1 dephosphorylation leads to the activation of RIG-I or MDA5 (Hu et al, 2017). Besides SUMOylation, other proteins such as HLA-F adjacent transcription 10 (FAT10) also modulate RIG-I activity by non-covalent binding to the CARDs domain of RIG-I and inhibit IFN activation via IRF3 and NF-κB. FAT 10 also binds to TRIM 25 and stabilize the TRIM 25 and blocks the active RIG-I from interacting with mitochondria (Nguyen et al, 2016). The protein SEC14L1 is involved in negatively regulating RIG-I signalling by binding to RIG-I CARDs and blocking CARDs from MAVS adaptor protein. The knockdown to SEC14L leads to a more robust antiviral response to Sendai virus infection and Newcastle disease Virus (NDV) (Li et al, 2013). Furthermore, several autophagy-related genes, such as Atg 5-12 have been shown to modulate RIG-I and suppresses the RIG-I signalling activation by interacting with CARDs domain of RIG-I and MAVS (Jounai et al, 2007). A mitochondria targeting protein was also shown to regulate the RIG-I activity. The 14-3-3 epsilon binds to RIG-I and translocate the RIG-I from the cytoplasmic milieu to the membrane of mitochondria and for assembly with MAVS and to activate the antiviral signalling (Liu et al, 2012). Most of the regulatory factors of RIG-I activation are summarised in table 1.2.

**Table 1.2**: The regulatory factors governing the activation or inhibition of RIG-I signalling and their mechanisms

| **Regulatory Factors** | **Mechanism** | **Upregulation/ Downregulation of IFN** | **References** |
|---|---|---|---|
| TRIM 25 | K63-linked ubiquitination at | Upregulation of IFN | (Gack et al, |

| | | | |
|---|---|---|---|
| | lys172 of RIG-I | expression | 2007; Sanchez et al, 2016) |
| TRIM 4 | K63-linked ubiquitination at lys 172 and Lys 164 of RIG-I | Upregulation of IFN expression | (Yan et al, 2014a) |
| RNF 125 | K48-linked ubiquitination at CARDs of RIG-I | Downregulation of IFN expression | (Arimoto et al, 2007) |
| RNF 135/Riplet | K63-linked ubiquitination at CTD of RIG-I | Upregulation of IFN expression | (Oshiumi et al, 2009) |
| c-CBL | K48 polyubiquitin chain on CTD of RIG-I | Downregulation of IFN expression | (Chen et al, 2013b) |
| MEX3C | K63-linked ubiquitination of RIG-I | Upregulation of IFN expression | (Kuniyoshi et al, 2014) |
| HDAC 6 | Deacetylation of Lys 909 in RIG-I | Upregulation of IFN expression | (Choi et al, 2016) |
| PFAS | Deamidation of RIG-I | Upregulation of IFN expression | (He et al, 2015) |
| CYLD | removes Lys 63-linked polyubiquitin chains | Downregulation of IFN expression | (Friedman et al, 2008) |
| PP1α/γ | MDA5 and RIG-I dephosphorylation | Upregulation of IFN expression | (Wies et al, 2013) |
| CKII | Phosphorylation of Thr770 or Ser854 to Ser855 of RIG-I | Downregulation of IFN expression | (Sun et al, 2011) |
| PKC α/β | Phosphorylation of Ser8 and Thr 170 of RIG-I | Downregulation of IFN expression | (Maharaj et al, 2012) |
| IFI35 | Interact with RIG-I to suppress dephosphorylation of RIG-I and K48-linked ubiquitination | Downregulation of IFN expression | (Das et al, 2014) |
| USP4 | deubiquitination and stabilisation of RIG-I | Upregulation of IFN expression | (Wang et al, 2013) |
| CHIP | K48-linked ubiquitination | Downregulation of IFN expression | (Zhao et al, 2016b) |

| | | | |
|---|---|---|---|
| PRKRIR | blocks poly-ubiquitination and protein degradation of RIG-I | Upregulation of IFN expression | (Now & Yoo, 2011) |
| LMW FGF2 | binds to the caspase recruitment domains block RIG-I-MAVS interaction | Downregulation of IFN expression | (Liu et al, 2015b) |
| USP3 | Binds to CARDs of RLR and cleave the polyubiquitin chain | Downregulation of IFN expression | (Cui et al, 2014) |
| USP21 | deubiquitination of RIG-I | Downregulation of IFN expression | (Fan et al, 2014) |
| LUBAC | Compete with TRIM25 to bind RIG-I and induce proteasomal degradation of RIG-I | Downregulation of IFN expression | (Inn et al, 2011) |
| DDX 60 | Promotes binding of RIG-I to dsRNA | Upregulation of IFN expression | (Miyashita et al, 2011) |
| DDX3 | Binds to MAVS and RLRs | Upregulation of IFN expression | (Oshiumi et al, 2010b) |
| DHX9 | Binds to MAVS to sense RNA | Upregulation of IFN expression | (Zhang et al, 2011) |
| ARL16 | Binds to CTD of RIG-I | Downregulation of IFN expression | (Yang et al, 2011) |
| OASL | Binds to RIG-I | Upregulation of IFN expression | (Zhu et al, 2014) |
| MFN 1 | Binds to MAVS | Upregulation of IFN expression | (Castanier et al, 2010) |
| MFN1 | Binds to MAVS | Downregulation of IFN expression | (Yasukawa et al, 2009) |
| NLRX 1 | Binds to MAVS | Downregulation of IFN expression | (Moore et al, 2008) |
| NLRC5 | Interacts with RIG-I | Upregulation of IFN expression | (Ranjan et al, 2015) |

| | | | |
|---|---|---|---|
| EYA4 | Interacts with MAVS | Upregulation of IFN expression | (Okabe et al, 2009 |
| Ankrd17 | Interacts with RIG-I, MDA5 and MAVS | Upregulation of IFN expression | (Wang et al, 2012a) |
| 14-3-3ε | Binding to RIG-I as translocation complex | Upregulation of IFN expression | (Liu et al, 2012) |
| PACT | Binds CTD of RIG-I | Upregulation of IFN expression | (Kok et al, 2011) |
| ZAPS | Associate with RIG-I to promote oligomerisation of RIG-I | Upregulation of IFN expression | (Hayakawa et al, 2010) |
| RAVER1 | Interacts with MDA5 | Upregulation of IFN expression | (Chen et al, 2013a) |
| FAK | Interacts with MAVS | Upregulation of IFN expression | (Bozym et al, 2012) |
| gC1qR | Interacts with MAVS | Downregulation of IFN expression | (Xu et al, 2009) |
| Tetraspanin 6 | Interacts with MAVS to interfere with RLR binding | Downregulation of IFN expression | (Wang et al, 2012b) |
| FAT10 | Binds to CARDs to inhibit TRIM 25 | Downregulation of IFN expression | (Nguyen et al, 2016) |
| SEC14L | Interacts with RIG-I CARD to compete with RIG-I and MAVs binding | Downregulation of IFN expression | (Li et al, 2013) |

## 1.4 Development of RIG-I-like receptors as antiviral, vaccine adjuvants or oncotherapeutics

### 1.4.1 Pan-antivirals targeting RIG-I

RLRs are one of the most important PRRs which trigger antiviral immune responses against a broad group of viruses. Therefore, they serve as good targets for antiviral therapeutics development. The trend for antiviral intervention strategy focuses on the usage of direct acting antivirals (DAAs) in combination with interferons and other immune-modulatory compounds (Halfon & Sarrazin, 2012). Direct acting antivirals targets the essential components of the virus life cycle and acts specifically against certain viruses. However, due to error-prone replication of RNA virus genome, new quasispecies with reduced susceptibility to DAA have emerged. The long term use of DAAs could lead to resistant mutations and create a population of viruses escaping the DAA therapies (Asselah & Marcellin, 2013). To circumvent the problem of resistance, a broadly targeting antiviral must be used in combination with the DAAs to completely eliminate the viruses before resistant mutants could emerge. RIG-I agonist could serve as a novel group of promising antiviral candidates. The antivirals discussed here are shown in table 1.3.

### 1.4.2 Nucleotide based antivirals

SB9200 is a small compound derived from dinucleotide which has been shown to induce IFN via two distinct innate immune sensor pathways, RIG-I and NOD2. The compound SB9200 induces long-lasting induction of IFNα, IFNβ and ISGs expression in

liver tissue with concomitant increase in RIG-I, NOD2 and IRF3 (Korolowicz et al, 2016b). The initial study of this compound was carried out in woodchucks infected with WHV (Woodchuck Hepatitis Virus). Treatment of the woodchuck with SB9200 was non-toxic and lowered the antigen of WHV and viral nucleic acid in the liver. The treatment of WHV infected woodchuck with SB9200 and entecavir (ETV), a Hepatitis B antiviral, lowered the WHV viremia and a delayed the re-emergence of viral replication. Treatment with SB 9200 reduced viral infection to a similar extent to the usage of current antivirals such as Emtricitabine, Tenofovir and Adefovir (Suresh et al, 2017). The treatment of patients with HCV infection showed that SB9200 is effective as a treatment option after the failure of DAA and interferon treatment. Hence, SB9200 is a promising alternative to patients developing resistance to the current regimen of DAA therapy (Jones et al, 2017). The compound SB9200 interacts with RIG-I and NOD2 bound to the pre-genomic RNA. This interaction hinders the viral RDRP form replicating the genomic RNA of HBV (Sato et al, 2015). In the phase 1 human clinical trial, treatment of adult patients with chronic hepatitis C reduces the viral RNA which correlates with high SB9200 in plasma of the patients (Clinical trial no NCT01803308). Currently, SB9200 is being tested in phase 2 human clinical trial for adults chronically infected with the Hepatitis B virus.

### 1.4.3 RNA based antiviral candidates

From previous studies, it is clear that 5’ triphosphorylated and diphophorylated short double stranded RNA are RIG-I specific ligand(Goubau et al, 2014; Hornung et al, 2006; Kato et al, 2011; Schmidt et al, 2009). Several different groups are trying to develop this RNA agonist as antivirals. In a study by Goulet et al., the RNA ligand with

a 5’ triphosphate moiety triggers the activation of IRF3, IRF 7, NFkB and ISGs. The priming of lung epithelial cells, A549 with 5’pppRNA protected the cells from VSV (vesicular stomatitis virus), vaccinia virus and DENV (dengue virus). The 5’ppp RNA also confers protection against HIV in CD4+ T cells and HCV in Huh 7.5 cells (Goulet et al, 2013). The 5’pppRNA also protects against influenza virus *in vitro* and *in vivo*. Priming mice with 5’pppRNA was shown to reduce pneumonia in the mice when challenged with influenza virus (Goulet et al, 2013). In a study by Olagnier etal, 5’pppRNA triggers RIG-I specific activation to reduce the infection of DENV and CHIKV (chikungunya virus) in human myeloid, fibroblast and epithelial cells (Olagnier et al, 2014).

The specific features of 5’pppRNA were studied to determine the effect of sequence, length and structure of 5’pppRNA which enhances the antiviral activation of RIG-I(Chiang et al, 2015; Lee et al, 2018). The 5’pppRNA which consist of 99 nucleotide and forms a hairpin structure with uridine rich tract (M8) were more potent in activating RIG-I compared to RIG-I aptamer and poly IC. This unique RNA triggers RIG-I specifically without activating MDA5 or TLR3. M8 was also shown to confer prophylactic and therapeutic activities in cells against Dengue virus (DENV) and influenza A (IAV) infections. Furthermore, priming mice with M8 prior to influenza virus challenge reduces mortality in mice and result in a low virus titre in the lung 3 days post-infection (Chiang et al, 2015). Lee et al. also showed that short hairpin RNA with bent  stem structure and phosphorothioate backbone confers better protection than oseltamivir against influenza A H1N1 virus *in vitro* (Lee et al, 2018). In addition, short duplex stem-loop RNA also triggers a robust type I interferon response *in vivo*.

These short stem-loop RNAs (SLR) induce antiviral genes with effector function and repress genes involved in T cell maturation. The specificity of SLR makes it an important and highly effective antiviral or vaccine adjuvant candidate (Linehan et al, 2018).

### 1.4.4 Small molecular compounds

IFN and IFN stimulating genes are involved in the activation of innate and adaptive immune responses to establish an antiviral state in the host cells. As such, small molecules stimulating IFN and IFN are potential antiviral therapeutics. The high throughput screening of small molecule compounds carried out by Bedard et al., identified innate immune pathway agonist. The isoflavone-like compound was tested as antiviral and confers protection against Hepatitis C virus and Influenza A virus *in vitro*. The isoflavone compounds activates a narrow subset of innate immunity genes and could potentially be useful as a more targeted antiviral without causing issues with toxicity (Bedard et al, 2012).

In another study by Pattabhi et al., a group of hydroxyquinoline compound were identified to induce antiviral genes in cell culture. The genes upregulated when challenged with the hydroxyquinolines compound were the genes involved in the innate immunity such as RIG-I, IFIT1, IFIT 2, IFITM1, OAS3 and MX1. However, these compounds were shown to trigger high antiviral gene expression but not excessive activation of type I and type III interferon. Hence the hydroxyuinolines could be activating an alternative antiviral pathways not involving RIG-I. These hydroxyquinolines compounds were shown to be effective antivirals against RNA viruses from the families Flaviviridae, Filoviridae, Paramyxoviridae, Arenaviridae, and

Orthomyxoviridae. Interestingly, hydroxyquinoline compounds also showed prophylactic and therapeutic activity against viral (Pattabhi et al, 2016).

**Table 1.3 Pan-antivirals targeting RIG-I-like receptors. Adapted from (Yong & Luo, 2018)**

| **Pan-antivirals/ Formula** | **Target pathway** | **Referemces** |
|---|---|---|
| SB9200 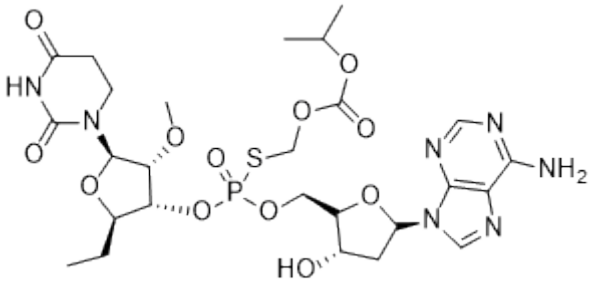 | RLR and NLR | (Jones et al, 2017; Korolowicz et al, 2016a; Korolowicz et al, 2016b; Suresh et al, 2017) |
| 5'ppp RNA derived from the 5' and 3' UTRs of the negative-strand RNA virus Vesicular Stomatitis Virus | RLR | (Goulet et al, 2013; Olagnier et al, 2014) |
| 5'ppp RNA (M8) | RLR | (Chiang et al, 2015) |
| 5'OH RNA with kink (CBS-13-BPS) | RIG-I, ISG56 | (Lee et al, 2018) |
| 5'PPP SLR<br>Stem-loop RNA with the length of 10 and 14 base pair | RIG-I | (Linehan et al, 2018) |
| KIN 100 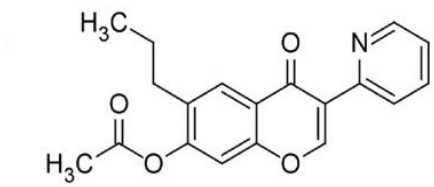 | IRF 3 | (Bedard et al, 2012) |
| KIN101 | IRF 3 | (Bedard et al, |

| | | |
|---|---|---|
| 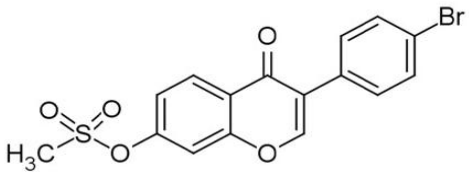 | | 2012) |
| KIN1000 | IRF 3 | (Pattabhi et al, 2016) |
| 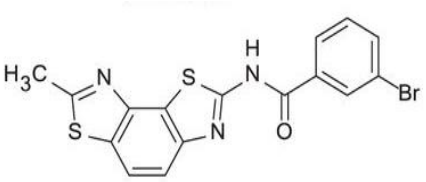 | | |
| KIN1400 | IRF 3 | (Pattabhi et al, 2016) |
| 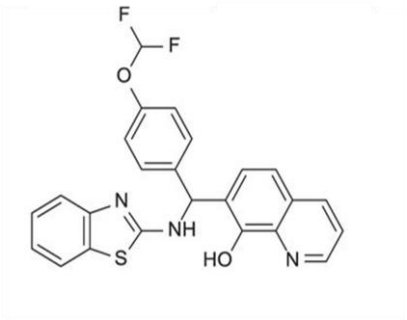 | | |
| KIN1408 | IRF 3 | (Pattabhi et al, 2016) |
| 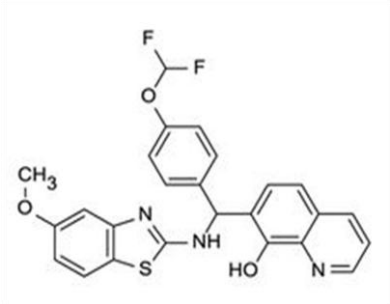 | | |
| KIN1409 | IRF 3 | (Pattabhi et al, 2016) |

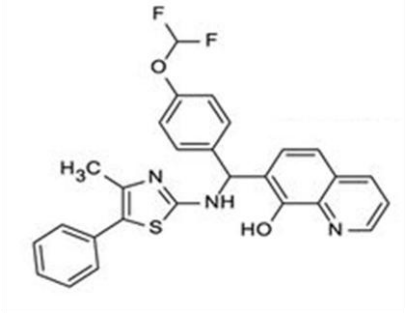


### 1.4.5 Innate immune potentiator as vaccine adjuvants

Vaccines developed traditionally are geared towards the activation of adaptive arm of immunity. Adjuvants acts as immune enhancer to vaccine via a broad cell and molecular based mechanism. Initially only two general classes of adjuvant have been approved for use in human vaccines; alum and oil in emulsion MF59. These adjuvants when administered with vaccines increases antigen uptake activates pro-inflammatory responses (Dupuis et al, 1998; Morefield et al, 2005; Mosca et al, 2008). In the later years, several other adjuvants were introduced such as AS03 (oil in water emulsion), AS04 (aluminium with monophosphoryl lipid A) and virosomes (Lee & Nguyen, 2015). The main mechanism of action for Alum mainly is the activation Th2 cellular immune responses. Alum was shown to be ineffective against HCV and HIV. Morever, there were also reports of Alum triggering hypersensitivity responses and erythema (Clements & Griffiths, 2002; Trollfors et al, 2005). With the recent insights into the molecular mechanisms of innate immune responses, the agonist of innate immunity may serve as a better candidate of targeted vaccine adjuvants. The list of innate immune potentiator used as vaccine adjuvant is shown in table 1.3.

Probst et al studied a small molecule compound named KIN 1148. This compound triggers the activation of IRF3 and protects mice against lethal influenza virus strain A/California/04/2009 when used as adjuvant with the H1N1 A/California/07/2009vaccine. KIN1148 stimulates IL-10 and Th-2 response to T cells in lung and lung-draining lymph nodes. The immunisation of influenza A vaccine with KIN 1148 increased the Influenza specific IgG antibodies detected. This study proves that KIN1148 could be used as vaccine adjuvant against influenza strain A/California/04/2009 (Table 1.4) (Probst et al, 2017).

The 5'triphosphorylated RNA, M8 was also tested as vaccine adjuvant with VLP with hemagglutinin and neuraminidase epitope from H5N1. The RNA was shown to enhance protective immunity and decrease the mortality rate of H5N1 infected mice when compared to VLP alone. More importantly, the combination of VLP and M8 increase influenza specific antibody titer when compared to other adjuvant such as addavax, alum and poly IC. In addition, the combination of VLP and M8 triggers TH1- biased CD4 T cells response in mice (Beljanski et al, 2015) . A Sendai virus defective interfering RNA (SeV DI RNA) derived 5' triphosphate RNA when used in combination with H1N1 pandemic vaccine induces influenza specific IgG and IgA antibodies. (Martinez-Gil et al, 2013).

While RLR agonists are still in the early stage of development as vaccine adjuvant, the Toll-like receptor agonist have been tested as potential vaccine adjuvant for viruses in clinical trials. The cationic peptide complexed with TLR 9 oligonucleotide known as IC31 is currently tested in phase II clinical trial (Olafsdottir et al, 2009). Another class of TLR7 ligand also known as imiquimod which was

approved as topical cream was also used as vaccine adjuvant in conjunction with intradermal vaccination and is currently in phase III clinical trial for influenza vaccine. The usage of this adjuvant improves seroconversion of the influenza vaccine in elderly patients (Hung et al, 2014). In a hepatitis B vaccine, Dynavax's HEPLISAVTM, a combination of recombinant antigen with TLR9 agonist, CpG-ODN is used and have been approved by FDA for used in humans.(clinical trial numbers NCT00426712, NCT00498212, NCT01282762, NCT00435812, NCT00511095, NCT00985426, NCT01195246, and NCT01005407). In addition a derivative of poly IC with mismatches in uracil and guanosine was shown to induces Th1 cells, cytokine IL-12 and IL-10 (Navabi et al, 2009). The trade name for this TLR3 agonist known as Ampligen® displayed a wide ranging antiviral activity against HIV, influenza, chronic fatigue syndrome, and hepatitis B and C infection(Navabi et al, 2009).

**Table 1.4**: Innate immune potentiator as virus vaccine adjuvants Adapted from (Yong & Luo, 2018)

| **Adjuvant** | **Target** | **Status** | **Virus vaccine** | **References** |
|---|---|---|---|---|
| KIN 1148 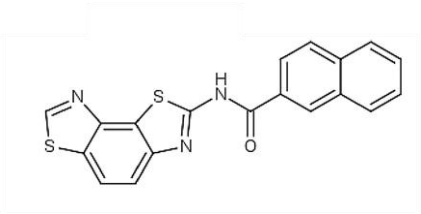 | IRF3 | Laboratory testing | Influenza H1N1 A/California/07/2009 | (Probst et al, 2017) |
| M8 5'pppRNA GACGAAGACCACAAAACCAGA UAAAAAAAAAAAAAAAAAAA AAAAAAUAAUUUUUUUUUUU UUUUUUUUUUUUUUUUAUC UGGUUUUGUGGUCUUCGUC | RLR | Laboratory testing | H5N1 influenza | (Beljanski et al, 2015) |
| 5'pppRNA Derived from SeV DI RNA | RLR | Laboratory testing | H1N1 2009 | (Martinez-Gil et al, 2013) |

| | | | | |
|---|---|---|---|---|
| Ampligen ® poly(I:C12U) | TLR3 | Phase IIb NCT00035893 | HIV | (Navabi et al, 2009) |
| CpG- ODN | TLR9 | Approved HEPLISAVTM | Hepatitis B | NCT00426712, NCT00498212, NCT01282762, NCT00435812, NCT00511095, NCT00985426, NCT01195246, and NCT01005407 |
| Imiquimod 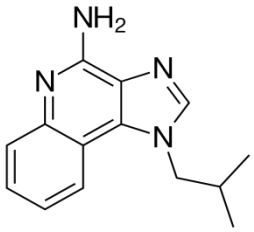 | TLR 7 | Phase III | Influenza A | (Hung et al, 2014) |

### 1.4.6 Targeting cytosolic nucleic acid-signalling as potential cancer immunotherapies

Cancer has been described previously as “wound that do not heal” by Dvorak (Dvorak et al, 1986). Cells that are injured or stressed release nucleic acid such as DNA, mRNA or microRNA that is highly secreted in the tumor microenvironment. The release of nucleic acid is mediated by processes such as apoptosis, necrotic cell death and secretion by the cancer cells (Suraj et al, 2017). The released of nucleic acid from

cancer cells are termed damage associated molecular patterns (DAMPs) could essentially target the same PPRs that acts as cytosolic nucleic acid sensors. In a recent study, it was shown that, damaged nucleic acids from cancer cells are released by cells in tumor microenvironment leading to activation of PRRs in CD8α dendritic cells via cGAS-STING or RIG-I and MDA5 antiviral signalling. This leads to the secretion of type I IFN and the migration of CD8α dendritic cells to the draining lymph nodes and the dendritic cells cross-primed the naive $CD8^+$ T lymphocytes (Duewell et al, 2014; Ellermeier et al, 2013; Klarquist et al, 2014; Woo et al, 2014).

In the tumor microenvironment the activation of RIG-I could potentially trigger programme cell death (PCD) and cytokine activation of macrophages and natural killer cells. This would lead to the enhanced cross priming of the adaptive immune effectors (Okamoto et al, 2017). Programme cell death that are triggered by RIG-I includes pyroptosis and apoptosis. In the example of prostate cancer cells, RIG-I activation at the tumour microenvironment triggers expression of Fas, tumor necrosis factor (TNF), TNF-related apoptosis inducing ligand (TRAIL) and TRAIL receptors, resulting in caspase-8 activation and apoptosis (Kaneda, 2013). In the IFN rich tumor microenvironment triggered by RIG-I, the cell death by leukocyte, NK cells and macrophages also increases. The maturation of macrophages and dendritic enhance antigen presentation of T-lymphocytes in the tumor draining lymph nodes (Elion & Cook, 2018).

Given the effectiveness of the innate immune system in destroying cancer cells, RIG-I agonist are now being studied as anti-cancer treatment in the clinical and pre-clinical trial for hepatocellular carcinoma, leukemia, melanoma and prostate

cancer (Besch et al, 2009; Hou et al, 2014; Kawaguchi et al, 2009; Li et al, 2017). A pre-clinical study of the compound specific for RIG-I under Merck/Rigontec, RGT100 is in the phase I/II clinical trials for advanced solid tumors, liver tumor and lymphomas (NCT03065023). Another company that works with small molecule compound targeting RLRs, Kineta Inc. is also testing compound as an onco-immunological target, although this study has not been reported in peer reviewed articles.

Besides RIG-I specific agonist which only targets RIG-I like receptor pathway, several other compounds are reported to indirectly activate RIG-I-like receptor signalling pathway, for example the inactivated Sendai virus particles. These inactivated particles have been tested in phase I/II clinical trials for late stage malignant melanoma and prostate cancer (Fujita et al, 2017; Tanemura et al, 2013). Another therapeutic agent for cancer therapy is the DNA methyltransferases (DNMTs) inhibitors. DNMT inhibitors such as 5-azacitidine (AZA) showed potential in therapeutic treatments of non small cell lung cancer, solid tumor and ovarian cancer (Matei et al, 2012). Currently, DNMT inhibitor is used in phase II clinical trials together with HDAC inhibitors, entinostat (Wrangle et al, 2013). A study to dissect the different signalling pathway involved in usage of DNMT inhibitors revealed that there are up-regulation of several immunomodulatory pathways including the RLR signalling pathway (Li et al, 2014).

Another agonist of RLR and TLR signalling pathway, the synthetic nucleic acid poly ICLC is also being investigated in clinical trials. Poly ICLC is a polyinosinic-polycytidylic acid with poly-l-lysine and carboxymethylcellulose as a stabilizer. When tested in patients with Stage IV anaplastic astrocytoma, the treatment with poly ICLC

increased survival to more than 8 years as compared to 2 years using chemotherapy alone (Salazar et al, 1996). In addition, poly ICLC was tested as adjuvant for several cancer such as gliomas, breast cancer, pancreatic cancer, ovarian cancer, and multiple myeloma (Dillon et al, 2017; Mehrotra et al, 2017; Okada et al, 2015; Sabbatini et al, 2012; Tsuji et al, 2013). The potential of polyICLC in treating various cancer is immense when used in combination with other therapeutics or as an adjuvant. The RIG-I agonists used in cancer immunotherapy and their respectively clinical trial stages are listed in table 1.5.

**Table 1.5** Cytosolic nucleic acid sensors RLRs targeted for cancer immunotherapy. Adapted from (Iurescia et al, 2018)

| **Clinical trial Identifier and the phase of study** | **Compound** | **Cancer condition** | **Status of trial** | **References** |
|---|---|---|---|---|
| UMIN000002376, I/II | Inactivated Sendai virus particles | Malignant melanoma stage IIIC or stage IV | Phase I finished in 2016 | (Tanemura et al, 2013) |
| UMIN000006142, I/II | Inactivated Sendai virus particles | Castration-resistant prostate cancer | Currently recruiting participants | (Fujita et al, 2017) |
| NCT01105377, II | Azacitidine/Entinostat | Metastatic colorectal cancer | Completed Update on August 2014 | (Li et al, 2014) |

| | | | | |
|---|---|---|---|---|
| NCT01349959, II | Azacitidine/Entinostat | Advanced breast cancer; triple-negative and hormone-refractory | Ongoing, but not recruiting participantsUpdate on December 2016 | (Li et al, 2014) |
| NCT01928576, II | Azacitidine/Entinostat/Nivolumab | Recurrent metastatic non-small cell lung cancer | Currently recruiting participants Updated on October 2017 | (Wrangle et al, 2013) |
| NCT03065023, 1/II | RGT100 | advanced solid tumors, liver tumor and lymphomas | Halted and will be continued with new protocol | - |

In spite of the potential use of RLR agonist as a potent antivirals and the use in cancer immunotherapy, stringent care should be taken into account the off-target activation of autoimmunity should be carefully evaluated to prevent cytokine storm that could potentially hinders the safety and efficacy of these treatments(Trinchieri, 2010). It is also important to note that RIG-I are ubiquitously expressed in most human cells and could trigger systemic inflammation. Therefore, to prevent uncontrolled activation, many immune checkpoint inhibitor based treatments are managed with the presence of corticosteroid as an immunosuppressor (Elion & Cook, 2018)

### 1.4.7 Harnessing the innate immune sensing pathways for immunotherapy

Given the ability of nucleic acid to trigger robust interferon production and the ability of basal level nucleic acid sensor to quickly mount an effective response, RLRs would be a suitable target for immunotherapy. RLRs are also ideally contained within the cytosol of cells preventing systemic IFN-associated inflammation (Junt & Barchet, 2015). Besides, the ability of this sensor protein to discriminate self and foreign RNA has been extensively proven in previous studies (Anchisi et al, 2015; Lassig et al, 2015; Louber et al, 2015; Rawling et al, 2015). Furthermore, uncontrolled activation of nucleic acid sensors by agonist is also kept in check within the cells with the constitutive presence of nucleases (Morita et al, 2004; Rice et al, 2007).

The idea of packaging nucleic acid into virus-like-particle (VLP) as a nanocarrier for immunotherapy serves two purposes; (1) For the targeted delivery of nucleic acid into cells in a protected environment to prevent undesired systemic immune activation, (2) VLP itself with its highly repetitive particulate structure is a potent activator of B cells (Jennings & Bachmann, 2009). CpG ODN a synthetic nucleic acid activating the TLR 9 of the innate immunity, packaged into VLP which have been tested in clinical trial for potential to be used as vaccine against many infectious diseases and cancer (reviewed in (Scheiermann & Klinman, 2014). RLR specific agonist could potentially be applied for used as immunodrugs or adjuvant for vaccines (Figure1.14).

Several VLPs have been successfully used as commercial vaccines most notably for the treatment of HPV (Human Papilloma virus), HBV (Hepatitis B virus) and HEV (Hepatitis E virus). Some example of recombinant based VLP vaccines include

GlaxoSmithKline's Engerix® (hepatitis B virus) and Cervarix® (human papillomavirus), and Merck and Co., Inc.'s Recombivax HB® (hepatitis B virus), Gardasil® (human papillomavirus) and Hecolin (Hepatitis E virus) Xiamen Innovax Biotech(Christensen et al, 1996; Deschuyteneer et al, 2010; Li et al, 2005; Marais et al, 2006; Mulder et al, 2012; Waters et al, 1987; Wei et al, 2014; Zhang et al, 2014). The VLP based vaccines are also being developed and tested at various stages of clinical trials for Influenza virus, rotavirus, Norwalk virus and parvovirus(Antonis et al, 2006; Galarza et al, 2005; LoBue et al, 2006; O'Neal et al, 1998; Pushko et al, 2005; Tacket et al, 2003). However, the use of VLP as nanocarrier has not been tested in any human clinical trial. Several different cargoes were reported to be loaded onto VLP to functionalise and deliver therapeutics inclucing, antibody, cytokines, nucleic acid, metal and small molecule drugs (Gleiter & Lilie, 2003; Kimchi-Sarfaty et al, 2003; Oh et al, 2004; Zhao et al, 2011).

Developing VLP into nanocarrier as a vehicle for immunotherapy comes with challenges such as targeted delivery of the therapeutic agent, efficient cargo loading, VLP stability, pharmacokinetics of immunotherapy agent and surface functionalization (Rohovie et al, 2017). Besides that, VLP are also prone to clearance by phagocytes before reaching the targeted site for cargo delivery. For VLP usage solely as nanocarrier for delivery, the immune activation events associated with virus recognition may not be desirable feature of the VLP. The VLPs used for such purposes can be PEGylated to prevent unwanted immune activation during therapeutics delivery to the targeted cells(Jain & Jain, 2008). Besides that, the process of large

scale packaging of VLP with therapeutic agents can be a major roadblock to the functionalisation of VLP as nanocarrier(Naskalska & Pyrc, 2015).

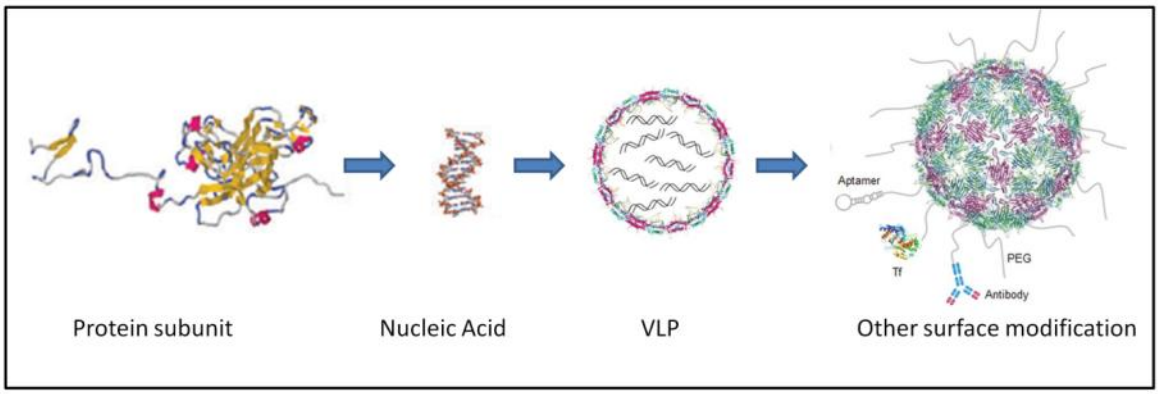


**Figure 1.14 :** PAMPs of RLR could be assembled into VLP for targeted cell delivery (Yan et al, 2014b; Zhang et al, 2015). The protein subunit for VLPs is easily produced in large scale via recombinant bacterial expression. Immune-modulatory RNA of interest can then be packaged into the VLPs via *in vitro* assembly.

**1.5: Aim of the thesis**

RIG-I-like receptors (RLRs) are crucial as the first line of cellular defence against viral invasion. RLRs act as an important class of pathogen recognition receptors (PRRs) and are able to mount an antiviral response against infections such as Influenza, Dengue, Ebola and many other dangerous viral pathogens. RIG-I is able to distinguish viral nucleic acid signatures as non-self and mount an effective immune response by ultimately inducing the secretion of type 1 interferon and pro-inflammatory cytokines. MDA5 and LGP2 are other members of the RIG-I-like receptors and are also known to bind to and detect double stranded RNA. MDA5 is involved in many autoimmune conditions while LGP2 acts as either a positive or negative regulator of RIG-I-like signalling.

Many studies were carried out previously to determine the PAMPs that are able to activate RIG-I and trigger the innate immune activation. Of the many different RNA ligands, blunt-ended dsRNA with 5’ triphosphate moiety is known as a potent RNAs that activates RIG-I. Recently, the Pyle lab showed that the short stem-loop RNAs with stable tetraloop at one end with 5’ triphosphate are strong RIG-I activator.

In this study, we employ biochemical and cell based assay to determine the ability of short stem-loop RNA in triggering RIG-I activation and the potential to package this RNAs in virus-like particles as a means to deliver the RNA into cells. Specific aims:

1) Development of immune modulatory RNA (ImmRNA) with robust RIG-I activation
2) The packaging of ImmRNA into virus-like particle

## Chapter 2: Materials and methods

### 2.1 Protein expression and purification

Genes of interest in plasmid pET-SUMO vector (Invitrogen) were transformed into *Escherichia coli* Rosetta$^{TM}$ 2 (DE3)(Novagen). Transformants were grown in Luria Broth (LB) broth supplemented with Kanamycin (50 mg/L) and Chloramphenicol (37 mg/L) at 37°C and induced at $OD_{600}$ of 0.8-1.0 with 0.5 mM IPTG. The overexpression of the recombinant protein was carried out for 16 hr at 18°C. Cells were harvested by centrifugation at 5000 rpm for 20 minutes at 4°C. Cells were resuspended in lysis buffer containing 25 mM 4-(2-hydroxyethyl)-1-piperazineethanesulfonic acid (HEPES), pH 8.0, 500 mM sodium chloride (NaCl), 5 mM β-Mercaptoethanol (β-ME), 5% glycerol, 10 mM imidazole at a ratio of 20ml of lysis buffer per 5 g of cell pellet. Cells were lysed with homogenizer (GEA Niro Soavi) at 900 bar for 5-10 minutes and clarified by centrifugation at 40,000 rpm for 40 minutes at 4°C. The soluble fraction was collected and incubated with Ni-NTA Agarose beads slurry (Thermo) for 2 hours at 4°C. The bound recombinant proteins were passed through a drip column and the Ni-NTA beads with protein were washed extensively with lysis buffer containing 20-40 mM imidazole and lysis buffer with high salt (1M). The proteins were eluted with lysis buffer containing 300 mM imidazole. The SUMO tag was cleaved with Ulp1 protease in dialysis buffer containing 25 mM HEPES, pH 7.5, 150 mM NaCl, 2 mM DTT, 5% glycerol overnight. The SUMO tag and the Ulp1 protease were removed by running through Ni-NTA Agarose beads. The protein was then further polished by running through HiTrap Heparin HP 5 ml column (GE Healthcare) and eluted in buffer containing 25 mM HEPES, pH 7.5, 600 mM NaCl, 5 mM β-Mercaptoethanol (β-ME), 10

% glycerol. Eluted fractions were pooled, concentrated and injected into HiLoad 16/600 Superdex 200 pg (GE Healthcare) column for size exclusion chromatography. Eluted fractions were collected, concentrated using Vivaspin 20 (Molecular weight cut off 30 kDa) (Sartorius) and analysed by sodium dodecyl sulfate-polyacrylamide gel electrophoresis (SDS-PAGE), and then quantified using NanoDrop® spectrophotometer (Thermo Fisher Scientific, USA) by measuring the absorbance at 280 nm. The purified protein was then flash frozen and stored in small aliquot in -80$^{o}$C.

**2.2 *In vitro* transcription of RNA**

RNAs were transcribed using complementary DNA oligo pairs chemically synthesised from IDT (IDTSg). The 5' end of the primer contains T7 recognition sequence followed by the RNA sequence to be transcribed. Briefly, complementary DNA oligo pairs were annealed by heating to 95$^{o}$C and cooling it slowly to room temperature. *In vitro* transcription reaction were carried out in 30 mM HEPES pH 7.4, 30 mM $MgCl_2$, 2 mM spermidine, 10 mM DTT, 0.01 % Triton-X100, 4.5 mM GTP and 4 mM NTP (CTP, ATP and UTP), 1 µM annealed DNA template, 400 nM T7 RNA polymerase, 0.2 U/mL thermostable inorganic pyrophosphatase for overnight at 37°C. The transcribed RNAs were purified by phenol:chloroform:isoamyl alcohol (25:24:1, v/v) extraction followed by ethanol precipitation in the presence of 0.3 M sodium acetate pH 5.2 and 100% ethanol overnight at -80 °C. RNA pellet was resuspended in 10 mM HEPES buffer pH 7.4 and subjected to further purification by Hi-Trap Q HP column. The two heparin buffers consist of 10 mM HEPES pH 7.4 and 10 mM HEPES pH 7.4 with 1M NaCl. The RNA was eluted in a salt gradient. The eluted RNAs were subjected to ethanol

precipitation and run on 20% denaturing PAGE with 7 M Urea. The RNA with the expected size were excised from the gel and extracted in 0.3 M sodium acetate pH 5.2 followed by ethanol precipitation. Purified RNAs were resuspended in ME 50 buffer containing 10 mM MOPS pH 7, 1 mM EDTA and 50 mM NaCl. The resulting RNA was run on a 20 % denaturing PAGE with (7 M Urea) and stain with Stains-All. The sequence of the primer pairs used is shown in Appendix 1.

**2.3 Crystallisation screening**

For crystallisation, 80 µM protein hsRC2 were incubated with different RNAs at a molar ratio of 1:1.5 for 1 hour on ice. Protein-ligand complexes were subjected to centrifugation at 14, 000 rpm for 20 mins at 4$^{o}$C to remove aggregated protein. An automated initial crystallisation screen was carried out using Pheonix liquid handling system in 96 wells plate format in INTELLI-PLATE® 96 (ArtRobbinsInstruments) for 6 screening kits for different RNA-protein complexes. Protein drops and mother liquor were screened at 1:1 ratio using 0.15 µl per well and monitored over 21 days using the Rock Imager 1000 (Formulatrix) Crystallisation screening was carried out using the sitting drop vapor diffusion method.

Once crystal hits were obtained, optimisation was carried out in 24 well plate formats in hanging drop vapour diffusion method. Similarly, 80 µM protein hsRC2 were incubated with RNAs at a molar ratio of 1:1.5 for 1 hour on ice. Protein-RNA complexes were mixed at a ratio of 1:1 in a reservoir containing 0.25 M sodium thiocyanate and 0.1 M MOPS pH 7.4 with different concentration of PEG3350 ranging from 20%-30% (w/v). The 14 day old crystals were harvested and flash frozen in liquid nitrogen.

Crystallisation plate was also set up using the hanging drop vapour diffusion method with Additive Screen HT ™ (Hampton Research). Plates were manually set up using 0.1 µL of the additives with 0.9 µL reservoir and 1 µl pre-incubated protein RNA complex.

**2.4 Data collection, Structure determination and refinement**

Diffraction intensities were recorded at PXIII at Swiss Light Source, Switzerland and TPS 05A at National Synchrotron Radiation Research Centre, Taiwan. Diffraction intensities were integrated using iMOSFLM, XDS or HKL 3000 (Battye et al, 2011; Kabsch, 2010a; Kabsch, 2010b; Powell et al, 2007). Scaling and merging of the intensities were done using SCALA or AIMLESS from CCP4 suite (Diederichs & Karplus, 1997; Evans, 2007; Evans, 2011). The qualities of the data sets are assessed by POINTLESS in CCP4 suite (Evans, 2011; Winn et al, 2011). Data collection and refinement statistics for the crystals are stated in the table 3.1. The solution for hsRC2 with 3p10LA9 was solved using PHASER MR (CCP4 suite) with hsRC2 with GC 10 RNA (PDB id: 5F98) as the search model (Luo et al, 2008; McCoy, 2007; McCoy et al, 2007).

**2.5 NADH coupled ATPase assay**

ATPase assay was carried out for the full length RIG-I protein. Assay was carried out in buffer containing 25 mM MOPs pH7.4, 150 mM KCl, 2 mM DTT and 0.01% Triton X-100 in the presence of 5X assay mix containing 1 mM NADH, 100 U/ml lactic dehydrogenase, 500 U/ml pyruvate kinase, 2.5 mM phosphoenol pyruvate. For $K_M$ of ATP, 20 nM protein of interest for RIG-I protein was used. Saturating amount of RNA

was added at the concentration of 1 µM and incubated with the protein for 2 hours prior to the initiation of the reaction. The reaction was initiated by the addition of 1 to 1 molar ratio of ATP and $MgCl_2$ diluted to 8 different concentrations ranging from 5 µM to 5000 µM and were monitored over 10 mins at Abs of 340 nm in a 96 well plate format using Cytation 3 Cell Imaging Multimode Reader at room temperature. All data were obtained in triplicates and plotted as the rate of NADH hydrolysis as a function of ATP concentration using Michaelis-Menten equation with GraphPad Prism® version 6 program (GraphPad Software, Inc.). Rates were obtained over the duration of 10 minutes with 1 minute interval and are corrected for background NADH decomposition. The initial velocity was determined based on the ATPase activity determine as described by Kiianitsa et al. (Kiianitsa et al, 2003). The path length for the reaction volume was calculated using Beer-Lambert law after measuring a known concentration of NADH in the same assay volume. Initial velocities were calculated using the following equation from Kiianitsa et al.

Initial velocity ($\mu M \times s^{-1}$) = $-\frac{dA340}{dt}$ ($OD \times s^{-1}$) $\times K^{-1}_{path}$

$K^{-1}_{path}$ = molar absorption coefficient for NADH at a given optical length

$k_{cat} = V_{max}/[E_t]$

**2.6 Cell culture and IFN-β induction assays**

HEK-Lucia™ RIG-I cells derived from HEK293 cell, and THP1-Dual™ derived from THP-1 cells are cell lines generated to express the secreted Lucia luciferase reporter gene. This reporter gene is under the control of an IFN-inducible ISG54 promoter enhanced

by a multimeric IFN-stimulated response element (ISRE). Cells were maintained in T-75 flask in Dulbecco's Modified Eagle Medium (DMEM, GIBCO) supplemented with 10% fetal bovine serum for HEK-Lucia™ RIG-I cells and HEK-Lucia™ null cells. THP1-Dual™ cells were maintained in RPMI (GIBCO), supplemented with 10% fetal bovine serum. IFN-β induction assay was carried out in 96 well plates with a seeding density of 50, 000 cells/well for HEK-Lucia™ RIG-I cells and HEK-Lucia™ null and 100,000 cells/well for THP1-Dual™. Cells were transfected with RNA of varying concentration from 300 nM to 6 nM with LyoVec (InvivoGen) based on the manufacturer's instruction. After 24 hours, 10 µL of the cell culture medium for HEK-Lucia™ RIG-I and HEK-Lucia™ null cells was collected and mixed with 50 µl of QUANTI-Luc™ (an assay reagent containing all the components required to quantitatively measure the activity of Lucia luciferase). For THP1-Dual™ cells, the culture medium was harvested after 48 hours. Luminescence was measured using a Biotek Synergy H1 plate reader (Biotek, Winooski, VT, United States). Time point experiment was also carried out using 100 nM RNA in 96 well plate format for up to 72 hours.

Cell based inhibition assay was carried out using HEK-Lucia™ RIG-I cells. HEK-Lucia™ RIG-I cells were plated at a seeding density of 50,000 cells/well and transfected with 10 nM of 3p10L with different concentration of antagonist 3p10LG5 ranging from 300 nM to 6 nM using LyoVec as per the manufacturer's recommendation. After 24 hours, 10 µL of the cell culture medium was collected and mixed with 50 µl of QUANTI-Luc™ and luminescence was measured using Biotek Synergy H1 plate. All the assays were carried out in Corning 96-well plates in triplicates. The half maximal inhibitory concentration ($IC_{50}$) of an inhibitor was

determined using GraphPad Prism version 6 (GraphPad Software, La Jolla California, USA).

**2.7 Hydrogen/Deuterium exchange (HDX) coupled with mass spectrometry (HDX-MS)**

**(HDX-MS experiment and data analysis was carried out by Dr Zheng Jie from Prof. Griffin's lab)**

The full length RIG-I protein was incubated with 10 fold excess of RNA ligands 3p10LG5, 3p10LG9 and 3p10LA9 at 4 °C for 1 hour. The protein RNA complex were diluted into 20 µl $D_2O$ on exchange buffer (50 mM HEPES, pH 7.4, 150 mM NaCl, 5 mM $MgCl_2$, 2 mM DTT) and incubated at 4°C and quenched by mixing with 25 µl of ice-cold 4 M guanidium hydrochloride with 1% trifluoroacetic acid. Samples were incubated in $D_2O$ on exchange buffer containing 3 M guanidium hydrochloride (50 mM HEPES, pH 7.4, 150 mM NaCl, 5mM $MgCl_2$, 2 mM DTT and 3 M gHCL) overnight at room temperature.

The samples were immediately placed on dry ice after the quenching reactions until the samples were injected into the HDX platform. Samples injected to the HDX platform were passed through an immobilised pepsin column (2mm × 2cm) at 200 µl $min^{-1}$ and the digested peptides were captured on a 2mm × 1cm C8 trap column (Agilent) and desalted. The peptides were then separated across a 2.1mm × 5cm C18 column (1.9 □m Hypersil Gold, ThermoFisher) with a linear gradient of 4% - 40% acetonitrile and 0.3% formic acid, over 5 mins at 4°C. Mass spectrometric

data were acquired using an Orbitrap mass spectrometer (Q Exactive, ThermoFisher) with a measured resolving power of 65,000 at m/z 400. HDX analyses were performed in triplicates, with single preparations of each protein-ligand complex. The intensity weighted mean m/z centroid value of each peptide envelope was calculated and subsequently converted into a percentage of deuterium incorporation. Corrections for back-exchange were made based on an estimated 70% deuterium recovery, and accounting for the known 80% deuterium content of the deuterium exchange buffer. When comparing the two samples, the perturbation %D is determined by calculating the differences between the two samples. HDX Workbench colours each peptide according to the smooth colour gradient. HDX perturbation key (%D) shown in each indicated figure. Differences in %D between -5% to 5% are considered non-significant and are coloured gray according to the HDX perturbation key (Pascal et al, 2012). In addition, unpaired t-tests were calculated to detect statistically significant ($p<0.05$) differences between samples at each time point. At least one time point with a p-value less than 0.05 was present for each peptide in the data set further confirming that the difference was significant.

Data Rendering: the HDX data from all overlapping peptides were consolidated to individual amino acid values using a residue averaging approach. Briefly, for each residue, the deuterium incorporation values and peptide lengths from all overlapping peptides were assembled. A weighted function was applied in with shorter peptides weighted more heavily, and longer peptides were weighted less. Each of the weighted deuterium incorporation values was then averaged to produce a single value for each amino acid. The initial two residues of each peptide, as well as

prolines, were omitted from the calculations. This approach is similar to that previously described (Keppel & Weis, 2015).

**2.8 VLP cloning into pETSUMO and pNIC28-BSA4 expression vector**

The genes for MS2 and Q beta coat protein were synthesised by GenScript and were cloned into pETSUMO and pNIC28-BSA4 vector. The primers with overhang for the vector backbone were designed and purchased from Integrated DNA technologies, Singapore (IDT.sg). The PCR reaction was set up using Phusion Flash High-Fidelity PCR MasterMix or KOD HotStart Mastermix. In a 25 µl reactions, 50 ng plasmid template was used with 1 µL of forward and reverse primers at 10 µM, and 12.5 µL of 2xMastermix. The PCR reaction was carried out by heating to 95°C for 5 minutes, followed by 20-30 times repeat of PCR amplification cycle. The cycle consists of 30 seconds of denaturation at 95°C, 30 seconds of annealing at (Tm primer – 5) °C and extension at 20 seconds 72°C. The final extension step was carried out for 10 minutes at 72°C. The PCR product was purified using the QIAquick PCR Purification Kit from Qiagen. The PCR Product then serves as a primer for the extension of the template backbone. Another round of PCR was carried out with longer extension time according to the backbone size. The template plasmids were then digested by adding 0.5 µL of *DpnI* enzyme (NewEngland biolabs) and incubated for overnight at 37°C. The reaction was transformed into transformation competent *Ecoli*. The transformants were recovered by the addition of 400 µL of LB and incubating at 37°C, 300 rpm for two hours. The transformants were plated on LB agar plate supplemented with Kanamycin (50mg/L) and incubated at 37°C overnight. The positive colonies were

picked the next day and subsequently grown in 4 mL of LB broth with Kanamycin (50mg/L). Plasmids were exacted the following day and insertion of genes was confirmed by sequencing.

**2.9 Expression and purification of VLP by ammonium sulphate precipitation and sucrose gradient centrifugation**

From the minimal RNA ligand required for MS2 and Q beta scaffold, we designed several RNA as hybrids of 3p10LG9 and 3p10L as a test for RNA for binding to MS2 and Q beta VLP. The RNA sequence for 3p10L and 3p10LG9 was hereafter named MS2-3p10L, MS2-3p10LG9 and Q beta-3p10L. The sequence of the *in vitro* transcription primer and the RNA is shown in Appendix 2. The VLP was expressed in *E. coli* BL21 (DE3) Novagen as previously mentioned. Cells were lysed with homogenizer (GEA Niro Soavi) at 900 bar for 5-10 minutes and clarified by centrifugation at 40,000 rpm for 40 minutes at 4°C. Subsequently, cells were precipitated with increasing concentration of ammonium sulphate at the concentration of range of 20 -70% with 10% increment. The fraction corresponding to the presence of the coat protein was analysed in SDS-PAGE. The fraction which consists mostly of MS2 were pooled, dialysed overnight in buffer containing 25 mM HEPES pH7.4 100 mM NaCl and 10% (v/v) glycerol. The partially purified fractions were pooled and overlay in sucrose gradient cushion ranging from 20% to 70% (w/v) sucrose and were centrifuged for 35,000 rpm for 18 hours in rotor SW41-Ti at 4°C. The fractions were collected from top to bottom at 500 µL volume each and the fractions were run on SDS-PAGE to

determine the presence of the virus-like particles. The fraction was then dialysed extensively in buffer containing 25 mM HEPES pH7.4 100 mM NaCl.

### 2.10 Purification of coat protein pET-SUMO Q beta

For pET-SUMO, Q beta protein, the presence of the 11kD small ubiquitin-related modifier (SUMO) fusion tag and hexa-histidine tag at N-terminal prevent the coat protein from forming the VLP particles and hence was purified according to the method mentioned in section 2.1. Purified protein remained as coat protein and was used for *in vitro* assembly with the RNA.

### 2.11 Particles under negative staining EM

During the final step of protein purification, namely gel filtration, glycerol and sucrose were omitted in order to avoid dialysis of the protein sample. The sample for negative stain EM was collected off the superdex 200 pg column from the very apex of the corresponding protein peak. In doing so, the protein was obtained at high concentration and purity. Afterwards, the protein was diluted to working conditions (usually 0.01 mg/mL) using the same buffer as for gel filtration.

Carbon coated EM grids with copper, 10-12 nm carbon layer, 400 square mesh were used. For negative stain EM grid preparation, grids were first glow discharged for 60 sec (PDC-32G, HARRICK). Afterwards, 4 µL of protein sample was applied on top of the carbon surface for 1 min at room temperature and subsequently blotted with torn up Whatman paper. Immediately after, 4 µL of aqueous 2% uranyl acetate solution was applied on the same grid for 1 min and blotted. The EM grid was then air dried for 10 min before it was stored away or used for data collection.

### 2.12 Cell based assay in THP1-Dual™ for ImmRNA with VLP motif

THP1-Dual™ cells were maintained in RPMI (GIBCO), supplemented with 10% fetal bovine serum. IFN-β induction assay was carried out in 96 well plates with a seeding density of 100,000 cells/well for THP1-Dual™. Cells were transfected with RNA with LyoVec according to the manufacturer's instruction.

### 2.13 *In vitro* assembly of MS2 particles and Q beta coat protein with ImmRNA

Purified virus-like particles were dialysed overnight in buffer containing 20 mM HEPES pH7 with 1 mg/mL RNase A for every 2 mg/mL purified VLP in dialysis tubing with 3 kD MWCO. The dialysis was carried out at room temperature overnight. The dialysed particles were subjected to analytical gel filtration run using column S200 10/300pg and the Abs 260 and Abs 280 was checked for the presence of nucleic acid in the VLP. MS2 was subsequently soaked with MS2-3p10L or MS2-3p10LG9 at the concentration of 250 nM of RNA/mg of VLP and incubated overnight at room temperature in 20 mM HEPES pH7.

Another method used to incorporate RNA into is to treat MS 2 VLP with denaturing buffer and reassemble. Briefly, VLPs at 5 mg/mL were incubated in disassembly buffer (20 mM Tris-HCl, 50 mM NaCl, 6 M urea, 10 mM dithiothreitol) at 4°C for 4 hours and dialysed against 10 mM acetic acid and 50 mM NaCl. The coat protein was dialysed in the buffer containing 50 mM NaCl, 20 mM Tris-HCl, pH 7.5 with a 20-fold molar excess of RNA. The protein RNA complex was concentrated with 3 kD MWCO concentrator and resolved in analytical gel filtration S200 10/300pg.

For Q beta coat protein, dimer coat protein devoid of any nucleic acid was obtained. The *in vitro* assembly of Q beta was carried out using 200 µM protein and 200 µM RNA in 50 mL volume in buffer containing HEPES pH 7 10 mM and 0.3% (v/v) hydrogen peroxide to promote disulfide linkages formation. The protein RNA complexes were concentrated with Vivaspin 20 with a MWCO of 3 kD. Protein RNA complex was resolved in gel filtration S200 10/300pg. The fraction obtained was incubated in the assembly buffer with the addition of 6 mM coat protein dimer and resolved in gel filtration S200 10/300pg before carrying out negative staining EM.

## Chapter 3: Design and functional characterisation of ImmRNAs

### 3. 1 Background and rationale

RIG-I like receptors (RLRs) are a class of pattern recognition receptors involved in intracellular RNA sensing of viral infection (Kato et al, 2011; Schlee, 2013; Yoneyama et al, 2004). RLRs consist of three members which include Retinoic Acid-Inducible Gene (RIG-I), Melanoma Differentiation Associated Gene 5 (MDA5) and Laboratory of Genetics and Physiology 2 (LGP2) (Loo et al, 2008; Yoneyama et al, 2005b). At the core of the RIG-I like protein is a DExD/H-box RNA helicase which consists of HEL1, HEL2 and an insertion domain (Luo et al, 2011; Rawling & Pyle, 2014). The C-terminal domain (CTD) is involved in detection pathogenic RNA, while the N-terminal domain of RIG-I and MDA5 consists of tandem caspase activation and recruitment domain (CARDs) (Hiscott et al, 2006; Lu et al, 2011). In the cytoplasm, RIG-I exists in the autorepressed conformation with CARDs domain interacting with the HEL2i domain (Kowalinski et al, 2011; Zheng et al, 2015). When it encounters and bind to pathogenic RNA, conformational rearrangement occurs and coupled with ATP hydrolysis, the CARDs will be exposed to allow interaction with its protein partner, MAVS (mitochondria antiviral signalling protein) (Jiang & Chen, 2012; Kawai et al, 2005; Kowalinski et al, 2011; Luo et al, 2011; Meylan et al, 2005; Seth et al, 2005; Xu et al, 2005). Subsequently, MAVS will activate the downstream signalling via IRF3, IRF7 and NFκB transcription factor to trigger the production of type I interferon and pro-inflammatory cytokines (Hiscott et al, 2006; Iwanaszko & Kimmel, 2015; Peisley et al, 2014; Ramos & Gale, 2011; Seth et al, 2005).

The CTD domain of RIG-I confers RNA selectivity by high affinity binding with blunt-ended double stranded RNA (Lu et al, 2011). This is followed by conformational changes in the domains to accommodate the RNA ligand and subsequently the co-operative binding and hydrolysis of ATP (Louber et al, 2015). Previous studies have shown that binding of ATP is crucial for activation of RIG-I (Louber et al, 2015; Rawling et al, 2015). Upon binding of ATP, the movement of HEL2i domain scanning the RNA strand causes the expulsion of CARDs (Kohlway et al, 2013). A model proposed by Louber et al. (2015) suggest that the anchoring of non-self RNA such as 5'pppdsRNA to the CTD promotes favourable position for the rapid repetition of RNA helicase association and dissociation from ATP hydrolysis and this cycle promotes sustained CARDs exposure for effective signalling (Louber et al, 2015). Whereas, in the case of endogenous RNA, ATP hydrolysis is proposed to evict RNA from helicase domain due to the lack of CTD anchoring (Louber et al, 2015).

RIG-I CTD recognises and is activated by 5' triphosphorylated RNA which are RNA commonly generated during viral replication processes (Hornung et al, 2006). RIG-I recognises many different classes of RNA including RNAs from positive and negative stranded RNA virus (Kato et al, 2011) , RNA fragments generated by RNA polymerase III (Ablasser et al, 2009; Chiu et al, 2009), the cleavage product from RNAseL (Malathi et al, 2007; Malathi et al, 2010), synthetic polyI:C and even lncRNA (Bird, 2018; Jiang et al, 2018). The simplest RNA form described to be able to trigger the activation of RIG-I is 5' triphosphorylated double stranded RNA with a blunt end (Schlee et al, 2009; Schmidt et al, 2009). In addition, RIG-I was also shown to be activated by other molecular signatures such as 5' diphosphate and cap 0 (Devarkar

et al, 2016; Goubau et al, 2014). Therefore, the basic requirement of RIG-I activation is simply the duplex RNA although it has been shown that certain molecular feature such as 5' hydroxyl and cap 1 were unable to activate RIG-I (Devarkar et al, 2016; Rawling et al, 2015). Recent studies revealed that RIG-I has a higher preference for poly U/UC tract and AU-rich RNA (Runge et al, 2014; Schnell et al, 2012).

Previous studies have revealed that RIG-I is able to bind to short RNA duplex and is activated by RNA with the minimal length of 10 bp with RIG-I capable of forming multimer on longer duplexes (Kohlway et al, 2013; Patel et al, 2013; Peisley et al, 2014; Peisley et al, 2013). Firstly, we would like to validate the minimal length of RNA required for RIG-I activation is the 10 bp dsRNA. To this end, we designed a set of duplex hairpin immune-modulatory RNA (ImmRNA) with different length. We confirm from ATPase assay that the 3p10L was the most potent RIG-I activator. Next, we would like to enhance the activity of 3p10L and to accomplish that, we introduced guanosine insertions along the stem of the RNA with minimal length of 10 bp (3p10L). Using biochemical and cell-based approach, we tested a set of RNAs with kinks along the stem. We identified immRNA 3p10LG5 inhibits RIG-I activation and 3p10LG9 RNA triggers a more robust IFN production than the perfectly base-paired RNA. Further characterisation revealed that the guanosine residue in RNA 3p10LG9 could be replaced by adenosine to trigger comparable type I interferon responses. HDX-MS studies revealed that the tight binding of Helicase and CTD domains to 3p10LG9 is responsible for the higher type I interferon expression in the cell based assay.

### 3.2 Protein expression and purification

For RIG-I, two different constructs were expressed and purified. The two different constructs are the pET-SUMO with human full length RIG-I (hsRF) shown in (Figure 3.1A) and pET-SUMO human RIG-I without CARDs domain (hsRC2) shown in (Figure 3.1A) within the dotted line. Both proteins were recombinantly expressed in *E. coli* and the recombinant proteins are not post-translationally modified. The purity of both proteins was verified by SDS-PAGE. Monomeric peaks corresponding to the expected molecular weight of 78kD for hsRC2 (Figure 3.1B) and 107kD for hs RIG-I (Figure 3.1C) was observed for both proteins. The proteins were used for further characterisations and assays.

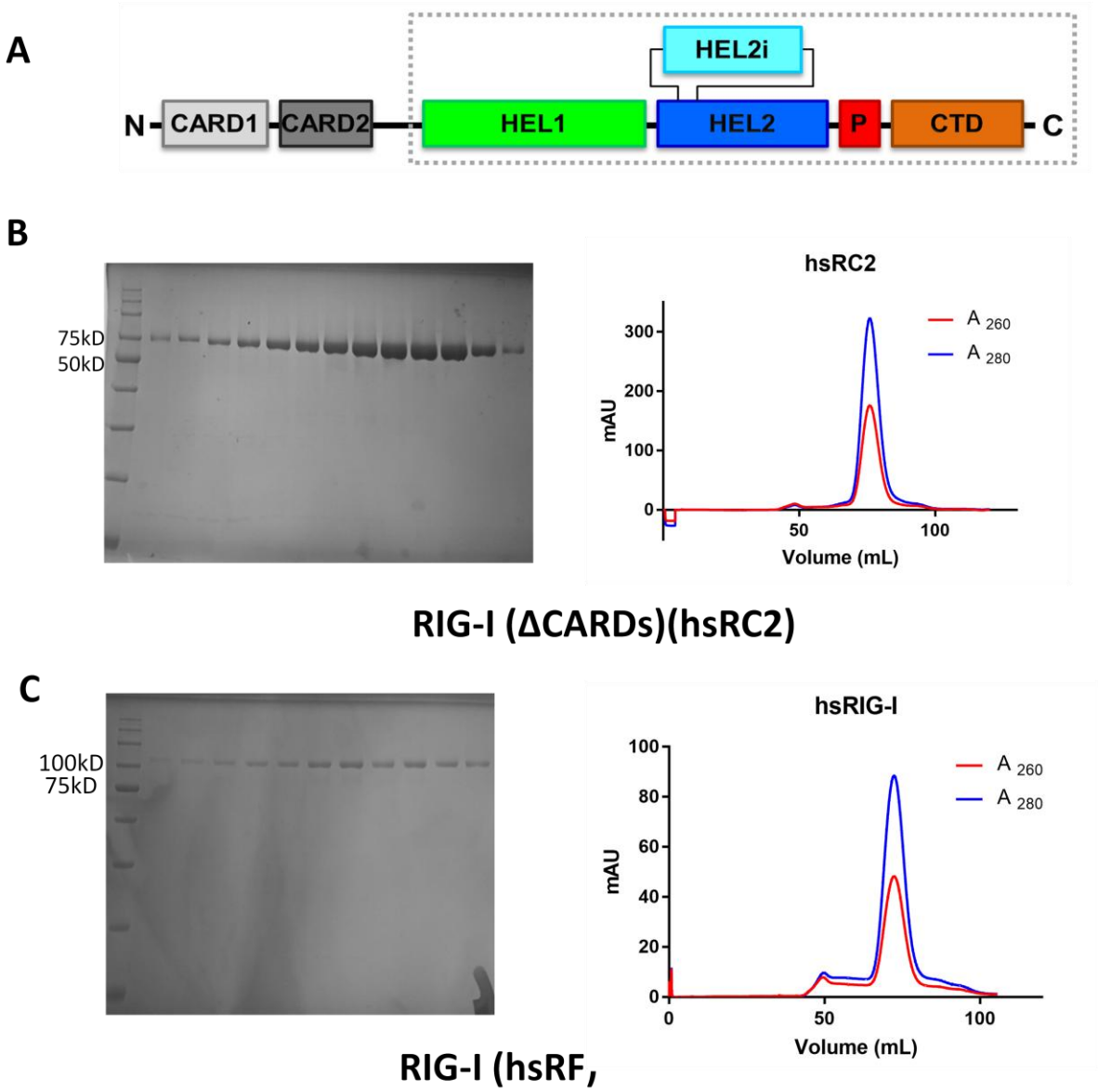


**Figure3.1.** Construct design and purification of the human RIG-I protein. (A) Schematic diagram of human RIG-I protein full length (hsRF) and human RIG-I protein without CARDS (highlighted in dotted-line box) The CARDs domain are in Grey, HEL1 domain in green, HEL2 domain in dark blue, HEL2i domain in cyan, Pincer in red and C-terminal domain in orange (B) The SDS-PAGE profile for purified hsRC2 corresponding to the size of 78kD and chromatogram indicating a symmetrical monomeric peak (C) The SDS-PAGE profile for purified hsRF corresponding to the size of 107kD and chromatogram indicating a symmetrical peak.

### 3.3 Design and *in vitro* transcription of ImmRNA

Several RNAs were generated based on the previously available structural model of hsRIG-I with RNA. For this study, we generated 6 RNAs with guanosine bulges along the stem and name them 3p10LG5, 3p10LG7, 3p10LG9, 3p10LG17, 3p10LG19 and 3p10LG21 and compare the relative activity of these RNAs with the 3p10L (5' triphosphorylated RNA with 10 base-paired stem region). The other modified RNAs with different nucleotide insertions in the stem at the position 9 are also shown in (Figure 3.2A) Transcribed RNA was checked for purity in 20% denaturing PAGE and were stained with Stains-All dye (Figure 3.2B).

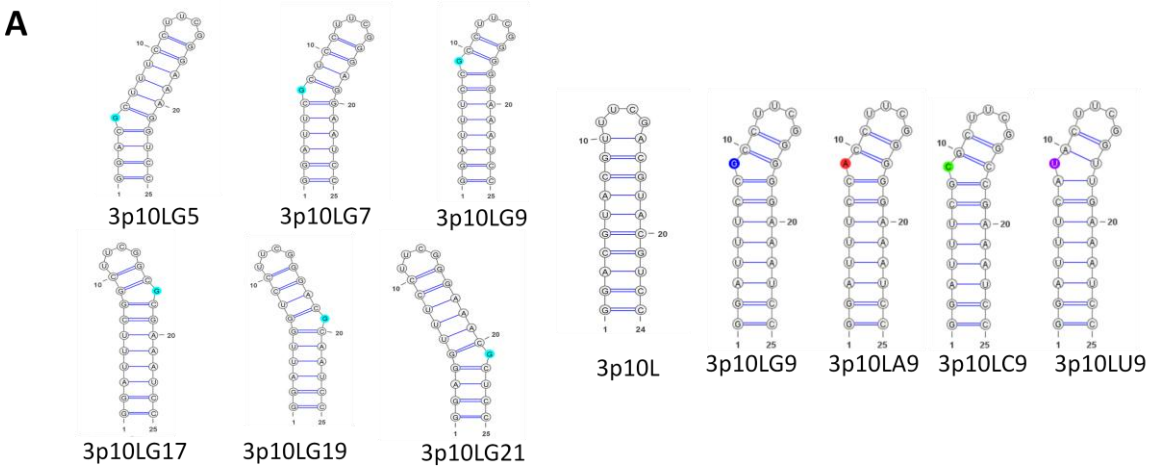


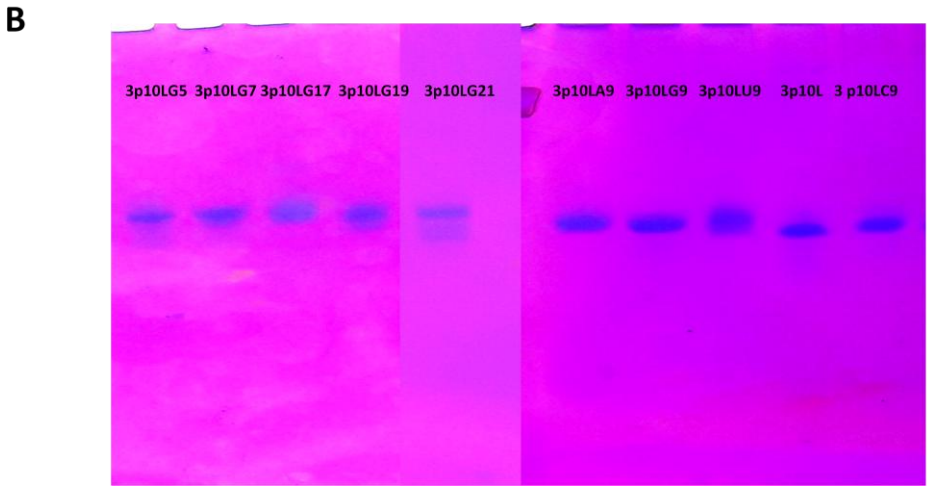

**Figure 3.2** ImmRNA constructs used (A) Schematic representation of RNA and its fold with guanosine bulge along the stem region of RNA and also different nucleotide insertion at the position 9 of the stem RNA (B) 20% denaturing PAGE (7 M Urea) for purified immRNA.

### 3.4 RNA minimal length for RIG-I activation

To more precisely determine the minimal length for RIG-I enzymatic activation, we measured the ATPase activity when stimulated by hairpin RNA with the size ranging from 6 to 20 base pairs. We measure the Michaelis constant for the RNAs and the catalytic constant with saturating amount of ATP. Table below showed the 3p10L showed the highest catalytic constant of 5.9 $s^{-1}$ (Figure 3.3B). The RNA longer than 3p10L however did not display such a high ATPase signalling activation with the $K_{cat}$ value of 3p11L 3p12L, 3p14L and 3p20L showing 4.5 $s^{-1}$, 3.6 $s^{-1}$, 3.4 $s^{-1}$ and 3.2 $s^{-1}$ respectively (Figure 3.3B). The cell based assay however, did not display a similar trend to the ATPase activity, with 3p14L and 3p20L stimulating the highest Interferon activation. The difference between 3p9L, 3p10L, 3p12L, 3p14L and 3p20L however, were not significant when the one-way ANOVA/ Tukey's comparison test between the different RNAs was carried out. Although it is not immediately clear why the 3p11L RNA showed a lower activity than other activating RNA, it could be due to issues with transfection or stem sequence preference of the RNA involved. This has to be further validated by confirming the cell based assay another newly transcribed 3p11L of different sequence. However, the range of type I interferon stimulation by different RNAs were comparable (Figure 3.3A). Considering the trend of the ATPase hydrolysis activity, 3p10L would be the minimal length required to stimulate a more robust RIG-I ATPase activity. However, from the cell based assay, the 3p9L could

potentially be the minimal ligand required type I interferon stimulation. In the subsequent sections and based on structural model of 3p10L, several derivatives of 3p10L were further characterised.

A

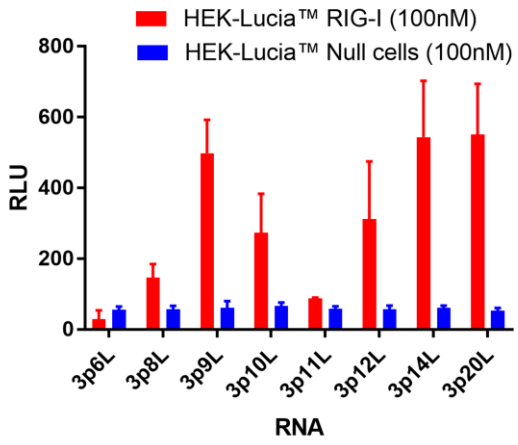


B

| RNA | Kcat($s^{-1}$) | Km (μM) | Kcat/Km ($s^{-1}$ $mM^{-1}$) |
|---|---|---|---|
| 3p6L | 0 | - | |
| 3p8L | 1.1±0.1 | 83.9±33 | 12.9±2.7 |
| 3p9L | 1.8±0.1 | 114.6±28.0 | 15.74±3.5 |
| 3p10L | 5.9±0.4 | 237.3±62.2 | 24.9±6.4 |
| 3p11L | 4.5±0.3 | 233.8±69.8 | 19.1±4.9 |
| 3p12L | 3.6±0.2 | 151.9±34.5 | 23.9±5.6 |
| 3p14L | 3.4±0.2 | 196.1±47.6 | 17.7±4.4 |
| 3p20L | 3.2±0.2 | 251.5±38.2 | 12.9±3.3 |

C

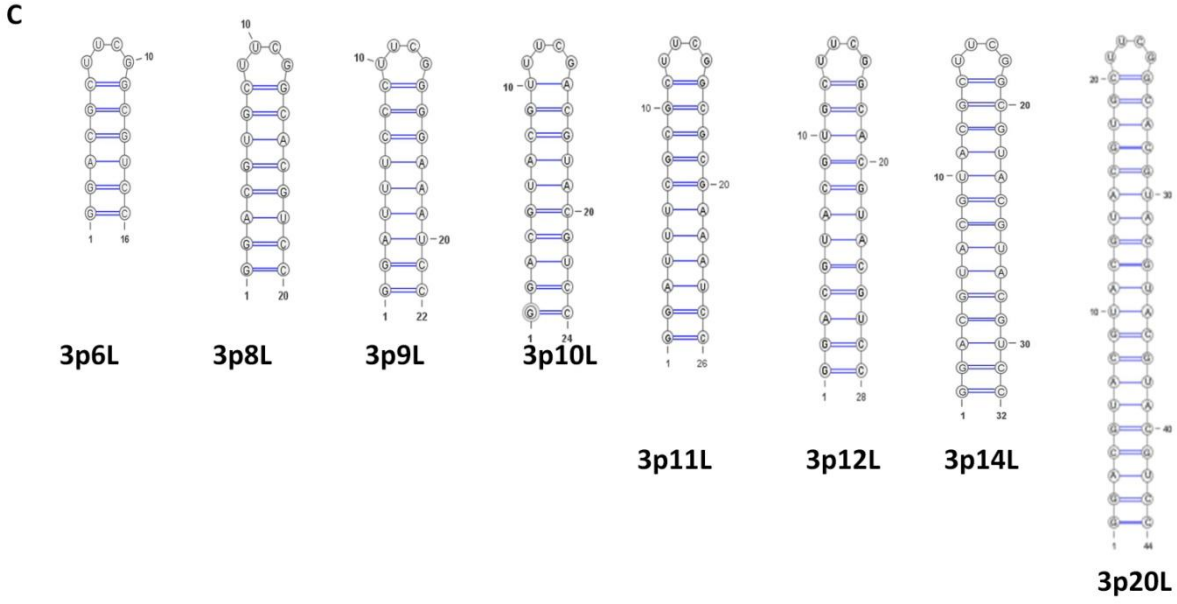


**Figure 3.3 Length of RNA effect the type I interferon activation and ATPase activity of RIG-I**

A) Cell based assay of different RNA in HEK-Lucia™ RIG-I and HEK-Lucia™ null. RNA of different length was transfected at a fix concentration of 100nM and luminescence was measured 24 hours post-transfection. Results are measured in triplicate and presented as

RLU. B) $K_{cat}$, $K_M$ and $K_{cat}/K_M$ of the RNA stimulating RIG-I ATPase activity C) Sequence of RNA with different stem length.

### 3.5 HEL2i domain samples the RNA PAMP for RIG-I activation

To infer the structural basis of RNA sensing by RIG-I protein, we compared the five available structures of human RIG-I HEL-CTD dsRNA complex structures (Figure 3.4A). By superpositioning the invariant HEL1-dsRNA-CTD domains, we found HEL2-HEL2i domains moved relatively along the dsRNA backbone. HEL2i plays the central role in releasing the CARDs domain upon binding to the RNA PAMP. This is mediated by the two opposing functional surfaces: one RNA sampling surface with conserved RNA recognising residues (K508-Q511 in human RIG-I) and one surface to interact with and sequester CARD2 domain from releasing (Luo, 2014; Zheng et al, 2015). Across the five structures, HEL2i samples approximately 5 base pairs (base pair 5-10, counting from the 5' end triphosphorylated nucleotide of the top strand) (Figure 3.4B). We speculate that any structural perturbation at this region will affect the intramolecular movement of the HEL-CTD domains relative to each other and alter the kinetics of CARDs release, i.e. the threshold of activation. To test this hypothesis, we introduce RNA nucleotide insertions and point mutations to the starting immRNA - 3p10L(5' triphosphorylated RNA with 10 base-paired stem region) (Kohlway et al, 2013) and evaluate them using both biochemical and cell based-assays.

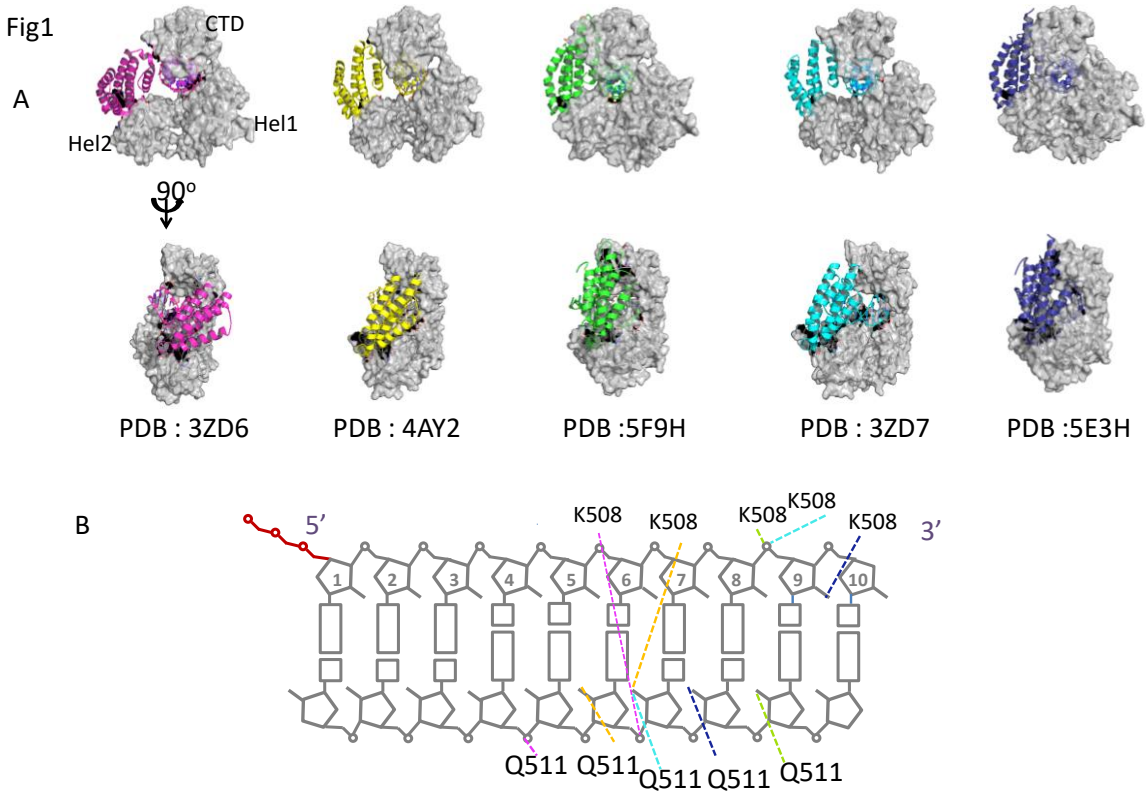


**Figure 3.4. The movement of HEL2i domain along the RNA strand**. A) Comparison of 5 different protein RNA complex of hsRC2. The HEL2i domain are highlighted in different colours for with different RNAs, hairpin with 8 base paired (yellow, PDB id: 4AY2), double stranded 10 base paired (magenta, PDB id: 3ZD6), double stranded 10 base paired with ADP (cyan, PDB id: 3ZD7), hairpin with 10 base paired (green, PDB id: 5F9H) and double stranded 12 base paired with ADP-BeF (dark blue, PDB id: 5E3H). B) Comparison of HEL2i domain and RNA interaction between the RNAs of different lengths. The residues K508 and Q511 from HEL2i domain were seen interacting with different residues of along the RNA strands.

### 3.6 3p10LG9 is a potent inducer of RIG-I activation and 3p10LG5 abolishes the activity of RIG-1

For this study, we generated 6 RNAs with guanosine bulges along the stem and named them 3p10LG5, 3p10LG7, 3p10LG9, 3p10LG17, 3p10LG19 and 3p10LG21 and compared the relative activity of these RNAs with the 3p10L (5' triphosphorylated RNA with 10 base-paired stem region) (Figure 3.5A). These RNAs were tested in cell-based assay using HEK-Lucia$^{TM}$ RIG-I and HEK-Lucia$^{TM}$ null to determine if the modification in the stem region could result in a higher IFN-β activity. One of the RNAs with an insertion of guanosine at position 9 of the stem in hairpin RNA was a potent inducer of RIG-I activation with at least 3 fold higher IFN-β compared to the parental strand of RNA (Figure 3.5B). The insertion of G at position 7 and 17 yielded similar expression as compared to the parental RNA (3p10L). The ATPase assay carried out using 20 nM of hsRIG-I protein with the saturating amount of RNA (1μM) also revealed a $K_{cat}$ of 9.01 $s^{-1}$ and 11.7 $s^{-1}$ for 3p10L and 3p10LG9 respectively (Figure 3.5C). Whereas, in the case of 3p10LG5, the cell based assay using in HEK-Lucia$^{TM}$ RIG-I was undetectable compared to those carried out in HEK-Lucia$^{TM}$ null. Similarly, ATPase assay carried out using hsRIG-I with saturating concentration of 3p10LG5 revealed no detectable ATP hydrolysis activity. Analytical gel filtration carried out with the purified protein of hsRC2 and 3p10LG5 revealed that the RNA forms complex and co-elutes as a complex indicating that 3p10LG5 binds but does not activate hsRIG-I (Figure 3.6A and 3.6B). Taken together, the insertion of guanosine along different positions of the RNA stem affects the robustness of IFN-β activity as well as the ATPase activity on hsRIG-I.

Fig 2

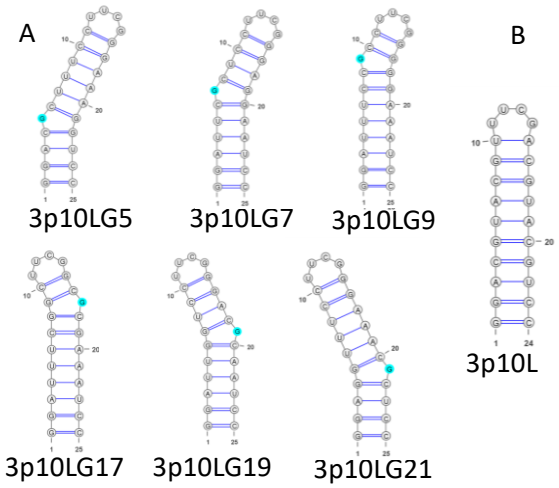





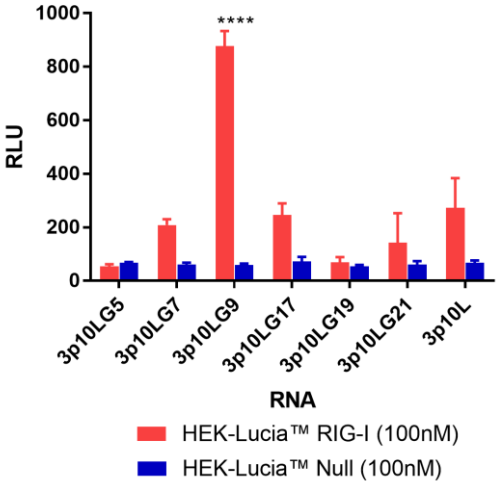


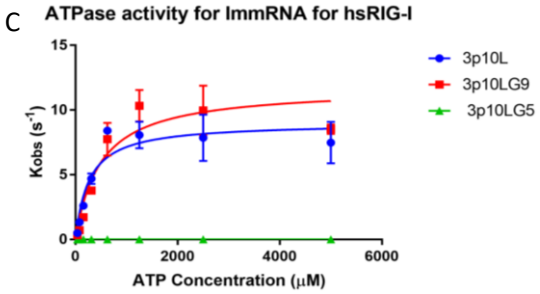


| RNA | Kcat($s^{-1}$) | Km (μM) | Kcat/Km ($s^{-1}$ $mM^{-1}$) |
|---|---|---|---|
| 3p10L | 9.0±0.6 | 261.8±67.1 | 34.4±8.9 |
| 3p10LG9 | 11.7±1 | 484±129.5 | 25.3±7.8 |
| 3p10LG5 | - | - | - |

**Figure 3.5. Insertion of guanosine along the RNA at different positions of hairpin RNA**. A) The design of hairpin RNA introducing bulges along the stem region of RNA. B) Cell based assay of different RNA in HEK-Lucia™ RIG-I and HEK-Lucia™ null. RNA was transfected at a fix concentration of 100nM and luminescence was measured 24 hours post-transfection. Results are measured in triplicate and presented as RLU. Asterisks indicate the significant differences based on one-way ANOVA/ Tukey's comparison test between the different RNAs (****= P ≤ 0.0001). The significance refers to the 3p10LG9 in comparison to 3p10L reference C) The ATPase activity of RNA with the highest cell based assay activity (3p10LG9) and lowest activity (3p10LG5) in comparison to the parental strand of RNA (3p10L). The data were fitted to the Michaelis-Menten equation and the $K_{m,ATP}$ and $K_{cat,ATP}$ was determined with saturating amount of RNA to hsRIG-I .

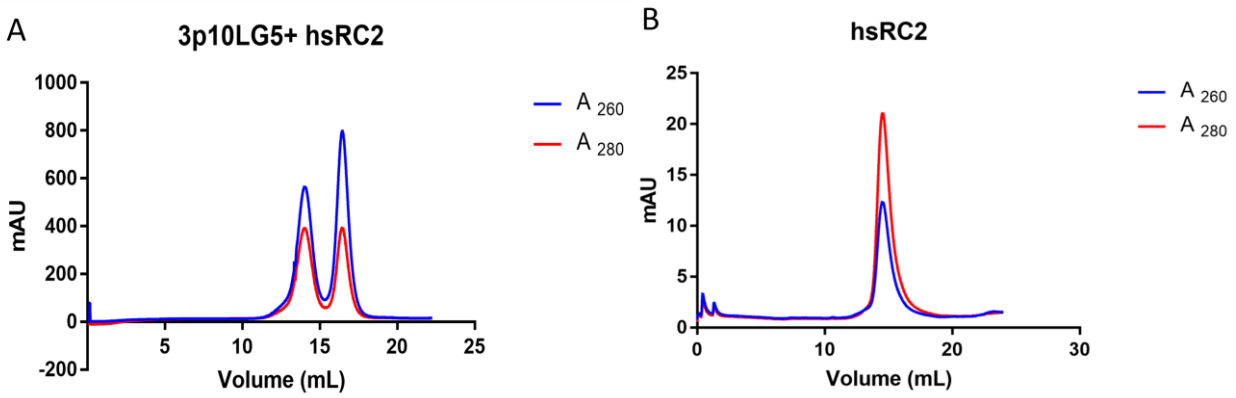


**Figure 3.6 : 3p10LG5 binds to hsRC2**. A) Purified protein was complexed with RNA at the molar ratio of 1:1.5 and injected onto a Superdex 200 10/300 column and eluted as a two symmetrical peak with the first peak representing the protein RNA complex and the second peak representing the excess RNA B) control hsRC2 alone elution peak

### 3.7 Insertion of different bases at the position 9 of hairpin RNA result in different levels of activation

Next, we tested the effect of substituting different bases at the position 9 of the hairpin RNA on the activity of RIG-I (Figure 3.7A). The sequence of the RNA along the stem were not conserved to obtain only a single possible folding with different nucleotide bulges introduced to the stem of the RNA. The guanosine residue of the RNA was substituted with adenosine, cytosine and uracil. The RNA activity tested in HEK-Lucia$^{TM}$ RIG-I and HEK-Lucia$^{TM}$ null revealed that the insertion of guanosine and adenosine at position 9 have similar IFN-β activation activity whereas the presence of uracil or cytosine at position 9 stimulate and approximately 2 fold lower activity (Figure 3.7B). The ATPase assay carried out using 20 nM of hsRIG-I protein with the saturating amount of RNA (1 μM) also revealed lower $K_{cat}$ for RNA with uracil or cytosine at position 9 with 7.29 $s^{-1}$ and 8.29 $s^{-1}$ respectively (Figure 3.7C). This result revealed the preference of purine at the bulge at position 9 in enhancing the overall stimulation of RIG-I activity.

Fig. 3

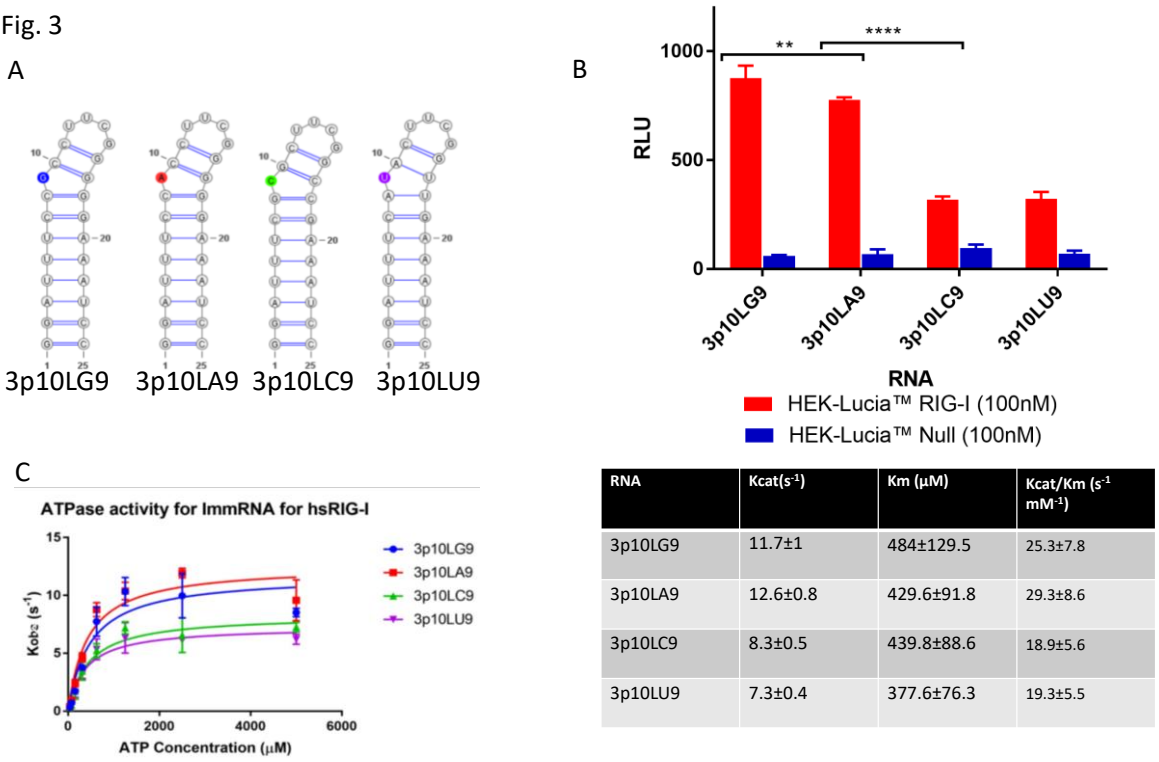


| RNA | Kcat($s^{-1}$) | Km (μM) | Kcat/Km ($s^{-1}$ $mM^{-1}$) |
|---|---|---|---|
| 3p10LG9 | 11.7±1 | 484±129.5 | 25.3±7.8 |
| 3p10LA9 | 12.6±0.8 | 429.6±91.8 | 29.3±8.6 |
| 3p10LC9 | 8.3±0.5 | 439.8±88.6 | 18.9±5.6 |
| 3p10LU9 | 7.3±0.4 | 377.6±76.3 | 19.3±5.5 |

**Figure 3.7 Insertion of different bases at position 9 along the hairpin RNA**. A) The design of hairpin RNA introducing different bases along the stem region at position 9 of RNA. B) Cell based assay of different RNA in HEK-Lucia™ RIG-I and HEK-Lucia™ null. RNA was transfected at a fix concentration of 100nM and luminescence was measured 24 hours post-transfection. Results are measured as triplicate and presented as RLU. Asterisks indicate the significant difference based on one-way ANOVA/ Tukey's comparison test between the different RNAs (** = $P \leq 0.01$) and (****= $P \leq 0.0001$) C) The ATPase activity of RNAs with different base insertion at position 9. The data were fitted to the Michaelis-Menten equation and the $K_{M,ATP}$ and $K_{cat,ATP}$ was determined with saturating amount of RNA to hsRIG-I.

### 3.8 Cell based assay comparing 3p10LG9, 3p10LA9 and 3p10L

The cell based assay was carried out using two different cell lines HEK-Lucia™ RIG-I and THP1-Dual™. HEK-Lucia™ RIG-I is a non immune cells derived from HEK 293T cells with a stable high level expression of human RIG-I. The $EC_{50}$ for 3p10LG9 is 133nM, 3p10LA9 is 199nM, 3p10L is 108nM (Figure 3.8A). The $EC_{50}$ value were comparable between the 3 RNA in the cells of HEK-Lucia™ RIG-I. The expression level for the 3 different RNA was first detected at 24 hours and the level increased at 48 hours and 72 hours post-transfection. The level of IFN-β activation was significantly different between 3p10LG9 and 3p10LA9 (*= $P \leq 0.05$) at 72 hours post-transfection (Figure 3.8B). In THP1-Dual™ cells, the $EC_{50}$ for 3p10LG9 is 91nM, 3p10LA9 is 51nM, 3p10L is 226nM (Figure 3.8C). The $EC_{50}$ for 3p10LG9 were almost two fold lower and the 3p10LA9 was approximately 4 fold lower than 3p10L indicating that 3p10LG9 and 3p10LA9 required a lower effective concentration to trigger type 1 interferon activation. The level of IFN-β activation was significantly different between 3p10L and 3p10LA9 (**=$P \leq 0.01$). The level of IFN-β activation of 3p10L was much lower than 3p10LA9 in THP1-Dual™ cells at 72 hours post-transfection (Figure 3.8D).

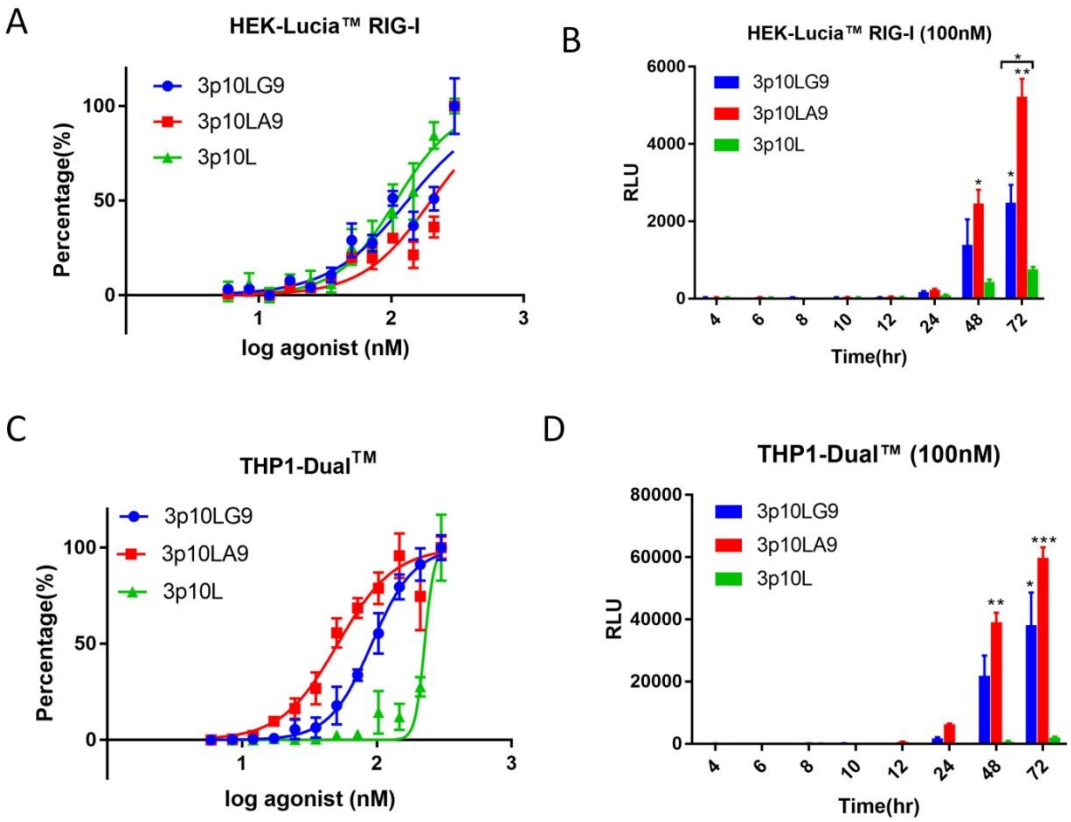


**Figure 3.8 Cell based assay for the 3p10LG9, 3p10LA9 and 3p10L in THP1-Dual™ and HEK-Lucia™ RIG-I.** A) RNA was transfected in HEK-Lucia™ RIG-I at a different concentration range of the RNA and luminescence was measured 24 hours post-transfection. Results were measured in triplicate and presented as normalised percentage vs log concentration.The $EC_{50}$ for 3p10L G9 is 133nM, 3p10LA9 is 199nM, 3p10L is 108 nM, B) RNA was transfected at a fix concentration of 100nM in HEK-Lucia™ RIG-I and luminescence was measured 4, 6, 8, 10, 12, 24, 48 and 72 hours post-transfection. Asterisks indicate the significant difference based on two-way ANOVA/ Tukey's comparison test between the different RNAs (*=P ≤ 0.05) and (**=P ≤ 0.01) C) RNA was transfected in THP1-Dual™ at a different concentration range of RNA and luminescence was measured 48 hours post-transfection. Results are measured in triplicate and presented as percentage vs log concentration. .The $EC_{50}$ for 3p10L G9 is 91 nM, 3p10LA9 is 51 nM, 3p10L is 226 nM D) RNA was transfected at a fix concentration of 100nM in THP1-Dual™ and luminescence was measured 4, 6, 8, 10, 12, 24, 48 and 72 hours post-transfection. Asterisks indicate the significant difference based on two-way ANOVA/ Tukey's comparison test between the different RNAs.

### 3.9 HDX-MS captured stronger allosteric effects upon 3p10LG9 binding to RIG-I than 3p10L. (Carried out in collaboration with Griffin lab)

HDX-MS is a sensitive and robust method to study protein dynamics upon ligand binding (Zheng et al, 2017; Zheng et al, 2015). We successfully captured the intra-molecular interactions between HEL2i and CARDs and the allosteric release of CARDs during RNA recognition by RIG-I (Zheng et al, 2015). Briefly, the protein-RNA complexes were exposed to deuterated water were denatured into peptides were subjected to LC-MS (Zheng et al, 2015). The HDX data were consolidated and mapped to the structure model using a residue averaging approach using HDX Workbench (Keppel & Weis, 2015; Pascal et al, 2012; Zheng et al, 2015).

To provide a mechanistic explanation for the increased enzymatic and cellular activities of 3p10LG9 over 3p10L, we used the method - hydrogen/deuterium exchange coupled to mass spectrometry (HDX-MS) to analyse the structural dynamics of hsRIG-I upon binding to 3p10LG9 and 3p10L (Fig. 3.9B). The HDX profiles revealed CARDs domain and in particular, the CARD2 latch peptide (Y103-114) exhibited higher deuterium incorporations for 3p10LG9 with hsRIG-I as compared to 3p10L (Figure 3.9C). Several key differences, also include a tighter binding of 3p10LG9 with hsRIG-I in HEL1 domain particularly, the motif Ia (F296-310), and Ic (I343-366) which are known to interact with RNA as compared to RNA 3p10L with hsRIG-I. Another interesting observation is the binding of CTD capping loop (F842-856) and CTD binding region (V893-904) to 3p10LG9 is also tighter as compared to the 3p10L. The modelled 3p10LG9 were shown to interact with the back surface of the HEL2i domain

and restrict the HEL2i movement and increase the HEL2i to a more extended conformation required to expel CARDs domain (Figure 3.9D).

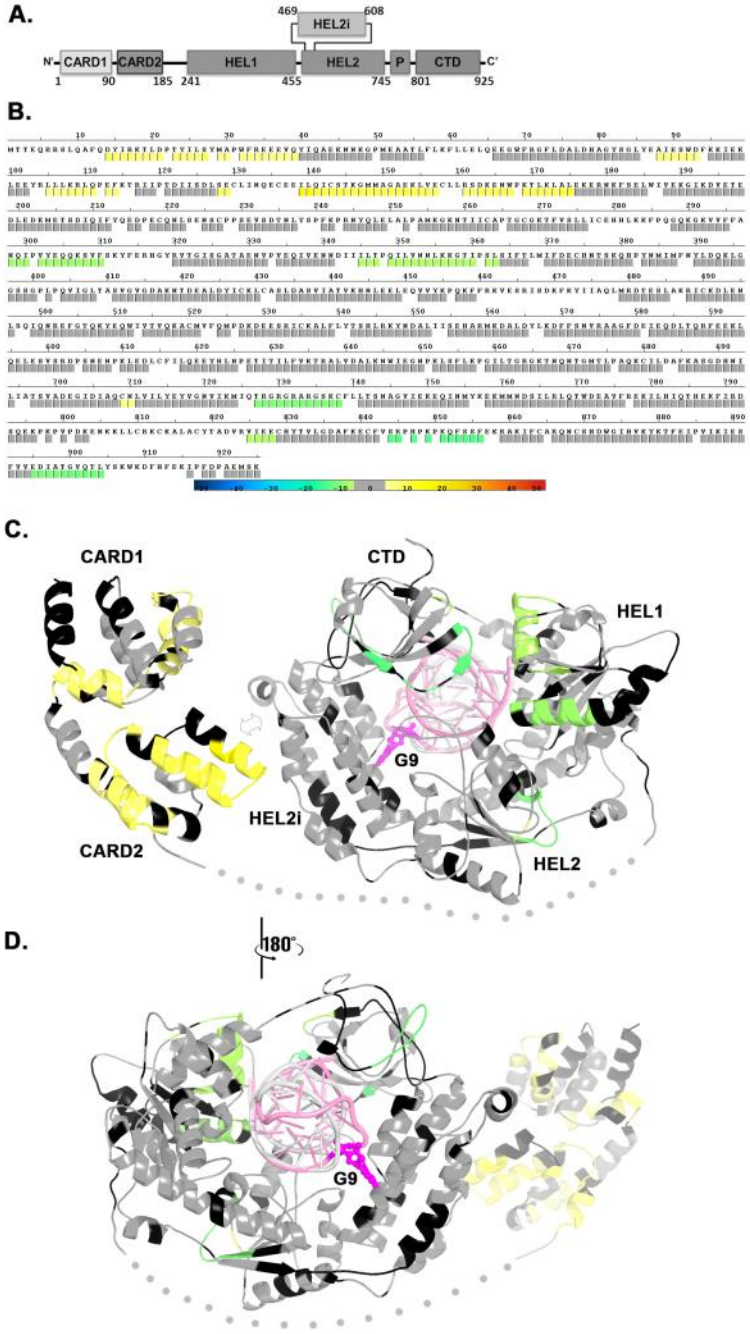


**Figure 3.9 HDX-MS difference map for 3p10LG9 vs 3p10L** A) The overall domain architecture of the human RIG-I. B) The overall difference map for hsRIG-I binding to 3p10LG9 vs 3p10L C) Regions that undergo higher hydrogen deuterium exchange are shown here in yellow (CARDs domain) and region that are more protected from hydrogen deuterium exchange are shown here in green (mainly the CTD and the HEL1 domain) D) The modelled RNA with the

guanosine 9 insertion revealed that the kinked guanosine interacts with the back surface of HEL2i. This RNA was modelled using RNA composer software and superposed with structure of hsRC2 (Biesiada et al, 2016a; Biesiada et al, 2016b).Therefore, G9 insertion restricted HEL2i movement and provided additional repellent force to release CARDs from HEL-CTD:3p10LG9 complex.

### 3.10 Crystallisation of hsRC2 with 3p10LA9 and 3p10LG9

The screening of hsRC2 in complex with 3p10LG9 and 3p10LA9 yielded crystals that grew into needle clusters within 3 days and were harvested within two weeks (Figure 3.10A and 3.10B). For hsRC2 and 3p10LG9 and 3p10LA9, the screening kits used includes PEG/Ion screen, Crystal Screen HT, Index Screen, PegRx from Hampton Research and Midas ™ from Molecular Dimension. A hit obtained from the PEG/Ion Screen with 0.2M Sodium thiocyanate and 20% PEG3350 pH 6.9. Crystals were optimized via grid expansion pH range and PEG concentration in a hanging drop vapour diffusion method and needle like crystal grew in condition of 25-30% PEG3350, 0.25 mM sodium thiocyanate and 0.1 M MOPS pH 7.4.

Further dehydration steps were carried out in 35% PEG3350, 0.25 mM sodium thiocyanate and 0.1 M MOPS pH 7.4 for 4 hours to improve the diffraction quality of the crystal. Individual needles were harvested and flash frozen in liquid nitrogen.

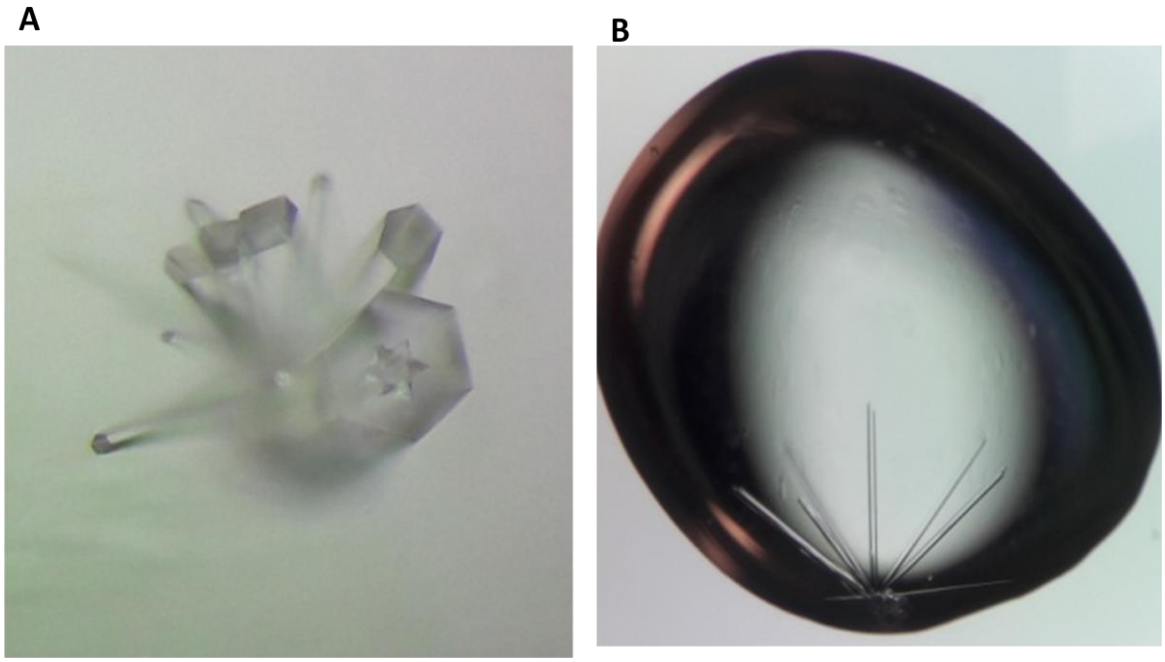


**Figure 3.10 12 day old crystal for hsRC2 and ImmRNA** .Crystals grown at 20°C hanging drop vapour diffusion with mother liquor containing 25-30% PEG3350, 0.25 mM sodium thiocyanate and 0.1 M MOPS pH 7.4 A) hsRC2 with 3p10LA9 and B) hsRC2 with 3p10G9.

The optimised crystals were harvested and tested in Swiss Light Source using the PX III beamline. The crystal diffracted to a low resolution of ~6-7 Å (Figure 3.11 A and 3.11B). To improve the resolution of the crystal, the crystals were grown in the same condition with the addition of additives from Additive Screen HT ™ (Hampton Research). Similarly, the crystals grew in needle-like morphology. Under several conditions such as the presence of 0.01 M EDTA, 4% v/v 1-Propanol, 3% v/v (+/-)-2-Methyl-2,4-pentanediol or 0.0 1 M Barium chloride dehydrate, the crystals grew bigger. Both hsRC2 with 3p10LA9 and 3p10LG9 were optimised in the condition with Additive Screen HT ™ (Hampton Research). These crystals were tested at TPS 05A at National Synchrotron Radiation Research Centre, Taiwan (Figure 3.12A-D). However, the resolution of the collected crystals remains low at 8-9 Å. The highest resolution data was obtained from hsRC2 with 3p10LA9 from SLS that with approximately 6Å resolution was determined by molecular replacement to the structure (PDB id: 5F98).

Although the structure was solved at a low resolution, the electron density map covers most part of the protein and RNA. In addition, there is a clear solvent shell around the RIG-I domains confirming the solution of the structure is correct (Figure 3.13). The data collection and refinement statistics table is shown in table 3.1

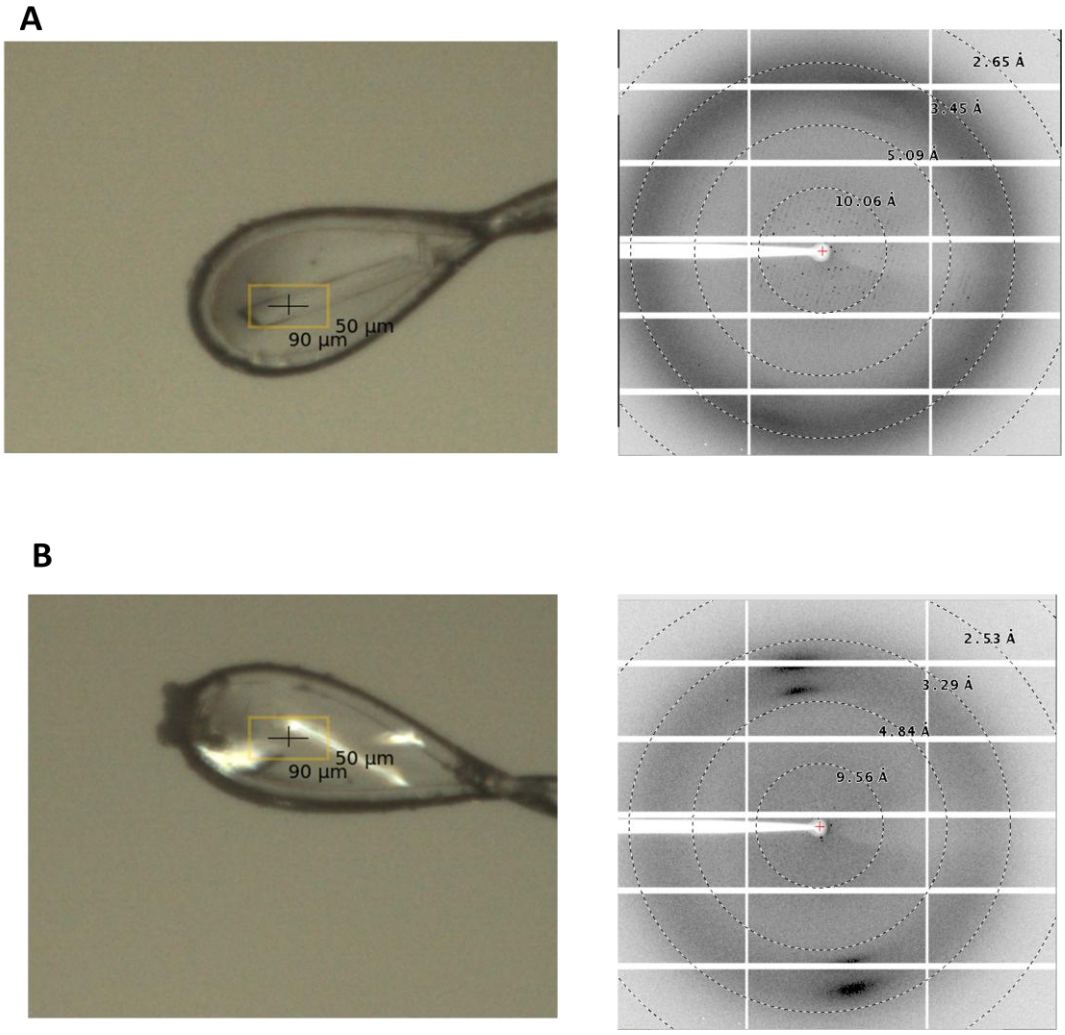


**Figure 3.11 Diffraction for crystal collected in Swiss Light Source** A) Crystal of hsRC2 and 3p10LA9 diffracted to 7Å and B) Very low resolution spot for the crystal of hsRC2 and 3p10LG9.

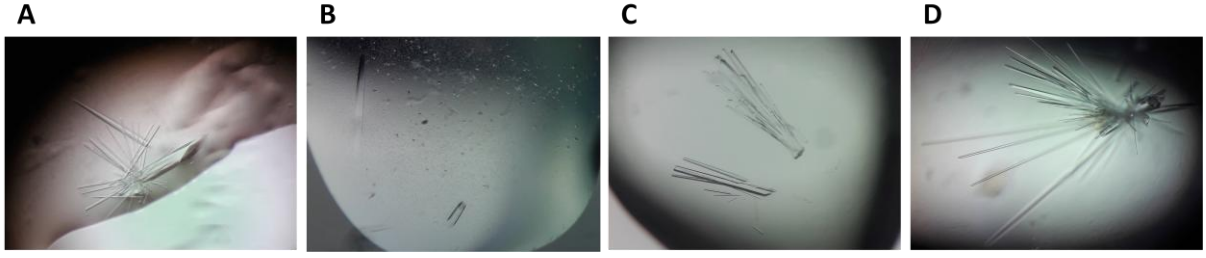

**Figure 3.12. The optimised crystal with Additive Screen HT ™.** Crystals grown at 20°C hanging drop vapour diffusion with mother liquor containing 35% PEG3350, 0.25 mM sodium thiocyanate and 0.1 M MOPS pH 7.4 A) with the addition of 0.01 M Barium chloride dehydrate B) with the addition of 3% v/v (+/-)-2-Methyl-2,4-pentanediol C) with the addition of 0.01 M EDTA D) with the addition 4% v/v 1-Propanol.

**Table 3.1 Data collection and refinement statistics for crystal structures of hsRC2 with 3p10LA9**

| **Data Collection Statistics** | **hsRC2+3p10LA9** |
|---|---|
| Wavelength (Å) | 1.00 |
| Resolution range (Å) | 46.99 – 6.00 (6.21-6.00) |
| Space group | $P6_5$ 2 2 |
| Unit cell a, b, c,<br>α, β, γ (Å) (°) | 177.29, 177.29, 110.84<br>90, 90, 120 |
| Total number of reflections | 95695 |
| Unique reflections | 5271 |
| Multiplicity | 18.20 |
| Completeness (%) | 99.13 (99.40) |
| I/σI | 6.10 (0.70) |
| Wilson B-factor (Å$^2$) | 147.89 |
| [a]$R_{merge}$ | 0.72 (5.20) |
| **Refinement Statistics** | |
| Resolution range (Å) | 46.99 - 6.00 |
| [b]$R_{work}$ (%) | 28.77 |
| [c]$R_{free}$ (%) | 36.55 |
| Number of non-hydrogen atoms | 5812 |
| Macromolecules | 5810 |
| RMSD (bonds) (Å) | 0.004 |
| [d]RMSD (angles) (°) | 0.84 |
| Ramachandran favoured (%) | 93.49 |
| Ramachandran outliers (%) | 1.4 |
| Clashscore | 20.18 |
| Average B-factor (Å$^2$) | 242.51 |

[a] $R_{merge} = \sum|I_j - < I > |/\sum I_j$, where $I_j$ is the intensity of an individual reflection, and $< I >$ is the average intensity of that reflection.

[b] $R_{work} = \sum||F_o| - |F_c||/\sum|F_c|$, where $F_o$ denotes the observed structure factor amplitude, and $F_c$ the structure factor amplitude calculated from the model.

[c] $R_{free}$ is as for $R_{work}$ but calculated with 5% (3044) of randomly chosen reflections omitted from the refinement.

[d]RMSD = root mean square deviations

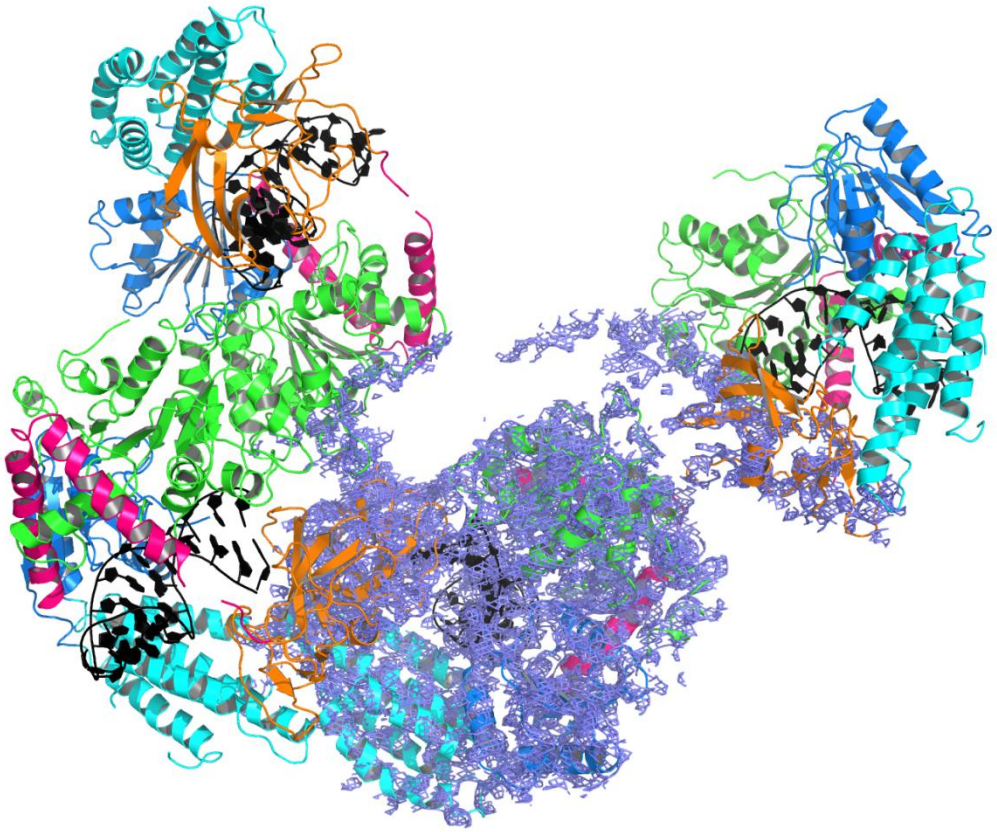

**Figure 3.13**. Crystal structure of hsRC2 in complex with 3p10LA9 at 6Å resolution.Four hsRC2 with 3p10LA9 were shown in this figure and the 2Fo-Fc maps contoured at 1σ displayed as a blue mesh is shown for 1 unit hsRC2: 3p10LA9.

### 3.11 Discussion

RIG-I is an important cytosolic sensor of viral infection by detecting the presence of foreign RNA in cells. The activation of RIG-I leads to the activation of host antiviral immune response via the production of type I interferon and pro-inflammatory cytokines (Iwasaki & Medzhitov, 2010; Kato et al, 2006; Loo et al, 2008). Interferon then activates the JAK-STAT signalling pathways which ultimately lead to the expression of interferon stimulated genes (ISGs). ISGs then inhibit the virus from spreading to surrounding cells by several mechanisms such as positive regulation of

IFN secretion, degrading nucleic acids and counteracting viral evasion strategy and apoptosis (Schneider et al, 2014; Schoggins & Rice, 2011). Hence RIG-I serves as an important therapeutic target for antiviral development as well as a therapeutic target for the treatment of cancer (Iurescia et al, 2018; Kaneda, 2013; Yong & Luo, 2018). Therefore, there is a need to understand the mechanism of RIG-I activation, in particular, the specific and targeted ligands triggering and activating RIG-I signalling in cells and in animal models.

Based on the previous studies by Kohlway et al, the double stranded RNA with the signature 5' triphosphate moiety with 10 bp long was the minimal length sufficient to trigger RIG-I activation (Kohlway et al, 2013). The crystallographic data obtained previously shown the CTD and HEL1 form the rigid hold on the first 4 nucleotides from the 5' and 3' end whereas the HEL2i domain interacts with the stem region up to the base 9 from the $5^{th}$ nucleotide onwards (PDB id: 4AY2, 5F9H, 3ZD6, 3ZD7 and 5E3H). The HEL2i domain was observedto scan along the stem region of the RNA. The relative position of HEL2i was shown to have an effect on the RIG-I activation because the CARDs domain are rested on the HEL2i domain in the inactive conformation (Devarkar et al, 2016; Jiang et al, 2012a; Kohlway et al, 2013; Luo et al, 2011). In this study, we first carried out an assay with RNA of different length. The ATPase assay data show that 3p10L stimulate the highest turnover number. We then set out to modify the structure of the minimal RNA 3p10L by introducing mismatch along the stem creating a kink in the hairpin RNA. We hypothesise that the kink in the stem of the RNA could potentially have an allosteric effect on the relative movement of the domain and perhaps effect the RIG-I activation to a different degree. In order

to systematically dissect the effect of the kink along the stem of the RNAs a guanosine nucleotide was introduced to create a mismatch on both strands from the 5$^{th}$ nucleotide onwards. These RNAs was designed as hairpin RNA terminated at one end with a thermodynamically stable UUCG tetraloop to ensure RIG-I binds in one orientation and therefore, the kink in the upper and lower strand could be studied effectively.

From the cell based assay it was shown that the position of the kink on the RNA effect the potency of RIG-I activation. The cell based assay showed the kink introduced at position 9 of the upper strand (3p10LG9) enhances the type I interferon activation. The type I interferon activation for 3p10LG9 was more than 2 fold higher than that of 3p10L. In the corresponding ATPase activity, 3p10LG9 showed the turnover number of 11.7 $s^{-1}$ as compared to the parental RNA, 3p10L with the $K_{cat}$ of 9.01 $s^{-1}$. In the study by Rawling et al, the binding of ATP and not the ATP hydrolysis was shown to be crucial for signalling activation of RIG-I (Rawling et al, 2015). Therefore, the relative fold of turnover number for both has little correlation to the fold of type I interferon activation. Based on the model of the 3p10LG9, the addition of the kinked present in 3p10LG9 interacts with the back surface of the helicase 2i domain of the RIG-I (Figure 3.14A). In the crystal structure captured with many different RNA ligands and ATP analogues, HEL2i domain is the most mobile domain and samples the RNA strand. The kink in position 9 could possibly lock the α- helical bundles in HEL2i in the extended conformation and in a position that expels CARDs domain resting on the HEL2i domain. Based on the proposed mechanism of ATPase activity and signalling, Louber et al (2015) proposed that RIG-I locked in an active

conformation for a longer duration would improve the ability to sustain type I Interferon production (Louber et al, 2015).

To further validate this hypothesis, HDX-MS was carried out to compare region within RIG-I that undergoes faster hydrogen deuterium exchange. In HDX-MS the more dynamic region will undergo a higher deuterium incorporation whereas the rigid region will have a lower deuterium incorporation (Masson et al, 2017). Several regions of RIG-I protein were observed with higher deuterium incorporation when bound to 3p10LG9 as compared to 3p10L. One of the regions that display a higher deuterium exchange is the latch peptide (Y103-114) of the CARD domain which in the inactive conformation is bound to RIG-I HEL2i domain. Hence, the when RIG-I is bound to 3p10LG9, the CARDs are more exposed and less protected from the deuterium incorporation as compared to RIG-I bound to 3p10L. Another region that displayed a high protection from deuterium incorporation when bound to 3p10LG9 is the motif Ia and motif Ic of the helicase 1 domain. This indicates that the 3p10LG9 is more tightly bound to the HEL1 domain as compared to 3p10L. Besides, HEL1 domain, the capping loop of CTD and the CTD binding site to 3p10LG9 also displayed a lower hydrogen-deuterium exchange indicating a tighter binding of 3p10LG9 as compared to 3p10L. Although HEL1 and CTD domain were not directly interacting with CARDs domain, the overall tighter binding HEL1 and CTD to the RNA indicates the overall compaction of helicase domain. From the previous biochemical and structural studies, the compaction of helicase in the event of ATP binding causes the CTD and the CARDs domain to come into close proximity and the clash of the domain releases the CARDs for downstream signalling events (Kohlway et al, 2013; Kowalinski et al,

2011; Rawling et al, 2015). From the HDX-MS we could conclude that the more compact the RIG-I helicase domain's interaction with the RNA due to tighter binding with 3p10LG9, the more sustained the release of CARDs was observed.

On the other hand, the kink created by the insertion of G at the position 5 (3p10LG5) of the hairpin RNA abolishes the activation of type I interferon. We showed from the analytical gel filtration and the inhibition assay that 3p10LG5 binds to RIG-I but is unable to activate the type I interferon expression. Based on the model of 3p10LG5, the kinked introduced to 3p10LG5 interacts with the HEL1 domain (Figure3.14B). The HEL1 is mainly involved in RNA binding. The region in which the kink interacts with the HEL1 domain is with the motif IIa. Based on the structures of SF2 helicases, the motif IIa is shown to interact with RNA and display a structural conservation within the DEAD-box family member (Luo et al, 2013). This motif IIa could be an important motif to form a stable interaction with RNA. As observed by Louber et al, the mutation of a residue Q380 to Proline a key residue in the motif IIa in hsRIG-I abolished the type I interferon activation (Louber et al, 2015). The kink introduced at position 5 of the upper strand of hairpin RNA could potentially perturb the RNA binding and the grip of HEL1 domain on the RNA that is required for RIG-I activation.

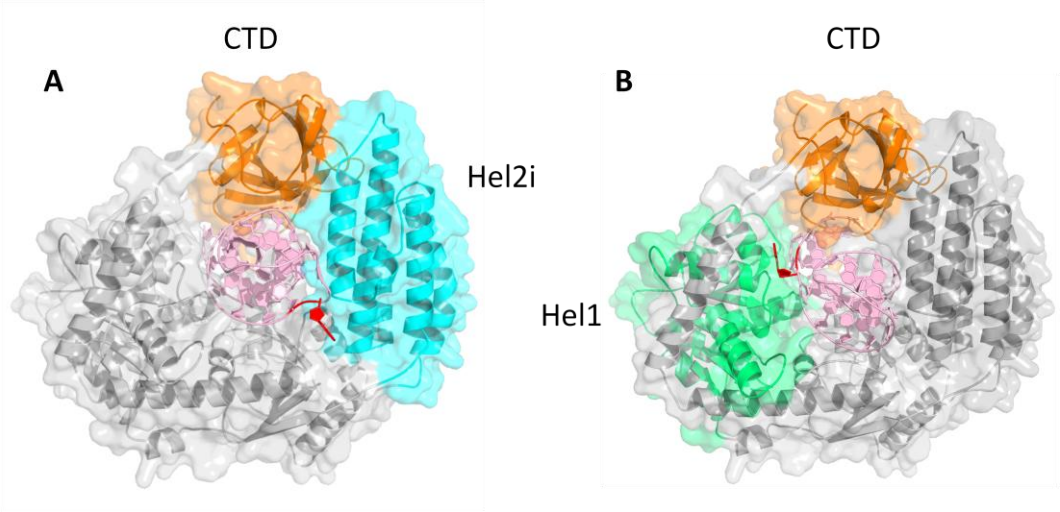


**Figure 3.14 Model of ImmRNA with hsRC2**. A) Model of 3p10LG9 with the kink shown in red interacting with HEL2i domain B) Model of 3p10LG5 with the kink shown in red interacting with HEL1 domain.

We next ask if the substitution of different nucleotides at the position 9 of the RNA could affect the type I interferon activation. We observe that the substitution of guanosine with adenosine at position 9 triggers similar level of expression of type I interferon expression whereas the substitution of cytosine or uracil at the position 9 of the RNA reduces the type I interferon expression by half. The ability of RIG-I to discriminate nucleotides and the preference towards some RNA with stretches of uracil had been reported previously (Lee et al, 2011; Runge et al, 2014; Saito et al, 2008; Schnell et al, 2012). For the different nucleotides at the kink position 9, it is more likely that the presence of bulkier purine is required for the HEL2i domain perturbation as compared the smaller side chain of pyrimidine. The sequence differences along the stem of the RNA were designed to ensure only a single possible conformation with different nucleotides as kink the hairpin RNA structure. We do not

expect the sequence difference to be a factor influencing the higher activation of type I interferon activity in RIG-I

Next, we tested the ability of RNAs such as 3p10L, 3p10LG9 and 3p10A9 to activate immune and non-immune cells. The cells used to verify the expression of type I interferon were the HEK 293T and THPI derived cells. Both cell lines have the Lucia luciferase reporter gene under the control of the ISG54 promoter and five IFN-stimulated response elements. When comparing the $EC_{50}$ value for the three RNA, the HEK-Lucia$^{TM}$ RIG-I shows quite similar $EC_{50}$ values with 133 nM for 3p10L G9, 199 nM for 3p10LA9 and 108 nM for 3p10L respectively. However, the difference in $EC_{50}$ values when the cell based assay was carried out in THP1-Dual$^{TM}$ was more prominent with 3p10L having very high $EC_{50}$ at 226 nM as compared to 3p10LG9 with 91nM and 3p10LA9 with 51nM respectively. The RLU for time point also showed that the 3p10L is much weaker in type I IFN expression at 72 hours post-transfection. This could be attributed to several possibilities such as the relative stability of the 3p10LG9 and 3p10LA9 as compared to 3p10L and therefore induces a higher expression of type I interferon at 72 hours post-transfection. Another reason is the higher initial type I interferon activation leads to a higher positive feedback of the RIG-I activation and increases in RIG-I expression in the cells.

In order to observe the structural difference induced by the binding of 3p10L, 3p10LG9 and 3p10LA9, we attempt to crystallise these RNAs with hsRIG-I without CARDs domain. Despite numerous attempts to crystallise these RNAs with hsRC2, the crystal diffracts poorly and was not of high enough resolution to observe the effect of the different RNAs on the domain arrangement. Although the protein was refined to

the correct solution with clearly visible solution shell, the resolution of the protein was low and the differences in the domain arrangement was not clear to explain the potential mechanism governing the preference for RNA with a kink at position 9. The success in crystallising a protein depends on many factors such as high purity, monodispersity, proper folding of the protein and the stability of the protein in the buffer (Page, 2008). Several optimisation steps could be done to improve the crystal diffraction including screening using more optimisation screen used such as Silver Bullet (Hampton), to check the monodispersity of the protein using circular dichroism, and also to slow the nucleation process to improve the crystal packing.

## Chapter 4 Packaging of ImmRNA in VLP

### 4.1 Background and rationale

The innate immune system plays an important role in the defence against pathogen infection, tumour recognition and contributes to the problem of autoimmunity (Akira et al, 2006). The innate immune system is involved in the antiviral defence as well as cancer sensing and there is much interest to develop innate immune system activators as therapeutics for antiviral application, to enhance vaccine efficacy and as oncotherapeutics (Gutjahr et al, 2016; Mancini et al, 2014; Moynihan & Irvine, 2017). The RLR responses are activated in the cell in the presence of foreign PAMPs, tissue damage or in the tumour microenvironment. This, in turn, triggers the localised activation of inflammation to limit the spread of the aberrant cell or foreign infectious components to the surrounding tissues (Fiuza & Suffredini, 2001; Tang et al, 2012). The direct administration of RIG-I activators could result in systemic distribution and inflammation (Appelbe et al, 2017). This challenge can be overcome by the use of controlled release methods such as nanocarriers which can deliver a large amount of loads at the targeted tissues or immunostimulatory antibody-drug conjugate (Liu et al, 2014; Ryu et al, 2017; Thomas et al, 2014).

RIG-I is an immune activator present in the cytosol of most cells, unlike other PRRs that are often expressed in immune cells. This allows the usage of RIG-I as a target for immune activator for application such as cancer immunotherapy independent of the subset of the cell population in tumour as well as vaccine adjuvants. However, this could potentially also activate a systemic antiviral reaction and could potentially lead to the problem of the cytokine storm. To circumvent this

problem, a solution is to develop targeted nanocarriers for delivery into different cells.

Virus-like particles (VLP) is one of the most versatile nanocarrier for targeted drug delivery and could also be used as vaccine adjuvants. VLP could be modified to potentially carry protein, nucleic acid and other small molecules to the targeted tissues before releasing the encapsulated cargo to the cells (Lua et al, 2014). One advantage of using VLP is the lack of genomic material of the viruses and hence there is no risk of reversion, unlike the live attenuated vaccines. Besides encapsulating materials in the interior of the VLP, the surface modification could also be carried out to functionalise the surface of the VLP to enhance specificity and other physical properties. The repetitive structure of VLP could be used for antigen presentation to enhance B cell receptor(BCR) cross linking (Zabel et al, 2014). The cross linking of BCR from multivalent antigen leads to BCR conformational changes and induces the active BCR microcluster formation and robust B cell signal activation (Geisberger et al, 2003). The repetitive nature of VLP also allows it to induce strong T-helper cells and to prime cytotoxic T lymphocytes (CTLs) (Cubas et al, 2009). VLP could also further activate dendritic cells (DC) and improve the recruitment of APC to the site which plays a role in capturing and processing the antigen and delivering them to secondary lymphoid organs (Zhang et al, 2004).

The potential usage of the agonist of PRRs as vaccine adjuvant has been studied previously. RLR agonist, , the 5'-triphosphate RNA was shown to trigger dose-sparing effects and provides protection against influenza virus challenge. The combination of VLP and RNA was able to increase the survival rate of mice infected

with H5N1 influenza virus as compared to VLP alone. The combination of VLP and M8 was able to induce higher antibody titer against influenza virus as compared to other adjuvants such as alum, addavax and poly IC. Furthermore, the vaccination with VLP and RNA stimulates TH1-biased CD4 T cells response in mouse sera (Beljanski et al, 2015). To date, VLP based vaccines have been developed extensively for more than 30 viruses and are being tested in various stages of clinical trials. However, currently, only 2 vaccines are approved for use in humans including the vaccine against Human Papilloma virus(HPV) which was approved in 2006, Hepatitis B Virus (HBV) which was approved in 1986. Several different types of VLPs are being generated as vaccines including VLP alone, VLP with envelope and chimeric VLP (Roldao et al, 2010).

In this study, we attempt to encapsulate Immune modulatory RNA (ImmRNA) in virus- like particles (VLP) of Q beta or MS2 which are RNA bacteriophages. Several Immune modulatory RNAs were designed to include the RNA scaffold recognition of MS2 and Q beta. We managed to package the VLP with RNA into Q beta coat protein. However, attempts to package the RNA in MS2 were not successful.

**4.2 Design of RNA binding to VLP**

The immRNA were modified to be incorporated into the VLP. The design of the immRNA is based on the minimal requirement of RNA residues from the translational operator (TR) of Q beta and MS2. Based on the crystal structure of the Q beta and MS2, both the coat protein dimer only share 20% identity and binds differently to their translational operator. In the Q beta coat protein, the operator requires a three nucleotide loop and a minimum of 8 base-paired stem. The only critical residue in the hairpin RNA of Q beta is the adenosine at the last position of the loop. Although an

adenosine bulge was observed in the stem at the fourth nucleotide from the loop, the removal of the adenosine was shown to have very minor effect on the affinity of binding of the TR to the Q beta coat protein (Figure 4.1A) (Lim et al, 1996; Witherell & Uhlenbeck, 1989). The binding of Q beta to the translational operator is tight and showed a dissociation constant (Kd) of 1nM (Lim et al, 1996). Whereas the binding of MS2 with its translational operator showed a dissociation constant of 3nM (Lim & Peabody, 1994).

The minimal requirement for the MS2 translational operator requires the hairpin RNA to be at least five base pair long. It also requires an unpaired purine nucleotide two base pair prior to the loop region of the helical RNA (Figure 4.1B). The tetraloop at the hairpin region requires Adenosine at the $1^{st}$ and $4^{th}$ nucleotide and a pyrimidine nucleotide at the $3^{rd}$ base of the RNA (Rumnieks & Tars, 2014). The binding of the TR RNA allows the stable formation of coat protein dimer and the RNA acts as a scaffold for the assembly of the coat protein into VLP (Figure 4.1C).

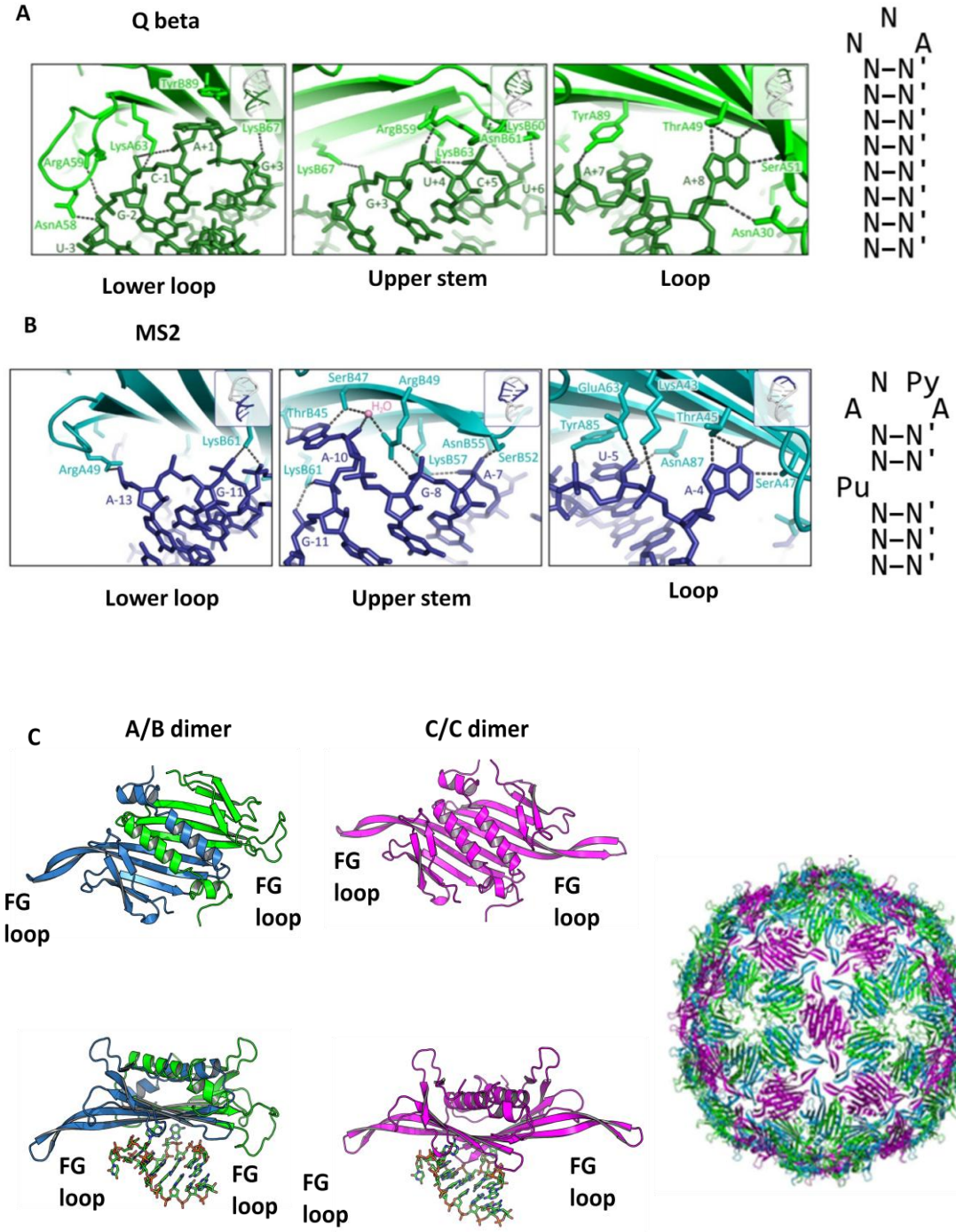


**Figure 4.1. The design of immRNA based on the translational operator of MS2 and Q beta** A) The overall structure of A) Q beta and B) MS2 coat protein dimer interacting with the translational operator (TR). The amino acids interacting with the nucleotide are labelled. The inset figure is the region of the TR hairpin interacting with the protein. The basic motif of the translational operator that is required to interact with the coat protein dimer and form the scaffold for the VLPs are shown on the right. Py, pyrimidine; Pu, purine; N, any nucleotide; N', a nucleotide complementary to N. C) The *in vitro* assembly of MS2 can be triggered by the

addition of hairpin RNA with the minimal important nucleic acid residues shown in figure A and B. The binding of the hairpin RNA to the coat protein induces a conformational change to form the CP dimer. Two different dimer conformations the A/B dimer and the C/C dimer could be formed. In the fully assembled capsid, the presence of A/B dimer and C/C dimer is at the ratio of 2:1 and there are a total of 60 repetitive dimer of A/B and C/C dimer to form the T=3 shell. Coat protein dimer shown is rendered from (PDB id: 1AQ3). Figure adapted from (Rumnieks & Tars, 2014; Stockley et al, 2016).

As a proof of concept, we designed immRNA based on 3p10LG9 and 3p10L for MS and 3p10L for Q beta from the previous section with the minimal RNA requirement for the RNA to bind to the coat protein dimer to initiate the assembly of VLP with package RNA in the interior. The RNA named MS2-3p10LG9, MS2-3p10L and Q beta-3p10L were shown here in (Figure 4.2) The RNAs were transcribed via *in vitro* transcription and purified (Figure 4.2).

**4.3 Cell based assay in THP1-Dual™**

To test if the modification made to the VLP based ImmRNA still retained its capability to trigger type I interferon activation, the RNAs were transfected into THP1-Dual™ cells. The VLP based ImmRNA showed slightly lower type I interferon activation activity as compared to the original ImmRNA sequence used in the previous chapter. However, we proceed to test this RNAs for VLP *in vitro* assembly (Figure 4.2B).

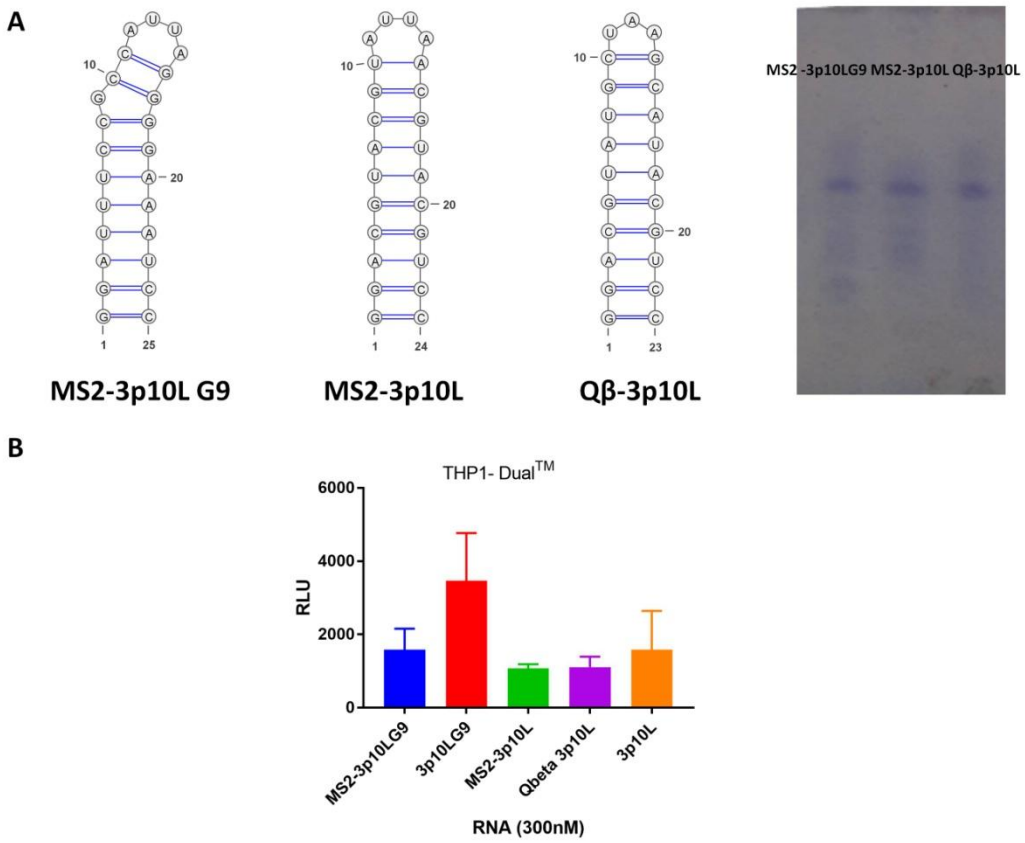


**Figure 4.2. ImmRNA for VLP**.A) The design for the three different RNA: MS2-3p10LG9, MS2-3p10L and Q beta-3p10L. Purified ImmRNA for all three RNA run in 20% denaturing PAGE. B) The cell based activity assay for VLP based ImmRNA in THP-1 Dual ™ cells.

### 4.4 Purification of MS2 VLP

The construct for MS2 coat protein was cloned into pNIC28-BSA4. This construct was MS2 gene was cloned into the pNIC28-BSA4 vector to exclude the hexa-histidine tag. In order to purify the construct without the hexa-histidine tag, the protein expressed were purified using ammonium sulphate precipitaton and sucrose gradient centrifugation. From the ammonium sulphate precipitation, the coat protein was present in the fraction of 30-40% ammonium sulphate (Figure 4.3A). Since the protein is devoid of tag at the N-terminal region and the expressed protein is purely the coat protein, we expect the protein to readily form virus-like particle. In order to further

obtain VLP, the ammonium sulphate fractions corresponding to coat protein were centrifuged in sucrose gradient centrifugation. Fractions collected (500 µL) were examined for the presence of coat protein in SDS-PAGE. From the sucrose gradient, the dense ring corresponding to the interface of 30-40% sucrose was observed (Figure 4.3B). This method of empty capsid purification was described previously by (Stonehouse & Stockley, 1993).

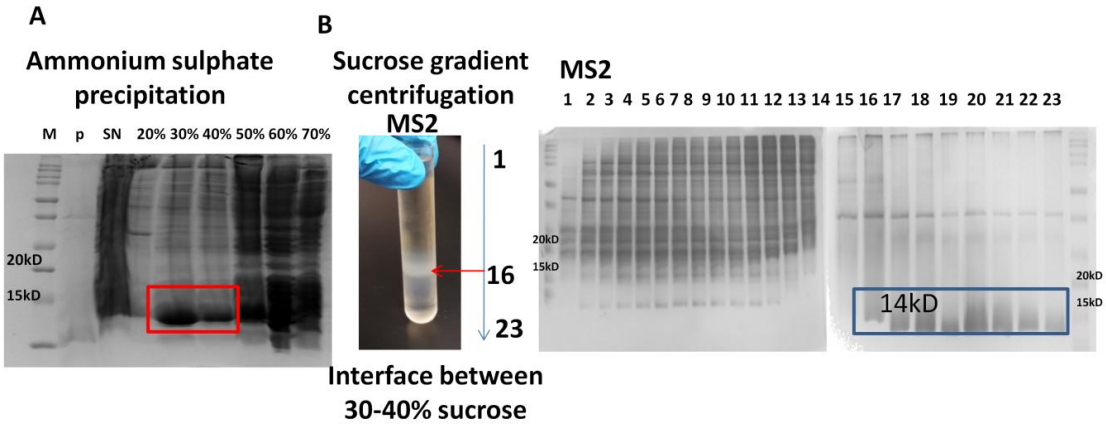


**Figure 4.3 Purification of MS2** VLP A) The ammonium sulphate precipitation fraction corresponding to the 30-40% showing ammonium sulphate B) Sucrose gradient centrifugation and the fraction corresponding to the VLP.SDS-PAGE revealed the presence of coat protein from fraction 16-23.

To verify the fraction purified form higher order assembly we run the analytical SEC using the column sepharose 6 Increase 10/300 for fraction 16 to 23 separately. MS2 VLP fraction 23 eluted at the largest size corresponding to volume of 11.74 mL after injection. The abs ratio for the peak showed that A260/280 higher than 1 indicating the presence of nucleic acid in the sample originating from the *E.coli* expression host (Figure 4.4A).

Next, to verify the fraction purified readily form VLP without the need to externally provide the transcriptional operator RNA (TR) negative staining was performed. The fraction 23 was pooled and dialysed extensively in buffer containing 25mM HEPES pH7.4 100mM NaCl to remove sucrose. Negative staining was performed for the sample. From the negative staining electron microscopy, the purified fraction from sucrose gradient centrifugation readily forms homogenous virus-like particles. The expected size for the T=3 icosahedral particle was reported previously at 27 nm and the size of the MS2 VLP was approximately 27nm in diameter (figure 4.4B).

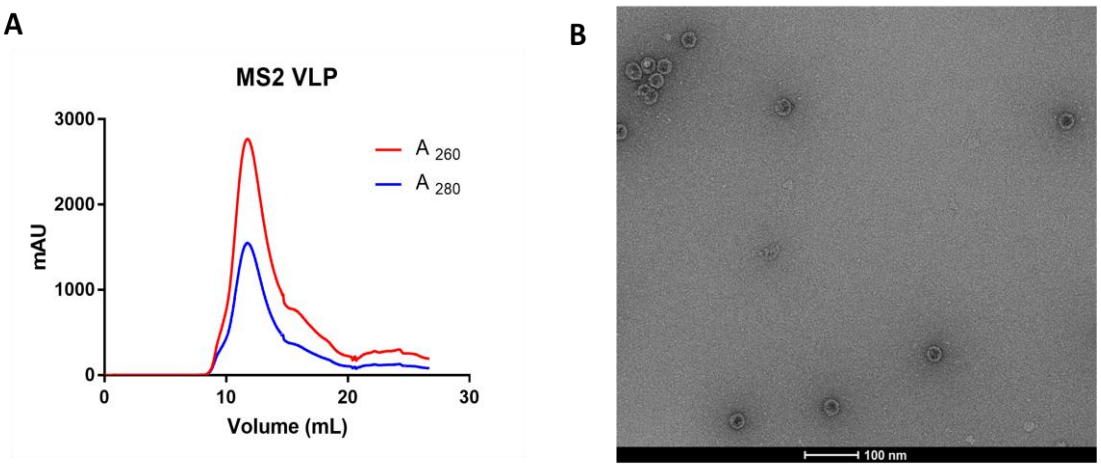


**Figure 4.4 Verification of VLP purification** A) Analytical gel filtration run on sepharose 6 increase 10/300 GL column for the fraction 23 from sucrose gradient centrifugation B) Negative staining electron microscopy of the sample corresponding to fraction 23 indicate the presence of VLP.

### 4.5 *In vitro* assembly of MS2 VLP with ImmRNA

Purified VLP were treated with RNase A as described previously in the materials and methods section. When the dialysed particles were subjected to analytical gel filtration column run s200 10/300pg, the abs 260/280 was higher than 1 indicating that the RNase A was unable to remove the RNA present in the VLP (Figure 4.5A). The

subsequent process of soaking the RNA with MS2-3p10L or MS2-3p10LG9 did not result in an increase of RNA incorporation as observed by the A 260 absorbance before and after soaking with RNA (Figure 4.5B).

Next, we treated the VLP in a denaturing buffer containing 6 M urea, 10 mM dithiothreitol. The presence of DTT is thought to disrupt the basic unit of the coat protein assembly, the dimer, which forms disulphide bond with other dimers. Urea is thought to bind to the protein and stabilises the denatured state. After treatment in Urea for 4 hours, the coat protein was dialysed to remove the Urea and dialysed in the assembly buffer with MS2-3p10L or MS2-3p10LG9. The protein and RNA complex was subsequently concentrated and run in analytical gel filtration S200 10/300pg column. The protein RNA was denatured and unable to form any higher order complex (Figure 4.5C) when compared with the VLP with elution volume of 9.7 mL.

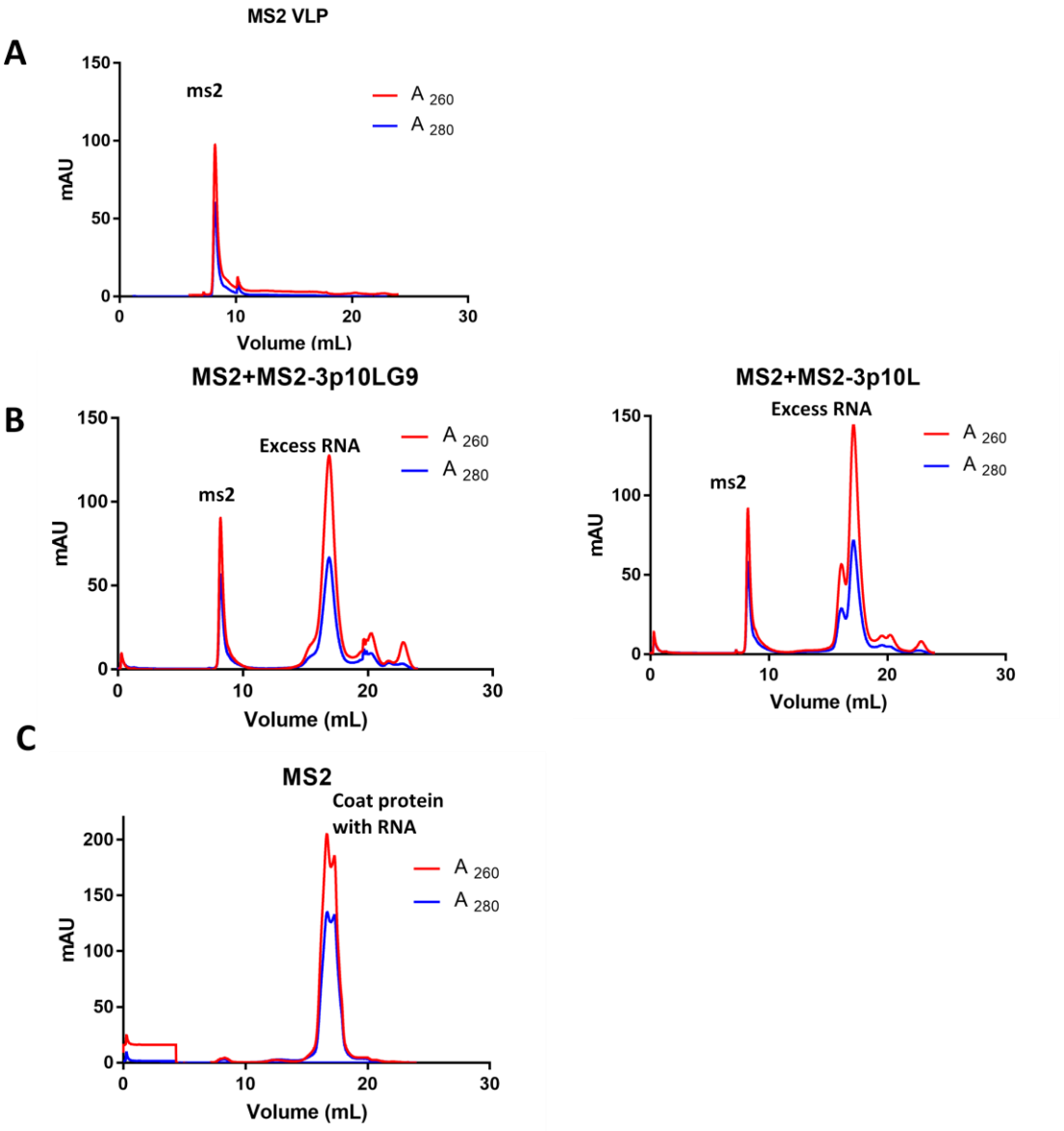


**Figure 4.5 *In vitro* assembly of MS2 VLP with ImmRNA** A) The analytical gel filtration of MS2 treated with RNase B) soaking of MS2-3p10L and MS2-3p10LG9 with MS2 VLP C) *In vitro* assembly of MS2 coat protein with RNA MS2-3p10L.

### 4.6 Purification of Q beta coat protein dimer

Since we encounter problem loading ImmRNA into the preformed VLP, we introduce an N-terminal SUMO tag by cloning Q beta in coat protein into the pETSUMO vector. We then proceed to purify the Q beta coat protein with Ni-NTA beads followed by the SUMO tag cleavage. This is followed by ion exchange chromatography and size

exclusion chromatography (SEC). The purification of pET-SUMO Q beta resulted in coat protein and a higher order assemble construct as shown in the SEC profile (Figure 4.6B). The peak corresponding to the VLP was shown to contain nucleic acid based on the Abs 280/260 of the peak. The coat protein showed the Abs 260/280 ratio of ~0.5 corresponding to clean protein without any nucleic acid (Figure 4.6B). The peak corresponding to a higher order assembly was verified by negative staining to be the fully formed VLP. Therefore, even in the presence of an N-terminal tag with a size of 11kD, the coat protein was still able to form virus-like particle (Figure 4.6C).

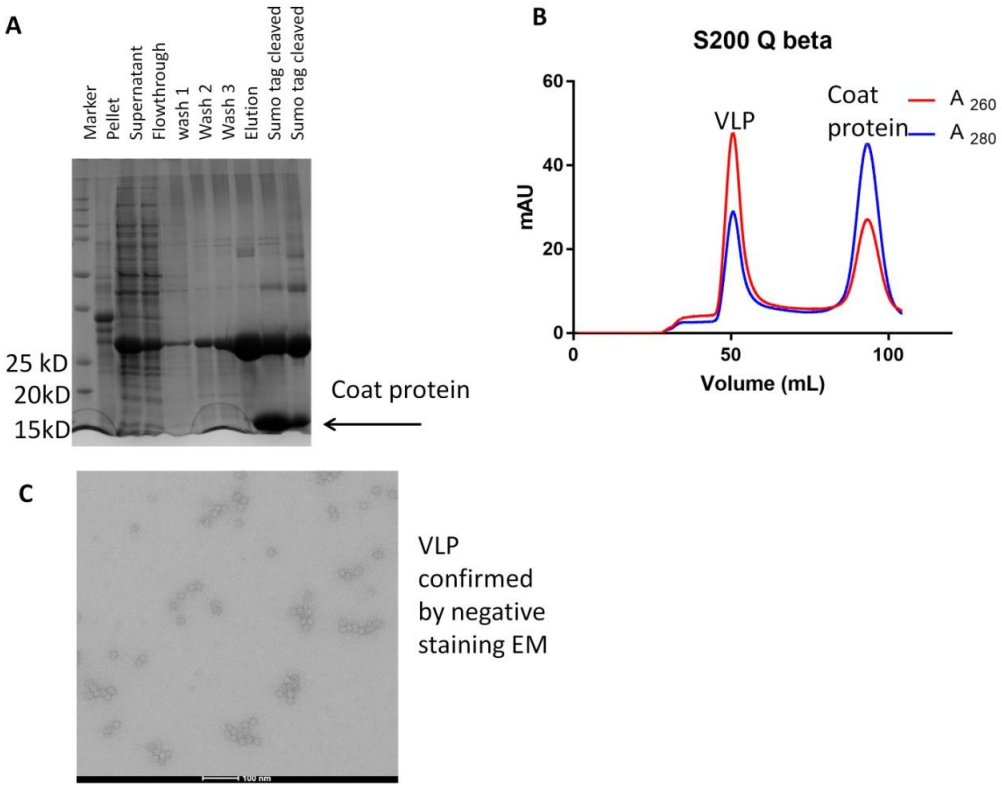


**Figure 4.6 Purification of Q beta coat protein** A) SDS PAGE profile for the Ni-NTA affinity purification stages. B) Size exclusion chromatography profile of Q beta coat protein and VLP C) Negative staining EM for the fraction labelled VLP.

### 4.7 *In vitro* assembly of Q beta coat protein with Q beta-3p10L

For Q beta coat protein, coat protein devoid of any nucleic acid was obtained. The *in vitro* assembly of Q beta was carried out using 200 µM protein and 200 µM RNA in 50mL volume in buffer containing HEPES pH 7 10mM and 0.3% (v/v) hydrogen peroxide to promote disulfide linkages formation. In principle, the formation of the VLP requires the ratio of RNA to the protein of 1:3 (Galaway & Stockley, 2013). The basic unit for the coat protein to assemble is the held together by disulphide bond formed by two cysteine residues at position 74 and 80 of the coat protein (Golmohammadi et al, 1996). The protein RNA complexes were concentrated with Vivaspin 20 with a MWCO of 3 kD. Protein RNA complex was resolved in gel filtration S200 10/300pg. Form the analytical SEC profile obtained it was shown that the Q beta coat protein form complex and one peak corresponding to a higher order RNA-protein complex were obtained as shown in the SEC profile with the elution volume of 10.16mL (Figure 4.7A). The RNA-protein complex from SEC was added with an excess amount of coat protein (6 mM) to the RNA protein complex to drive the formation of many other higher order species. From the SEC profile, the highest order species obtained eluted at 8.32mL (Figure 4.7B). The highest order assembly structure was verified to be homogenous VLP as shown by the negative staining EM. However, the yield of the *in vitro* assembled VLP was very low (Figure 4.7C).

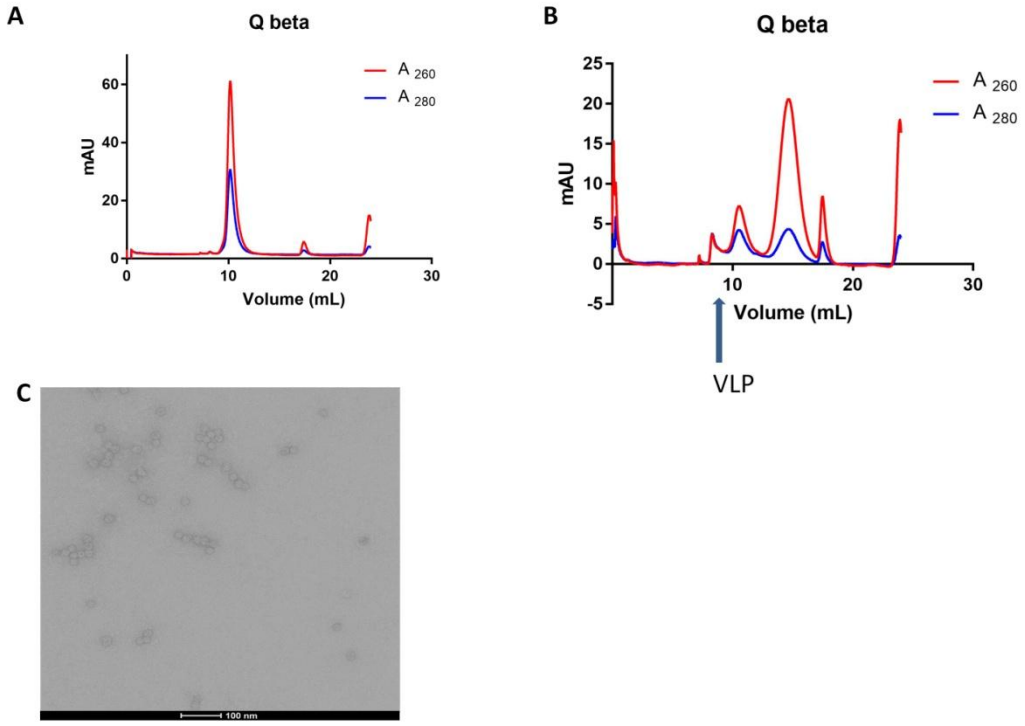


**Figure 4.7 *In vitro* assembly of Q beta coat protein with Q beta-3p10L** A) Size exclusion profile for the first stage of *in vitro* assembly using 1:1 ratio of coat protein dimer and Q beta-3p10L B) Size exclusion chromatography profile of Q beta coat protein and VLP with many higher order assembled structure C) Negative staining EM for the fraction labelled VLP.

## 4.8 Discussion

RNA is becoming more important in drug discovery and disease treatment due to the increase in understanding of the biological roles of RNA (Burnett & Rossi, 2012; Puerta-Fernandez et al, 2003). RNA based therapeutics include the inhibitors of mRNA translation, agent of RNA interference, ribozymes and RNA that binds to as ligands to other molecules. Although there are many application of RNA as therapeutics, the delivery of RNA into targeted cells remained challenging. Naked RNA are prone to degradation in cells by nucleases and could trigger systemic immune activation (Lieberman, 2018). The negatively charge RNA also pose a problem in delivery and this RNAs cannot passively traverse the cell membrane. Once in the cells, the RNA could readily be destroyed in the endosomes before exerting its cellular function (Kaczmarek et al, 2017). Challenges in the delivery, stability and specificity have driven numerous attempts to develop nucleic acid carriers or chemical modification to protect RNA.

Nanoparticle encapsulation of RNA is one of the most studied methods to protect nucleic acid from degradation and helps in the cellular uptake. One of the most versatile nanoparticles that can be used for therapeutic delivery into cells is the virus-like particles (Zdanowicz & Chroboczek, 2016). VLPs are stable in different temperature and pH, non-infectious and resistant to proteolytic degradation. Besides that, the surface of the repeating unit of coat protein could be manipulated to display nucleic acid, proteins and other chemical groups to functionalise the polyvalent scaffold for vaccine, therapeutics and diagnostics development (Brown et al, 2002; Garcea & Gissmann, 2004; Georgens et al, 2005; Jennings & Bachmann, 2008; Liepold

et al, 2007). Previous studies reported that the peptide display on the surface of the VLP enhances the cell-specific delivery (Brown et al, 2002; Pokorski et al, 2011). VLPs are also particularly attractive to be developed into vaccines as they can be trafficked to the lymph nodes and stimulate the B and T cells responses with the displayed epitopes. In particular, the repetitive nature of the VLPs surface allows better B cells activation and differentiation (Zabel et al, 2014).

VLPs from RNA bacteriophages such as Qβ and MS2 are hollow icosahedral nanoparticles which are form by 180 copies of coat protein (CP) (Golmohammadi et al, 1996; Machida & Imataka, 2015). Qβ and MS2 form a T=3 icosahedral structure with a small single stranded mRNA genome encoding four ORF. It was shown previously by Stockley et al. that the stem-loop RNA present in the MS2 viral genome interacts with the CP during assembly and up to 60 RNA stem-loop in the MS2 genome were identified (Dykeman et al, 2013; Hirao et al, 1998; Mills et al, 1990; Peabody, 1997). During the assembly, RNA protein interaction must first occur to stabilise the coat protein dimer formation. Subsequently, the cysteine 74 and 80 form disulphide linkages to hold the coat protein into a higher order assembly (Borodavka et al, 2012). The release of RNA involved the breakage of the disulphide linkages and destabilisation of VLP at low pH. In the cells, the low pH in the late endosomes and lysosomes may dissociate the VLPs and release the encapsulated nucleic acid. The attachment of targeting peptides also facilitate VLP uptake in human cells requiring less than 50 nmolar of VLP to efficient uptake (Galaway & Stockley, 2013; Pokorski et al, 2011; Wu et al, 1995). Furthermore, it was shown that the covalent attachment of histidine rich peptides on VLP surface could act as proton sponges to sequester

protons in the endosome causing the endosome to rupture and enhances the effect of the VLP delivery by a 100 fold (Ashley et al, 2011; Lachelt et al, 2014).

In our study, we attempt to encapsulate VLPs with immune modulatory RNA (ImmRNA). Since the nature of the hairpin RNA which acts as the translational operator and scaffold of MS2 and Q beta are quite similar to the immRNA, we incorporated minimal features required for the hairpin RNA to function as both scaffold and immRNA in the cells. The VLP based immRNA was able to trigger the type I IFN when transfected with LyoVec into THP1-Dual™. Attempt to purify MS2 VLP via ammonium sulphate precipitation and sucrose gradient centrifugation was successful. The MS2 coat was found to spontaneously form VLP when expressed in *E. coli* possibly with nucleic acid from the expression host incorporated as a scaffold. However, we failed in the attempt to disrupt the MS2 VLP into constituent coat protein components by using reducing agent and urea followed by reassembling the coat protein with VLP based immRNA. Several studies have shown that the VLPS of MS2 readily disassemble into coat protein the reassembly process was only accomplished with the viral genomic RNA (Borodavka et al, 2012; Rolfsson et al, 2008). Upon further investigation, the coat protein does not only interact with transcriptional operator (TR) but also many packaging signals (PSs) along the genomic RNA (Stockley et al, 2016). Although small individual hairpin RNA is crucial for the dimer formation, the presence of many dimers does not always come together into a formation that allows the VLPs to assemble into a correct conformation. PS are short RNA motifs present along the viral genomic RNA and facilitate protein-protein contacts and act as allosteric switches for the T=3 icosahedral shell formation

(Stockley et al, 2016). Since there were no traces of higher order assembled particles present from the reassembly, we also postulate that the harsh treatment to disassemble the VLP using 6 M urea might damage the coat protein.

Next, we attempted to purify coat protein instead of a preformed VLP. To accomplish that, we cloned the Q beta coat protein into the pETSUMO vector with the N terminal SUMO tag. The presence of SUMO tag hinders the spontaneous VLP formation for some of the expressed protein. However, a fraction of Q beta protein still manages to form VLP and was confirmed by negative staining EM. The coat protein was then reassembled with Qbeta-3p10L in the presence of hydrogen peroxide to promote disulphide bonds formation required for coat protein-coat protein interaction. In this condition, we manage to assemble coat protein and Qbeta-3p10L. Subsequently, we added the coat protein dimer at a very high ratio to the dimer-RNA complex in the buffer with hydrogen peroxide and we manage to obtain a small fraction of VLP. The ratio of A260/A280 indicates the presence of RNA and we confirm the presence of fully formed VLP via negative staining EM. The yield of VLP via *in vitro* assembly of Q-beta coat protein dimer was low. Although several higher order assembled protein-RNA complex was also obtained. According to Borodavka et al., most VLP assembly adopts a two stage process. In the initial stage, RNA is rapidly bound to the coat protein resulting in compact initiation complex. This is followed by the assembly with just the addition of CP subunits which are recruited to the growing shell (Borodavka et al, 2012). Hence it is possible to drive the formation of VLP with the addition of more coat protein once a higher order assembly is formed.

## 5 Conclusion

In this study we designed and identified immRNA minimal ligand to stimulate a robust immune response. The minimal ligand that is required to trigger the innate immune activation was determined to be at least 10 base-pair long in the stem region. The insertion of a guanosine kink at the position 9 of the stem RNA was shown to trigger a more robust type I interferon activation as compared to the parental RNA, 3p10L. HDX-MS comparison between the 3p10LG9 and 3p10L showed that the region corresponding to motif Ia and Ic of helicase 1 and the capping loop and the RNA binding site of CTD bind more tightly to 3p10LG9 as compared to 3p10L. The CARDs domain of hsRIG-I was also more exposed when bound to 3p10LG9 as compared to 3p10L. The substitution of the nucleotide at position 9 with adenosine of the immRNA 3p10LG9 was shown to trigger similar type I interferon response. However, the substitution of guanosine with uracil and cytosine were shown to reduce the type I interferon by half which leads us to conclude the presence of purine in position 9 is critical to improve the RIG-I activation. We also showed that the introduction of guanosine kink at the position 5 of the stem region of the RNA resulted in immRNA that binds to but is unable to activate hsRIG-I signalling.

For the packaging of immRNA into VLP, the modification was done to the sequence of the hairpin RNA to act as a scaffold for RNA binding and also to encapsulate the RNA. We observed that the changes to the sequence of VLP based immRNA reduce the type I interferon activation as compared to the original immRNA (3p10L and 3p10LG9) we manage to purify virus-like particle for MS2 from *E. coli.* However, we failed to reassemble the immRNA into the VLP using MS2. As for Q beta,

we manage to purify VLP and coat protein and were able to assemble VLP with immRNA with a two step incubation strategy, although the yield of assembled VLP carrying the immRNA was low.

**Future Directions**

As more understanding is obtained with regards to RIG-I mechanism of action and the contribution of deregulation of the protein to different disease state, the potential to develop agonist of RIG-I as therapeutics continues to grow. As discussed in the chapter1, the involvement of RIG-I in the induction of inflammation and targeted cell death makes RIG-I agonist an attractive tool for antiviral, adjuvant and oncotherapeutic development. However, caution must be taken to improve targeted delivery to prevent the unwanted outcome of triggering systemic immune activation and cytokine storm.

In order to understand the effect of the kink on the stem of the hairpin RNA, it would be ideal to obtain the crystal structure of immRNA bound to hsRC2. Effort should be focused to systematically dissect the condition to crystallise the ImmRNA with hsRC2 especially 3p10LA9, 3p10LG9 and 3p10LG5. Capturing the hsRC2 protein with immRNA would be invaluable to the understanding of the development of ImmRNA as an agonist of RIG-I. Next, the stability of immRNA in cells should be evaluated using radiolabelled immRNA to check for the integrity of immRNA overtime after transfection into cells.

To develop this RNA into potential therapeutics, the agonist of RIG-I (3p10LA9 and 3p10LG9) should further characterise in different human cell lines for its generation

of the antiviral and inflammatory responses. Besides that, therapeutic and prophylactic effect of the RIG-I agonist in a mouse model of viral infection could be evaluated. The ability of RIG-I agonist to act as an adjuvant for vaccines can also be tested in mouse model infected with certain viral diseases. The ability of ImmRNA to trigger the innate and adaptive response in the tumor microenvironment could also be evaluated in cancer mouse model as oncotherapeutics.

As for the delivery of ImmRNA into cells, a different method of packaging the ImmRNA should be explored to enhance the yield and stability of immRNA in nanocarrier. It was recently shown that short triphosphorylated RNA could be delivered to cells by conjugating the 5'ppp RNA with PEG via a cleavable linker (Palmer et al, 2018). Perhaps, this idea could be adapted to develop PEGylated VLP with surface conjugation of immRNA via Cu(I) catalysed click chemistry (Patel & Swartz, 2011). Besides that, for the downstream application, the VLP could be functionalized for targeted cell application. For example, a recent study identified a peptide SP94 as a peptide targeting specifically human hepatocellular carcinoma (HCC). By displaying the peptide on the surface of MS2 VLP, the VLP was able to deliver several different cargoes to the HCC specific cell line Hep3B without affecting other cell lines (Ashley et al, 2011).

**Appendix 1**

**Primer sequence for immRNA**

| Primer name | Primer sequence | RNA |
|---|---|---|
| OHYT49 | GTAATACGACTCACTATAGGACGCTTCGGCGTCC | 3p6L |
| OHYT50 | GGACGCCGAAGCGTCCTATAGTGAGTCGTATTAC | 3p6L |
| OHYT37 | GTAATACGACTCACTATA GG ACGT GC TTCG GC ACGT CC | 3p8L |
| OHYT38 | GGACGTGCCGAAGCACGTCCTATAGTGAGTCGTATTAC | 3p8L |
| OHYT65 | GTAATACGACTCACTATAGGATTTCCCTTCGGGGAAATCC | 3p9L |
| OHYT66 | GGATTTCCCCGAAGGGAAATCCTATAGTGAGTCGTATTAC | 3p9L |
| OHYT07 | GTAATACGACTCACTATAGGACGTACGTTTCGACGTACGTCC | 3p10L |
| OHYT08 | GGACGTACGTCGAAACGTACGTCCTATAGTGAGTCGTATTAC | 3p10L |
| OHYT15 | GTAATACGACTCACTATAGGATTTCGCGCTTCGGCGCGAAATCC | 3p11L |
| OHYT16 | GGATTTCGCGCCGAAGCGCGAAATCCTATAGTGAGTCGTATTAC | 3p11L |
| OHYT31 | GTAATACGACTCACTATA GGACGTACGTGC TTCG GCACGTACGTCC | 3p12L |
| OHYT32 | GGACGTACGT GC CGAA GC ACGTACGTCCTATAGTGAGTCGTATTAC | 3p12L |
| OHYT51 | GTAATACGACTCACTATA GGACGTACGTACGC ttcg GCGTACGTACGTCC | 3p14L |
| OHYT52 | GGACGTACGTACGCCGAAGCGTACGTACGTCCTATAGTGAGTC GTATTAC | 3p14L |
| OHYT29 | GTAATACGACTCACTATA GG ACGTACGTACGTACGTGC TTCGGCACGTACGTACGT ACGTCC | 3p20L |
| OHYT30 | GGACGTACGTACGTACGTGCCGAAGCACGTACGTACGTACGTC CTATAGTGAGTCGTATTAC | 3p20L |
| OHYT41 | GTAATACGACTCACTATA GGACGCTTTCCTTCGGGAAAGGTCC | 3p10LG5 |
| OHYT42 | GGACCTTTCCCGAAGGAAAGCGTCCTATAGTGAGTCGTATTAC | 3p10LG5 |
| OHYT17 | GTAATACGACTCACTATAGGATTCGCTCCTTCGGGAGGAATCC | 3p10LG7 |
| OHYT18 | GGATTCCTCCCGAAGGAGCGAATCCTATAGTGAGTCGTATTAC | 3p10LG7 |
| OHYT19 | GTAATACGACTCACTATAGGATTTCCGCCTTCGGGGGAAATCC | 3p10LG9 |
| OHYT20 | GGATTTCCCCCGAAGGCGGAAATCCTATAGTGAGTCGTATTAC | 3p10LG9 |
| OHYT13 | GTAATACGACTCACTATAGGATTTCGGCTTCGGCGCGAAATCC | 3p10LG17 |
| OHYT14 | GGATTTCGCGCCGAAGCCGAAATCCTATAGTGAGTCGTATTAC | 3p10LG17 |
| OHYT43 | GTAATACGACTCACTATA GGATTGGTCCTTCGGGACGCAATCC | 3p10LG19 |
| OHYT44 | GGATTGCGTCCCGAAGGACCAATCCTATAGTGAGTCGTATTAC | 3p10LG19 |
| OHYT11 | GTAATACGACTCACTATAGGAGGTTTCCTTCGGGAAACGCTCC | 3p10LG21 |
| OHYT12 | GGAGCGTTTCCCGAAGGAAACCTCCTATAGTGAGTCGTATTAC | 3p10LG21 |
| OHYT57 | GTAATACGACTCACTATAGGATTTCCACCTTCGGGGGAAATCC | 3p10LA9 |
| OHYT58 | GGATTTCCCCCGAAGGTGGAAATCCTATAGTGAGTCGTATTAC | 3p10LA9 |
| OHYT61 | GTAATACGACTCACTATAGGATTTCGCGCTTCGGCCGAAATCC | 3p10LC9 |
| OHYT62 | GGATTTCGGCCGAAGCGCGAAATCCTATAGTGAGTCGTATTAC | 3p10LC9 |
| OHYT59 | GTAATACGACTCACTATAGGATTTCATACTTCGGTTGAAATCC | 3p10LU9 |
| OHYT60 | GGATTTCAACCGAAGTATGAAATCCTATAGTGAGTCGTATTAC | 3p10LU9 |

## Appendix 2

### Primer sequence for immRNA-VLP

| Primer name | Primer sequence | RNA |
|---|---|---|
| OHYT73 | GTAATACGACTCACTATA GGACGTACGTATTAACGTACGTCC | MS2-3p10L |
| OHYT74 | GGACGTACGTTAATACGTACGTCCTATAGTGAGTCGTATTAC | MS2-3p10L |
| OHYT75 | GTAATACGACTCACTATA GGACGTACGTTAAACGTACGTCC | Q beta- 3p10L |
| OHYT76 | GGACGTACGTTTAACGTACGTCCTATAGTGAGTCGTATTAC | Q beta-3p10L |
| OHYT77 | GTAATACGACTCACTATA GGATTTCCGCCATTAGGGGAAATCC | MS2-3p10LG9 |
| OHYT78 | GGATTTCCCCTAATGGCGGAAATCCTATAGTGAGTCGTATTAC | MS2-3p10LG9 |

**Appendix 3: HDX-MS raw data for hsRIG-I with 3p10L or 3p10LG9 vs without RNA**

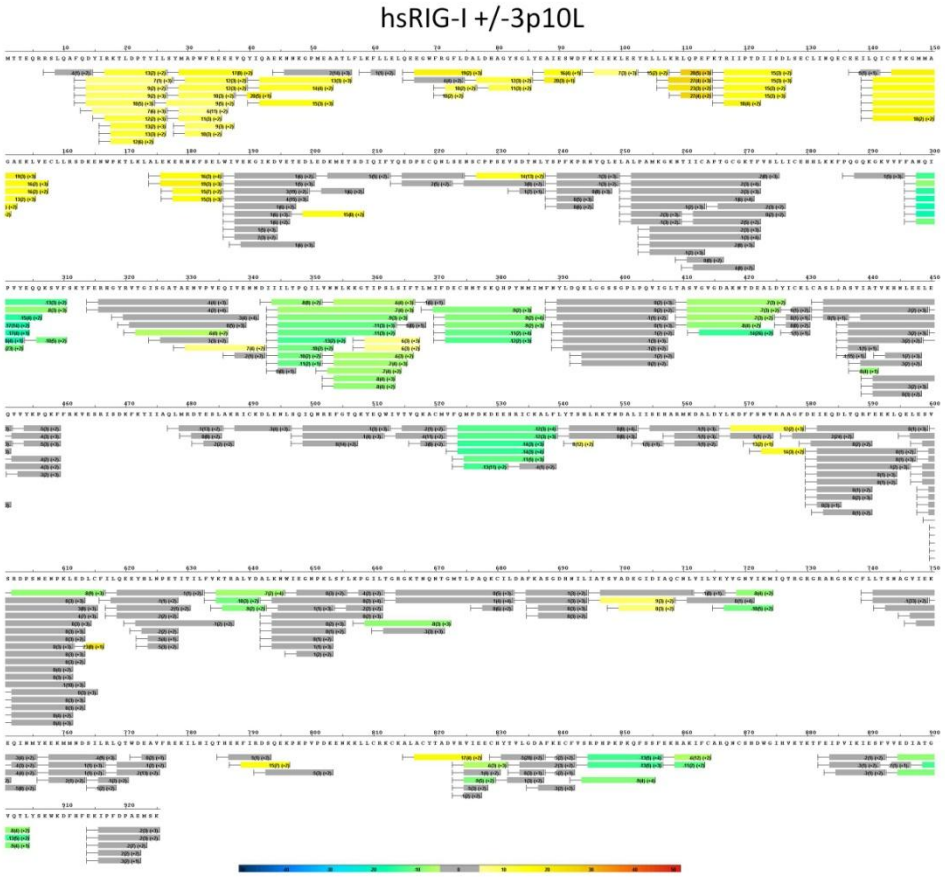

hsRIG-I +/- 3p10LG9

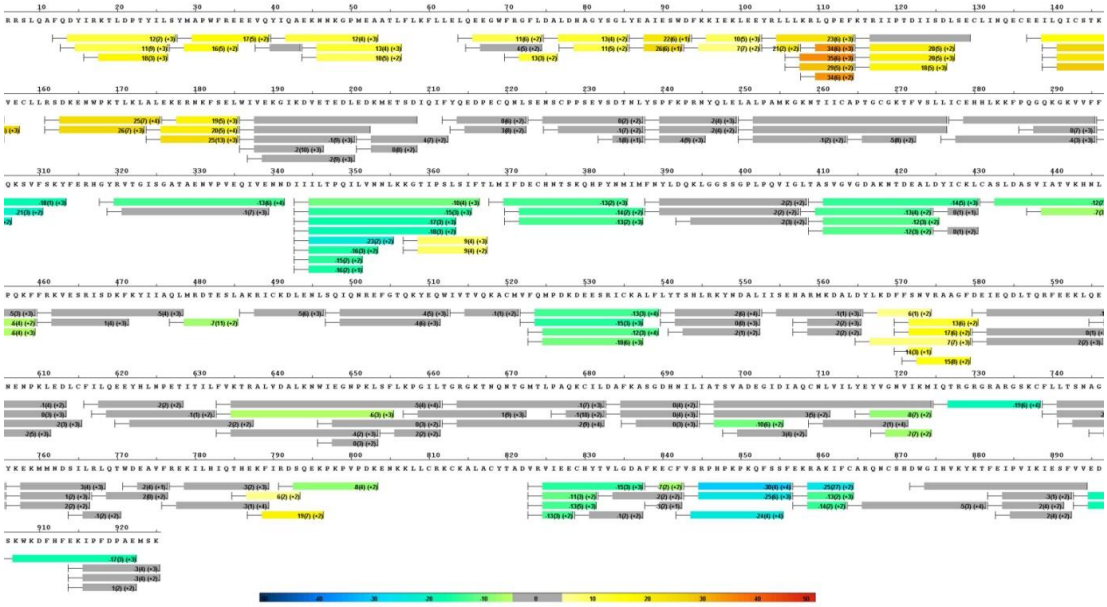

**List of publications**

3) Zheng J, **Yong HY**, Panutdaporn N, Liu CF, Tang K, Luo DH (2015) High-resolution HDX-MS reveals distinct mechanisms of RNA recognition and activation by RIG-I and MDA5. *Nucleic Acids Res* **43:** 1216-1230

4) **Yong HY**, Luo D (2018) RIG-I-Like Receptors as Novel Targets for Pan-Antivirals and Vaccine Adjuvants Against Emerging and Re-Emerging Viral Infections. *Front Immunol* **9:** 1379

**5)** Yong HY Luo D. RIG-I-Like Receptors . eLS: **Encyclopedia of Life Sciences**; 2015 www.els.net/WileyCDA/ElsArticle/refId-a0026237.html

**Manuscript in preparation**

1) Yong HY, Zheng J, Ho VCY, Fink K, Griffin PR, Luo D. Structure guided design of immunomodulatory RNAs specifically target RIG-I

**References:**


Ablasser A, Bauernfeind F, Hartmann G, Latz E, Fitzgerald KA, Hornung V (2009) RIG-I-dependent sensing of poly(dA:dT) through the induction of an RNA polymerase III-transcribed RNA intermediate. *Nat Immunol* **10:** 1065-U1040

Akira S, Takeda K (2004) Toll-like receptor signalling. *Nature reviews Immunology* **4:** 499-511

Akira S, Uematsu S, Takeuchi O (2006) Pathogen recognition and innate immunity. *Cell* **124:** 783-801

Alexopoulou L, Holt AC, Medzhitov R, Flavell RA (2001) Recognition of double-stranded RNA and activation of NF-kappaB by Toll-like receptor 3. *Nature* **413:** 732-738

Alff PJ, Gavrilovskaya IN, Gorbunova E, Endriss K, Chong Y, Geimonen E, Sen N, Reich NC, Mackow ER (2006) The pathogenic NY-1 hantavirus G1 cytoplasmic tail inhibits RIG-1- and TBK-1-directed interferon responses (vol 80, pg 9676, 2006). *J Virol* **80:** 12430-12430

Anchisi S, Guerra J, Garcin D (2015) RIG-I ATPase activity and discrimination of self-RNA versus non-self-RNA. *mBio* **6:** e02349

Antonis AFG, Bruschke CJM, Rueda P, Maranga L, Casal JI, Vela C, Hilgers LAT, Belt PBGM, Weerdmeester K, Carrondo MJT, Langeveld JPM (2006) A novel recombinant virus-like particle vaccine for prevention of porcine parvovirus-induced reproductive failure. *Vaccine* **24:** 5481-5490

Appelbe OK, Moynihan KD, Flor A, Rymut N, Irvine DJ, Kron SJ (2017) Radiation-enhanced delivery of systemically administered amphiphilic-CpG oligodeoxynucleotide. *Journal of controlled release : official journal of the Controlled Release Society* **266:** 248-255

Arimoto KI, Takahashi H, Hishiki T, Konishi H, Fujita T, Shimotohno K (2007) Negative regulation of the RIG-I signaling by the ubiquitin ligase RNF125. *P Natl Acad Sci USA* **104:** 7500-7505

Ashley CE, Carnes EC, Phillips GK, Durfee PN, Buley MD, Lino CA, Padilla DP, Phillips B, Carter MB, Willman CL, Brinker CJ, Caldeira JD, Chackerian B, Wharton W, Peabody DS (2011) Cell-Specific Delivery of Diverse Cargos by Bacteriophage MS2 Virus-like Particles. *Acs Nano* **5:** 5729-5745

Asselah T, Marcellin P (2013) Interferon free therapy with direct acting antivirals for HCV. *Liver international : official journal of the International Association for the Study of the Liver* **33 Suppl 1:** 93-104

Bakker AB, Baker E, Sutherland GR, Phillips JH, Lanier LL (1999) Myeloid DAP12-associating lectin (MDL)-1 is a cell surface receptor involved in the activation of myeloid cells. *Proc Natl Acad Sci U S A* **96:** 9792-9796

Bamming D, Horvath CM (2009) Regulation of signal transduction by enzymatically inactive antiviral RNA helicase proteins MDA5, RIG-I, and LGP2. *J Biol Chem* **284:** 9700-9712

Basler CF, Wang XY, Muhlberger E, Volchkov V, Paragas J, Klenk HD, Garcia-Sastre A, Palese P (2000) The Ebola virus VP35 protein functions as a type IIFN antagonist. *P Natl Acad Sci USA* **97:** 12289-12294

Battye TG, Kontogiannis L, Johnson O, Powell HR, Leslie AG (2011) iMOSFLM: a new graphical interface for diffraction-image processing with MOSFLM. *Acta crystallographica Section D, Biological crystallography* **67:** 271-281

Baum A, Sachidanandam R, Garcia-Sastre A (2010) Preference of RIG-I for short viral RNA molecules in infected cells revealed by next-generation sequencing. *Proc Natl Acad Sci U S A* **107:** 16303-16308

Bedard KM, Wang ML, Proll SC, Loo YM, Katze MG, Gale M, Iadonato SP (2012) Isoflavone Agonists of IRF-3 Dependent Signaling Have Antiviral Activity against RNA Viruses. *J Virol* **86:** 7334-7344

Beljanski V, Chiang C, Kirchenbaum GA, Olagnier D, Bloom CE, Wong T, Haddad EK, Trautmann L, Ross TM, Hiscott J (2015) Enhanced Influenza Virus-Like Particle Vaccination with a Structurally Optimized RIG-I Agonist as Adjuvant. *J Virol* **89:** 10612-10624

Berke IC, Modis Y (2012) MDA5 cooperatively forms dimers and ATP-sensitive filaments upon binding double-stranded RNA. *The EMBO journal* **31:** 1714-1726

Besch R, Poeck H, Hohenauer T, Senft D, Hacker G, Berking C, Hornung V, Endres S, Ruzicka T, Rothenfusser S, Hartmann G (2009) Proapoptotic signaling induced by RIG-I and MDA-5 results in type I interferon-independent apoptosis in human melanoma cells. *J Clin Invest* **119:** 2399-2411

Biesiada M, Pachulska-Wieczorek K, Adamiak RW, Purzycka KJ (2016a) RNAComposer and RNA 3D structure prediction for nanotechnology. *Methods* **103:** 120-127

Biesiada M, Purzycka KJ, Szachniuk M, Blazewicz J, Adamiak RW (2016b) Automated RNA 3D Structure Prediction with RNAComposer. *Methods in molecular biology* **1490:** 199-215

Bird L (2018) Reigning in RIG-I. *Nature reviews Immunology* **18:** 357

Bisaillon M, Bergeron J, Lemay G (1997) Characterization of the nucleoside triphosphate phosphohydrolase and helicase activities of the reovirus lambda1 protein. *J Biol Chem* **272:** 18298-18303

Borodavka A, Tuma R, Stockley PG (2012) Evidence that viral RNAs have evolved for efficient, two-stage packaging. *P Natl Acad Sci USA* **109:** 15769-15774

Bozym RA, Delorme-Axford E, Harris K, Morosky S, Ikizler M, Dermody TS, Sarkar SN, Coyne CB (2012) Focal adhesion kinase is a component of antiviral RIG-I-like receptor signaling. *Cell Host Microbe* **11:** 153-166

Brown WL, Mastico RA, Wu M, Heal KG, Adams CJ, Murray JB, Simpson JC, Lord JM, Taylor-Robinson AW, Stockley PG (2002) RNA bacteriophage capsid-mediated drug delivery and epitope presentation. *Intervirology* **45:** 371-380

Bruns Annie M, Leser George P, Lamb Robert A, Horvath Curt M (2014) The Innate Immune Sensor LGP2 Activates Antiviral Signaling by Regulating MDA5-RNA Interaction and Filament Assembly. *Molecular cell* **55:** 771-781

Burnett JC, Rossi JJ (2012) RNA-based therapeutics: current progress and future prospects. *Chemistry & biology* **19:** 60-71

Cadena C, Hur S (2017) Antiviral Immunity and Circular RNA: No End in Sight. *Mol Cell* **67:** 163-164

Cao W, Zhang L, Rosen DB, Bover L, Watanabe G, Bao M, Lanier LL, Liu YJ (2007) BDCA2/Fc epsilon RI gamma complex signals through a novel BCR-like pathway in human plasmacytoid dendritic cells. *PLoS biology* **5:** e248

Cardenas WB, Loo YM, Gale M, Hartman AL, Kimberlin CR, Martinez-Sobrido L, Saphire EO, Basler CF (2006) Ebola virus VP35 protein binds double-stranded RNA and inhibits alpha/beta interferon production induced by RIG-I signaling. *J Virol* **80:** 5168-5178

Castanier C, Garcin D, Vazquez A, Arnoult D (2010) Mitochondrial dynamics regulate the RIG-I-like receptor antiviral pathway. *Embo Rep* **11:** 133-138

Chae JJ, Wood G, Masters SL, Richard K, Park G, Smith BJ, Kastner DL (2006) The B30.2 domain of pyrin, the familial Mediterranean fever protein, interacts directly with caspase-1 to modulate IL-1 beta production. *P Natl Acad Sci USA* **103:** 9982-9987

Chan YK, Gack MU (2016) A phosphomimetic-based mechanism of dengue virus to antagonize innate immunity. *Nat Immunol* **17:** 523-530

Chau TA, McCully ML, Brintnell W, An G, Kasper KJ, Vines ED, Kubes P, Haeryfar SMM, McCormick JK, Cairns E, Heinrichs DE, Madrenas J (2009) Toll-like receptor 2 ligands on the staphylococcal cell wall downregulate superantigen-induced T cell activation and prevent toxic shock syndrome. *Nat Med* **15:** 641-U143

Chazal M, Beauclair G, Gracias S, Najburg V, Simon-Loriere E, Tangy F, Komarova AV, Jouvenet N (2018) RIG-I Recognizes the 5' Region of Dengue and Zika Virus Genomes. *Cell reports* **24:** 320-328

Chen H, Li Y, Zhang J, Ran Y, Wei J, Yang Y, Shu H-B (2013a) RAVER1 is a coactivator of MDA5-mediated cellular antiviral response. *J Mol Cell Biol* **5:** 111-119

Chen HW, Yang YK, Xu H, Yang WW, Zhai ZH, Chen DY (2015) Ring finger protein 166 potentiates RNA virus-induced interferon-beta production via enhancing the ubiquitination of TRAF3 and TRAF6. *Scientific reports* **5**

Chen WL, Han CF, Xie B, Hu X, Yu Q, Shi LY, Wang QQ, Li DL, Wang JL, Zheng P, Liu Y, Cao XT (2013b) Induction of Siglec-G by RNA Viruses Inhibits the Innate Immune Response by Promoting RIG-I Degradation. *Cell* **152:** 467-478

Chen X, Yang X, Zheng Y, Yang Y, Xing Y, Chen Z (2014) SARS coronavirus papain-like protease inhibits the type I interferon signaling pathway through interaction with the STING-TRAF3-TBK1 complex. *Protein & cell* **5:** 369-381

Chen ZJJ (2005) Ubiquitin signalling in the NF-kappa B pathway. *Nat Cell Biol* **7:** 758-U719

Chiang C, Beljanski V, Yin K, Olagnier D, Ben Yebdri F, Steel C, Goulet ML, DeFilippis VR, Streblow DN, Haddad EK, Trautmann L, Ross T, Lin RT, Hiscott J (2015) Sequence-Specific Modifications Enhance the Broad-Spectrum Antiviral Response Activated by RIG-I Agonists. *J Virol* **89:** 8011-8025

Childs K, Randall R, Goodbourn S (2012) Paramyxovirus V Proteins Interact with the RNA Helicase LGP2 To Inhibit RIG-I-Dependent Interferon Induction. *J Virol* **86:** 3411-3421

Childs K, Stock N, Ross C, Andrejeva J, Hilton L, Skinner M, Randall R, Goodbourn S (2007) mda-5, but not RIG-I, is a common target for paramyxovirus V proteins. *Virology* **359:** 190-200

Childs KS, Andrejeva J, Randall RE, Goodbourn S (2009) Mechanism of mda-5 Inhibition by Paramyxovirus V Proteins. *J Virol* **83:** 1465-1473

Chiu YH, MacMillan JB, Chen ZJJ (2009) RNA Polymerase III Detects Cytosolic DNA and Induces Type I Interferons through the RIG-I Pathway. *Cell* **138:** 576-591

Choi SJ, Lee HC, Kim JH, Park SY, Kim TH, Lee WK, Jang DJ, Yoon JE, Choi YI, Kim S, Ma J, Kim CJ, Yao TP, Jung JU, Lee JY, Lee JS (2016) HDAC6 regulates cellular viral RNA sensing by deacetylation of RIG-I. *Embo Journal* **35:** 429-442

Christensen ND, Dillner J, Eklund C, Carter JJ, Wipf GC, Reed CA, Cladel NM, Galloway DA (1996) Surface conformational and linear epitopes on HPV-16 and HPV-18 L1 virus-like particles as defined by monoclonal antibodies. *Virology* **223:** 174-184

Civril F, Bennett M, Moldt M, Deimling T, Witte G, Schiesser S, Carell T, Hopfner KP (2011) The RIG-I ATPase domain structure reveals insights into ATP-dependent antiviral signalling. *Embo Rep* **12:** 1127-1134

Clements CJ, Griffiths E (2002) The global impact of vaccines containing aluminium adjuvants. *Vaccine* **20 Suppl 3:** S24-33

Cubas R, Zhang S, Kwon SK, Sevick-Muraca EM, Li M, Chen CY, Yao QZ (2009) Virus-like Particle (VLP) Lymphatic Trafficking and Immune Response Generation After Immunization by Different Routes. *J Immunother* **32:** 118-128

Cui J, Song Y, Li Y, Zhu Q, Tan P, Qin Y, Wang HY, Wang RF (2014) USP3 inhibits type I interferon signaling by deubiquitinating RIG-I-like receptors. *Cell research* **24:** 400-416

Cui S, Eisenacher K, Kirchhofer A, Brzozka K, Lammens A, Lammens K, Fujita T, Conzelmann KK, Krug A, Hopfner KP (2008) The C-terminal regulatory domain is the RNA 5 '-triphosphate sensor of RIG-I. *Mol Cell* **29:** 169-179

Dambuza IM, Brown GD (2015) C-type lectins in immunity: recent developments. *Current opinion in immunology* **32:** 21-27

Das A, Dinh PX, Panda D, Pattnaik AK (2014) Interferon-Inducible Protein IFI35 Negatively Regulates RIG-I Antiviral Signaling and Supports Vesicular Stomatitis Virus Replication. *J Virol* **88:** 3103-3113

Davis WG, Bowzard JB, Sharma SD, Wiens ME, Ranjan P, Gangappa S, Stuchlik O, Pohl J, Donis RO, Katz JM, Cameron CE, Fujita T, Sambhara S (2012) The 3' untranslated regions of influenza genomic sequences are 5'PPP-independent ligands for RIG-I. *Plos One* **7:** e32661

Denes A, Lopez-Castejon G, Brough D (2012) Caspase-1: is IL-1 just the tip of the ICEberg? *Cell Death Dis* **3**

Deretic V (2011) Autophagy in immunity and cell-autonomous defense against intracellular microbes. *Immunol Rev* **240:** 92-104

Deschuyteneer M, Elouahabi A, Plainchamp D, Plisnier M, Soete D, Corazza Y, Lockman L, Giannini S, Deschamps M (2010) Molecular and structural characterization of the L1 virus-like particles that are used as vaccine antigens in Cervarix (TM), the AS04-adjuvanted HPV-16 and-18 cervical cancer vaccine. *Hum Vaccines* **6:** 407-419

Devarkar SC, Wang C, Miller MT, Ramanathan A, Jiang F, Khan AG, Patel SS, Marcotrigiano J (2016) Structural basis for m7G recognition and 2'-O-methyl discrimination in capped RNAs by the innate immune receptor RIG-I. *Proc Natl Acad Sci U S A* **113:** 596-601

Diederichs K, Karplus PA (1997) Improved R-factors for diffraction data analysis in macromolecular crystallography. *Nat Struct Biol* **4:** 269-275

Dillon PM, Petroni GR, Smolkin ME, Brenin DR, Chianese-Bullock KA, Smith KT, Olson WC, Fanous IS, Nail CJ, Brenin CM, Hall EH, Slingluff CL (2017) A pilot study of the immunogenicity of a 9-peptide breast cancer vaccine plus poly-ICLC in early stage breast cancer. *J Immunother Cancer* **5**

Drickamer K, Fadden AJ (2002) Genomic analysis of C-type lectins. *Biochemical Society symposium***:** 59-72

Duewell P, Steger A, Lohr H, Bourhis H, Hoelz H, Kirchleitner SV, Stieg MR, Grassmann S, Kobold S, Siveke JT, Endres S, Schnurr M (2014) RIG-I-like helicases induce immunogenic cell death of pancreatic cancer cells and sensitize tumors toward killing by CD8(+) T cells (vol 21, pg 1825, 2014). *Cell Death Differ* **21:** 1984-1984

Dupuis M, Murphy TJ, Higgins D, Ugozzoli M, van Nest G, Ott G, McDonald DM (1998) Dendritic cells internalize vaccine adjuvant after intramuscular injection. *Cellular immunology* **186:** 18-27

Dvorak HF, Flier J, Frank H (1986) Tumors - Wounds That Do Not Heal - Similarities between Tumor Stroma Generation and Wound-Healing. *New Engl J Med* **315:** 1650-1659

Dykeman EC, Stockley PG, Twarock R (2013) Packaging signals in two single-stranded RNA viruses imply a conserved assembly mechanism and geometry of the packaged genome. *J Mol Biol* **425:** 3235-3249

Elinav E, Strowig T, Kau AL, Henao-Mejia J, Thaiss CA, Booth CJ, Peaper DR, Bertin J, Eisenbarth SC, Gordon JI, Flavell RA (2011) NLRP6 Inflammasome Regulates Colonic Microbial Ecology and Risk for Colitis. *Cell* **145:** 745-757

Elion DL, Cook RS (2018) Harnessing RIG-I and intrinsic immunity in the tumor microenvironment for therapeutic cancer treatment. *Oncotarget* **9:** 29007-29017

Ellermeier J, Wei J, Duewell P, Hoves S, Stieg MR, Adunka T, Noerenberg D, Anders HJ, Mayr D, Poeck H, Hartmann G, Endres S, Schnurr M (2013) Therapeutic efficacy of bifunctional siRNA combining TGF-beta1 silencing with RIG-I activation in pancreatic cancer. *Cancer research* **73:** 1709-1720

Errett JS, Suthar MS, McMillan A, Diamond MS, Gale M, Jr. (2013) The essential, nonredundant roles of RIG-I and MDA5 in detecting and controlling West Nile virus infection. *J Virol* **87:** 11416-11425

Evans PR (2007) An introduction to stereochemical restraints. *Acta crystallographica Section D, Biological crystallography* **63:** 58-61

Evans PR (2011) An introduction to data reduction: space-group determination, scaling and intensity statistics. *Acta crystallographica Section D, Biological crystallography* **67:** 282-292

Fan Y, Mao R, Yu Y, Liu S, Shi Z, Cheng J, Zhang H, An L, Zhao Y, Xu X, Chen Z, Kogiso M, Zhang D, Zhang H, Zhang P, Jung JU, Li X, Xu G, Yang J (2014) USP21 negatively regulates antiviral response by acting as a RIG-I deubiquitinase. *The Journal of experimental medicine* **211:** 313-328

Fang R, Jiang QF, Zhou X, Wang CG, Guan YK, Tao JL, Xi JZ, Feng JM, Jiang ZF (2017) MAVS activates TBK1 and IKK epsilon through TRAFs in NEMO dependent and independent manner. *Plos Pathog* **13**

Feng Q, Hato SV, Langereis MA, Zoll J, Virgen-Slane R, Peisley A, Hur S, Semler BL, van Rij RP, van Kuppeveld FJM (2012) MDA5 Detects the Double-Stranded RNA Replicative Form in Picornavirus-Infected Cells. *Cell reports* **2:** 1187-1196

Fiuza C, Suffredini AF (2001) Human models of innate immunity: local and systemic inflammatory responses. *Journal of endotoxin research* **7:** 385-388

Foy E, Li K, Wang C, Sumpter R, Jr., Ikeda M, Lemon SM, Gale M, Jr. (2003) Regulation of interferon regulatory factor-3 by the hepatitis C virus serine protease. *Science* **300:** 1145-1148

Franchi L, Eigenbrod T, Munoz-Planillo R, Nunez G (2009) The inflammasome: a caspase-1-activation platform that regulates immune responses and disease pathogenesis. *Nature immunology* **10:** 241-247

Friedman CS, O'Donnell MA, Legarda-Addison D, Ng A, Cardenas WB, Yount JS, Moran TM, Basler CF, Komuro A, Horvath CM, Xavier R, Ting AT (2008) The tumour suppressor CYLD is a negative regulator of RIG-I-mediated antiviral response. *Embo Rep* **9:** 930-936

Fujita K, Nakai Y, Kawashima A, Ujike T, Nagahara A, Nakajima T, Inoue T, Lee CM, Uemura M, Miyagawa Y, Kaneda Y, Nonomura N (2017) Phase I/II clinical trial to assess safety and efficacy of intratumoral and subcutaneous injection of HVJ-E in castration-resistant prostate cancer patients. *Cancer gene therapy* **24:** 277-281

Gack MU, Nistal-Villan E, Inn KS, Garcia-Sastre A, Jung JU (2010) Phosphorylation-Mediated Negative Regulation of RIG-I Antiviral Activity. *J Virol* **84:** 3220-3229

Gack MU, Shin YC, Joo CH, Urano T, Liang C, Sun LJ, Takeuchi O, Akira S, Chen ZJ, Inoue SS, Jung JU (2007) TRIM25 RING-finger E3 ubiquitin ligase is essential for RIG-I-mediated antiviral activity. *Nature* **446:** 916-U912

Galarza JM, Latham T, Cupo A (2005) Virus-like particle (VLP) vaccine conferred complete protection against a lethal influenza virus challenge. *Viral Immunol* **18:** 244-251

Galaway FA, Stockley PG (2013) MS2 viruslike particles: a robust, semisynthetic targeted drug delivery platform. *Molecular pharmaceutics* **10:** 59-68

Garcea RL, Gissmann L (2004) Virus-like particles as vaccines and vessels for the delivery of small molecules. *Curr Opin Biotech* **15:** 513-517

Gay NJ, Gangloff M, Weber ANR (2006) Opinion - Toll-like receptors as molecular switches. *Nature Reviews Immunology* **6:** 693-698

Geijtenbeek TB, Gringhuis SI (2009) Signalling through C-type lectin receptors: shaping immune responses. *Nature reviews Immunology* **9:** 465-479

Geisberger R, Crameri R, Achatz G (2003) Models of signal transduction through the B-cell antigen receptor. *Immunology* **110:** 401-410

Georgens C, Weyermann J, Zimmer A (2005) Recombinant virus like particles as drug delivery system. *Curr Pharm Biotechno* **6:** 49-55

Gitlin L, Barchet W, Gilfillan S, Cella M, Beutler B, Flavell RA, Diamond MS, Colonna M (2006) Essential role of mda-5 in type I IFN responses to polyriboinosinic:polyribocytidylic acid and encephalomyocarditis picornavirus. *Proc Natl Acad Sci U S A* **103:** 8459-8464

Gleiter S, Lilie H (2003) Cell-type specific targeting and gene expression using a variant of polyoma VP1 virus-like particles. *Biological chemistry* **384:** 247-255

Golmohammadi R, Fridborg K, Bundule M, Valegard K, Liljas L (1996) The crystal structure of bacteriophage Q beta at 3.5 A resolution. *Structure* **4:** 543-554

Goubau D, Schlee M, Deddouche S, Pruijssers AJ, Zillinger T, Goldeck M, Schuberth C, Van der Veen AG, Fujimura T, Rehwinkel J, Iskarpatyoti JA, Barchet W, Ludwig J, Dermody TS, Hartmann G, Sousa CRE (2014) Antiviral immunity via RIG-I-mediated recognition of RNA bearing 5 '-diphosphates. *Nature* **514:** 372-+

Goulet ML, Olagnier D, Xu ZY, Paz S, Belgnaoui SM, Lafferty EI, Janelle V, Arguello M, Paquet M, Ghneim K, Richards S, Smith A, Wilkinson P, Cameron M, Kalinke U, Qureshi S, Lamarre A, Haddad EK, Sekaly RP, Peri S, Balachandran S, Lin RT, Hiscott J (2013) Systems Analysis of a RIG-I Agonist Inducing Broad Spectrum Inhibition of Virus Infectivity. *Plos Pathog* **9**

Gutjahr A, Tiraby G, Perouzel E, Verrier B, Paul S (2016) Triggering Intracellular Receptors for Vaccine Adjuvantation. *Trends in immunology* **37:** 716

Halfon P, Sarrazin C (2012) Future treatment of chronic hepatitis C with direct acting antivirals: is resistance important? *Liver international : official journal of the International Association for the Study of the Liver* **32 Suppl 1:** 79-87

Haller O, Kochs G, Weber F (2006) The interferon response circuit: induction and suppression by pathogenic viruses. *Virology* **344:** 119-130

Hartman AL, Bird BH, Towner JS, Antoniadou ZA, Zaki SR, Nichol ST (2008) Inhibition of IRF-3 activation by VP35 is critical for the high level of virulence of ebola virus. *J Virol* **82:** 2699-2704

Hashimoto C, Hudson KL, Anderson KV (1988) The Toll gene of Drosophila, required for dorsal-ventral embryonic polarity, appears to encode a transmembrane protein. *Cell* **52:** 269-279

Hayakawa S, Shiratori S, Yamato H, Kameyama T, Kitatsuji C, Kashigi F, Goto S, Kameoka S, Fujikura D, Yamada T, Mizutani T, Kazumata M, Sato M, Tanaka J, Asaka M, Ohba Y, Miyazaki T, Imamura M, Takaoka A (2010) ZAPS is a potent stimulator of signaling mediated by the RNA helicase RIG-I during antiviral responses. *Nat Immunol* **12:** 37

He SP, Zhao J, Song SS, He XJ, Minassian A, Zhou Y, Zhang JJ, Brulois K, Wang YQ, Cabo J, Zandi E, Liang CY, Jung JU, Zhang XW, Feng PH (2015) Viral Pseudo-Enzymes Activate RIG-I via Deamidation to Evade Cytokine Production. *Mol Cell* **58:** 134-146

He ZJ, Zhu X, Wen WT, Yuan J, Hu YW, Chen JH, An S, Dong XH, Lin CJ, Yu JC, Wu JH, Yang Y, Cai JC, Li J, Li MF (2016) Dengue Virus Subverts Host Innate Immunity by Targeting Adaptor Protein MAVS. *J Virol* **90:** 7219-7230

Heaton SM, Borg NA, Dixit VM (2016) Ubiquitin in the activation and attenuation of innate antiviral immunity. *Journal of Experimental Medicine* **213:** 1-13

Helminen O, Huhta H, Lehenkari PP, Saarnio J, Karttunen TJ, Kauppila JH (2016) Nucleic acid-sensing toll-like receptors 3, 7 and 8 in esophageal epithelium, barrett's esophagus, dysplasia and adenocarcinoma. *Oncoimmunology* **5**

Hirao I, Spingola M, Peabody D, Ellington AD (1998) The limits of specificity: an experimental analysis with RNA aptamers to MS2 coat protein variants. *Molecular diversity* **4:** 75-89

Hiscott J, Lin RT, Nakhaei P, Paz S (2006) MasterCARD: a priceless link to innate immunity. *Trends Mol Med* **12:** 53-56

Horner SM, Park HS, Gale M, Jr. (2012) Control of innate immune signaling and membrane targeting by the Hepatitis C virus NS3/4A protease are governed by the NS3 helix alpha0. *J Virol* **86:** 3112-3120

Hornung V, Ellegast J, Kim S, Brzozka K, Jung A, Kato H, Poeck H, Akira S, Conzelmann KK, Schlee M, Endres S, Hartmann G (2006) 5 '-triphosphate RNA is the ligand for RIG-I. *Science* **314:** 994-997

Hou J, Zhou Y, Zheng YY, Fan J, Zhou WP, Ng IOL, Sun HC, Qin LX, Qiu SJ, Lee JMF, Lo CM, Man K, Yang Y, Yang Y, Yang YY, Zhang Q, Zhu XH, Li N, Wang ZX, Ding GS, Zhuang SM, Zheng LM, Luo XL, Xie Y, Liang AM, Wang ZG, Zhang M, Xia Q, Liang TB, Yu YZ, Cao XT (2014) Hepatic RIG-I Predicts Survival and Interferon-alpha Therapeutic Response in Hepatocellular Carcinoma. *Cancer Cell* **25:** 49-63

Howell MD, Fitzsimons C, Smith PA (2018) JAK/STAT inhibitors and other small molecule cytokine antagonists for the treatment of allergic disease. *Ann Allerg Asthma Im* **120:** 367-375

Hu MM, Liao CY, Yang Q, Xie XQ, Shu HB (2017) Innate immunity to RNA virus is regulated by temporal and reversible sumoylation of RIG-I and MDA5. *Journal of Experimental Medicine* **214:** 973-989

Hung IFN, Zhang AJ, To KKW, Chan JFW, Li C, Zhu HS, Li P, Li C, Chan TC, Cheng VCC, Chan KH, Yuen KY (2014) Immunogenicity of Intradermal Trivalent Influenza Vaccine With Topical Imiquimod: A Double Blind Randomized Controlled Trial. *Clin Infect Dis* **59:** 1246-1255

Inn KS, Gack MU, Tokunaga F, Shi M, Wong LY, Iwai K, Jung JU (2011) Linear ubiquitin assembly complex negatively regulates RIG-I- and TRIM25-mediated type I interferon induction. *Mol Cell* **41:** 354-365

Iurescia S, Fioretti D, Rinaldi M (2018) Targeting Cytosolic Nucleic Acid-Sensing Pathways for Cancer Immunotherapies. *Front Immunol* **9**

Iwanaszko M, Kimmel M (2015) NF-kappaB and IRF pathways: cross-regulation on target genes promoter level. *BMC genomics* **16:** 307

Iwasaki A, Medzhitov R (2010) Regulation of adaptive immunity by the innate immune system. *Science* **327:** 291-295

Jain A, Jain SK (2008) PEGylation: An approach for drug delivery. A review. *Crit Rev Ther Drug* **25:** 403-447

Jankowsky E (2011) RNA helicases at work: binding and rearranging. *Trends in biochemical sciences* **36:** 19-29

Jennings GT, Bachmann MF (2008) The coming of age of virus-like particle vaccines. *Biological chemistry* **389:** 521-536

Jennings GT, Bachmann MF (2009) Immunodrugs: therapeutic VLP-based vaccines for chronic diseases. *Annual review of pharmacology and toxicology* **49:** 303-326

Jensen MA, Niewold TB (2015) Interferon regulatory factors: critical mediators of human lupus. *Translational research : the journal of laboratory and clinical medicine* **165:** 283-295

Jiang FG, Ramanathan A, Miller MT, Tang GQ, Gale M, Patel SS, Marcotrigiano J (2012a) Structural insights into RNA recognition and activation by innate immune pattern-recognition receptor RIG-I. *Faseb J* **26**

Jiang M, Zhang S, Yang Z, Lin H, Zhu J, Liu L, Wang W, Liu S, Liu W, Ma Y, Zhang L, Cao X (2018) Self-Recognition of an Inducible Host lncRNA by RIG-I Feedback Restricts Innate Immune Response. *Cell* **173:** 906-919 e913

Jiang QX, Chen ZJ (2012) Structural insights into the activation of RIG-I, a nanosensor for viral RNAs. *Embo Rep* **13:** 7-8

Jiang XM, Kinch LN, Brautigam CA, Chen X, Du FH, Grishin NV, Chen ZJJ (2012b) Ubiquitin-Induced Oligomerization of the RNA Sensors RIG-I and MDA5 Activates Antiviral Innate Immune Response. *Immunity* **36:** 959-973

Jones M, Cunningham ME, Wing P, DeSilva S, Challa R, Sheri A, Padmanabhan S, Iyer RP, Korba BE, Afdhal N, Foster GR (2017) SB 9200, a novel agonist of innate immunity, shows potent antiviral activity against resistant HCV variants. *Journal of Medical Virology* **89:** 1620-1628

Jounai N, Takeshita F, Kobiyama K, Sawano A, Miyawaki A, Xin KQ, Ishii KJ, Kawai T, Akira S, Suzuki K, Okuda K (2007) The Atg5 Atg12 conjugate associates with innate antiviral immune responses. *Proc Natl Acad Sci U S A* **104:** 14050-14055

Junt T, Barchet W (2015) Translating nucleic acid-sensing pathways into therapies. *Nature reviews Immunology* **15:** 529-544

Kabsch W (2010a) Integration, scaling, space-group assignment and post-refinement. *Acta crystallographica Section D, Biological crystallography* **66:** 133-144

Kabsch W (2010b) Xds. *Acta crystallographica Section D, Biological crystallography* **66:** 125-132

Kaczmarek JC, Kowalski PS, Anderson DG (2017) Advances in the delivery of RNA therapeutics: from concept to clinical reality. *Genome medicine* **9:** 60

Kaneda Y (2013) The RIG-I/MAVS signaling pathway in cancer cell-selective apoptosis. *Oncoimmunology* **2**

Kang JY, Lee JO (2011) Structural Biology of the Toll-Like Receptor Family. *Annual Review of Biochemistry, Vol 80* **80:** 917-941

Kato H, Takahasi K, Fujita T (2011) RIG-I-like receptors: cytoplasmic sensors for non-self RNA. *Immunol Rev* **243:** 91-98

Kato H, Takeuchi O, Mikamo-Satoh E, Hirai R, Kawai T, Matsushita K, Hiiragi A, Dermody TS, Fujita T, Akira S (2008) Length-dependent recognition of double-stranded ribonucleic acids by retinoic acid-inducible gene-I and melanoma differentiation-associated gene 5. *The Journal of experimental medicine* **205:** 1601-1610

Kato H, Takeuchi O, Sato S, Yoneyama M, Yamamoto M, Matsui K, Uematsu S, Jung A, Kawai T, Ishii KJ, Yamaguchi O, Otsu K, Tsujimura T, Koh CS, Reis e Sousa C, Matsuura Y, Fujita T, Akira S (2006) Differential roles of MDA5 and RIG-I helicases in the recognition of RNA viruses. *Nature* **441:** 101-105

Kawaguchi Y, Miyamoto Y, Inoue T, Kaneda Y (2009) Efficient eradication of hormone-resistant human prostate cancers by inactivated Sendai virus particle. *Int J Cancer* **124:** 2478-2487

Kawai T, Takahashi K, Sato S, Coban C, Kumar H, Kato H, Ishii KJ, Takeuchi O, Akira S (2005) IPS-1, an adaptor triggering RIG-I- and Mda5-mediated type I interferon induction. *Nat Immunol* **6:** 981-988

Kell AM, Gale M, Jr. (2015) RIG-I in RNA virus recognition. *Virology* **479-480:** 110-121

Keller M, Ruegg A, Werner S, Beer HD (2008) Active caspase-1 is a regulator of unconventional protein secretion. *Cell* **132:** 818-831

Keppel TR, Weis DD (2015) Mapping Residual Structure in Intrinsically Disordered Proteins at Residue Resolution Using Millisecond Hydrogen/Deuterium Exchange and Residue Averaging. *Journal of the American Society for Mass Spectrometry* **26:** 547-554

Kiianitsa K, Solinger JA, Heyer WD (2003) NADH-coupled microplate photometric assay for kinetic studies of ATP-hydrolyzing enzymes with low and high specific activities. *Anal Biochem* **321:** 266-271

Kimchi-Sarfaty C, Arora M, Sandalon Z, Oppenheim A, Gottesman MM (2003) High cloning capacity of in vitro packaged SV40 vectors with no SV40 virus sequences. *Hum Gene Ther* **14:** 167-177

Klarquist J, Hennies CM, Lehn MA, Reboulet RA, Feau S, Janssen EM (2014) STING-Mediated DNA Sensing Promotes Antitumor and Autoimmune Responses to Dying Cells. *J Immunol* **193:** 6124-6134

Kobayashi K, Inohara N, Hernandez LD, Galan JE, Nunez G, Janeway CA, Medzhitov R, Flavell RA (2002) RICK/Rip2/CARDIAK mediates signalling for receptors of the innate and adaptive immune systems. *Nature* **416:** 194-199

Kobayashi KS, van den Elsen PJ (2012) NLRC5: a key regulator of MHC class I-dependent immune responses. *Nat Rev Immunol* **12:** 813-820

Kohlway A, Luo DH, Rawling DC, Ding SC, Pyle AM (2013) Defining the functional determinants for RNA surveillance by RIG-I. *Embo Rep* **14:** 772-779

Kok KH, Lui PY, Ng MH, Siu KL, Au SW, Jin DY (2011) The double-stranded RNA-binding protein PACT functions as a cellular activator of RIG-I to facilitate innate antiviral response. *Cell Host Microbe* **9:** 299-309

Kolakofsky D, Kowalinski E, Cusack S (2012) A structure-based model of RIG-I activation. *Rna* **18:** 2118-2127

Komuro A, Horvath CM (2006) RNA- and virus-independent inhibition of antiviral signaling by RNA helicase LGP2. *Journal of virology* **80:** 12332-12342

Koonin EV, Aravind L (2000) The NACHT family - a new group of predicted NTPases implicated in apoptosis and MHC transcription activation. *Trends in biochemical sciences* **25:** 223-224

Korolowicz K, Balarezo M, Iyer R, Padmanabhan S, Cleary D, Gimi R, Sheri A, Suresh M, Yon C, Tucker R, Afdhal N, Menne S (2016a) Antiviral Efficacy and Host Immune Response Induction with Sb 9200, an Oral Prodrug of the Dinucleotide Sb 9000, in Combination with Entecavir in the Woodchuck Model of Chronic Hepatitis B. *J Hepatol* **64:** S602-S602

Korolowicz KE, Iyer RP, Czerwinski S, Suresh M, Yang JM, Padmanabhan S, Sheri A, Pandey RK, Skell J, Marquis JK, Kallakury BV, Tucker RD, Menne S (2016b) Antiviral Efficacy and Host Innate Immunity Associated with SB 9200 Treatment in the Woodchuck Model of Chronic Hepatitis B. *Plos One* **11**

Kowalinski E, Lunardi T, McCarthy AA, Louber J, Brunel J, Grigorov B, Gerlier D, Cusack S (2011) Structural basis for the activation of innate immune pattern-recognition receptor RIG-I by viral RNA. *Cell* **147:** 423-435

Kuniyoshi K, Takeuchi O, Pandey S, Satoh T, Iwasaki H, Akira S, Kawai T (2014) Pivotal role of RNA-binding E3 ubiquitin ligase MEX3C in RIG-I-mediated antiviral innate immunity. *P Natl Acad Sci USA* **111:** 5646-5651

Lachelt U, Kos P, Mickler FM, Herrmann A, Salcher EE, Rodl W, Badgujar N, Brauchle C, Wagner E (2014) Fine-tuning of proton sponges by precise diaminoethanes and histidines in pDNA polyplexes. *Nanomed-Nanotechnol* **10:** 35-44

Lassig C, Matheisl S, Sparrer KMJ, Mann CCD, Moldt M, Patel JR, Goldeck M, Hartmann G, Garcia-Sastre A, Hornung V, Conzelmann KK, Beckmann R, Hopfner KP (2015) ATP hydrolysis by the viral RNA sensor RIG-I prevents unintentional recognition of self-RNA. *eLife* **4**

Latz E, Verma A, Visintin A, Gong M, Sirois CM, Klein DCG, Monks BG, McKnight CJ, Lamphier MS, Duprex WP, Espevik T, Golenbock DT (2007) Ligand-induced conformational changes allosterically activate Toll-like receptor 9 (vol 8, pg 772, 2007). *Nature immunology* **8:** 1266-1266

Lee J, Park EB, Min J, Sung E, Jang Y, Shin JS, Chun D, Kim KH, Hwang J, Lee MK, Go YY, Kwon D, Kim M, Kang SJ, Choi BS (2018) Systematic editing of synthetic RIG-I ligands to produce effective antiviral and anti-tumor RNA immunotherapies. *Nucleic Acids Res* **46:** 1635-1647

Lee MH, Lalwani P, Raftery MJ, Matthaei M, Lutteke N, Kirsanovs S, Binder M, Ulrich RG, Giese T, Wolff T, Kruger DH, Schonrich G (2011) RNA helicase retinoic acid-inducible gene I as a sensor of Hantaan virus replication. *J Gen Virol* **92:** 2191-2200

Lee NR, Kim HI, Choi MS, Yi CM, Inn KS (2015) Regulation of MDA5-MAVS Antiviral Signaling Axis by TRIM25 through TRAF6-Mediated NF-kappa B Activation. *Mol Cells* **38:** 759-764

Lee S, Nguyen MT (2015) Recent advances of vaccine adjuvants for infectious diseases. *Immune network* **15:** 51-57

Lei Y, Wen HT, Yu YB, Taxman DJ, Zhang L, Widman DG, Swanson KV, Wen KW, Damania B, Moore CB, Giguere PM, Siderovski DP, Hiscott J, Razani B, Semenkovich CF, Chen X, Ting JPY (2012) The Mitochondrial Proteins NLRX1 and TUFM Form a Complex that Regulates Type I Interferon and Autophagy. *Immunity* **36:** 933-946

Lemaitre B, Nicolas E, Michaut L, Reichhart JM, Hoffmann JA (1996) The dorsoventral regulatory gene cassette spatzle/Toll/cactus controls the potent antifungal response in Drosophila adults. *Cell* **86:** 973-983

Li D, Gale RP, Liu Y, Lei B, Wang Y, Diao D, Zhang M (2017) 5'-Triphosphate siRNA targeting MDR1 reverses multi-drug resistance and activates RIG-I-induced immune-stimulatory and apoptotic effects against human myeloid leukaemia cells. *Leukemia research* **58:** 23-30

Li H, Chiappinelli KB, Guzzetta AA, Easwaran H, Yen RW, Vatapalli R, Topper MJ, Luo J, Connolly RM, Azad NS, Stearns V, Pardoll DM, Davidson N, Jones PA, Slamon DJ, Baylin SB, Zahnow CA, Ahuja N (2014) Immune regulation by low doses of the DNA methyltransferase inhibitor 5-azacitidine in common human epithelial cancers. *Oncotarget* **5:** 587-598

Li MT, Di W, Xu H, Yang YK, Chen HW, Zhang FX, Zhai ZH, Chen DY (2013) Negative Regulation of RIG-I-Mediated Innate Antiviral Signaling by SEC14L1. *J Virol* **87:** 10037-10046

Li SW, Zhang J, Li YA, Ou SH, Huang GY, Huang GY, He ZQ, Ge SX, Xian YL, Pang SQ, Ng MH, Xia NS (2005) A bacterially expressed particulate hepatitis E vaccine: antigenicity, immunogenicity and protectivity on primates. *Vaccine* **23:** 2893-2901

Li X, Ranjith-Kumar CT, Brooks MT, Dharmaiah S, Herr AB, Kao C, Li P (2009a) The RIG-I-like receptor LGP2 recognizes the termini of double-stranded RNA. *J Biol Chem* **284:** 13881-13891

Li XJ, Lu C, Stewart M, Xu HY, Strong RK, Igumenova T, Li PW (2009b) Structural basis of double-stranded RNA recognition by the RIG-I like receptor MDA5. *Arch Biochem Biophys* **488:** 23-33

Lieberman J (2018) Tapping the RNA world for therapeutics. *Nat Struct Mol Biol* **25:** 357-364

Liepold L, Anderson S, Willits D, Oltrogge L, Frank JA, Douglas T, Young M (2007) Viral capsids as MRI contrast agents. *Magn Reson Med* **58:** 871-879

Lim F, Peabody DS (1994) Mutations That Increase the Affinity of a Translational Repressor for Rna. *Nucleic Acids Res* **22:** 3748-3752

Lim F, Spingola M, Peabody DS (1996) The RNA-binding site of bacteriophage Q beta coat protein. *J Biol Chem* **271:** 31839-31845

Linehan MM, Dickey TH, Molinari ES, Fitzgerald ME, Potapova O, Iwasaki A, Pyle AM (2018) A minimal RNA ligand for potent RIG-I activation in living mice. *Sci Adv* **4**

Liu GQ, Park HS, Pyo HM, Liu Q, Zhou Y (2015a) Influenza A Virus Panhandle Structure Is Directly Involved in RIG-I Activation and Interferon Induction. *J Virol* **89:** 6067-6079

Liu H, Moynihan KD, Zheng Y, Szeto GL, Li AV, Huang B, Van Egeren DS, Park C, Irvine DJ (2014) Structure-based programming of lymph-node targeting in molecular vaccines. *Nature* **507:** 519-522

Liu HM, Jiang FG, Loo YM, Hsu SZ, Hsiang TY, Marcotrigiano J, Gale M (2016) Regulation of Retinoic Acid Inducible Gene-I (RIG-I) Activation by the Histone Deacetylase 6. *Ebiomedicine* **9:** 195-206

Liu HM, Loo YM, Horner SM, Zornetzer GA, Katze MG, Gale M (2012) The Mitochondrial Targeting Chaperone 14-3-3 epsilon Regulates a RIG-I Translocon that Mediates Membrane Association and Innate Antiviral Immunity. *Cell Host Microbe* **11:** 528-537

Liu S, Chen J, Cai X, Wu J, Chen X, Wu YT, Sun L, Chen ZJ (2013) MAVS recruits multiple ubiquitin E3 ligases to activate antiviral signaling cascades. *eLife* **2:** e00785

Liu X, Luo DY, Yang N (2015b) Cytosolic Low Molecular Weight FGF2 Orchestrates RIG-I-Mediated Innate Immune Response. *J Immunol* **195:** 4943-4952

LoBue AD, Lindesmith L, Yount B, Harrington PR, Thompson JM, Johnston RE, Moe CL, Baric RS (2006) Multivalent norovirus vaccines induce strong mucosal and systemic blocking antibodies against multiple strains. *Vaccine* **24:** 5220-5234

Loo YM, Fornek J, Crochet N, Bajwa G, Perwitasari O, Martinez-Sobrido L, Akira S, Gill MA, Garcia-Sastre A, Katze MG, Gale M, Jr. (2008) Distinct RIG-I and MDA5 signaling by RNA viruses in innate immunity. *J Virol* **82:** 335-345

Loo YM, Owen DM, Li K, Erickson AK, Johnson CL, Fish PM, Carney DS, Wang T, Ishida H, Yoneyama M, Fujita T, Saito T, Lee WM, Hagedorn CH, Lau DT, Weinman SA, Lemon SM, Gale M, Jr. (2006) Viral and therapeutic control of IFN-beta promoter stimulator 1 during hepatitis C virus infection. *Proc Natl Acad Sci U S A* **103:** 6001-6006

Louber J, Brunel J, Uchikawa E, Cusack S, Gerlier D (2015) Kinetic discrimination of self/non-self RNA by the ATPase activity of RIG-I and MDA5. *BMC biology* **13:** 54

Lu C, Ranjith-Kumar CT, Hao L, Kao CC, Li P (2011) Crystal structure of RIG-I C-terminal domain bound to blunt-ended double-strand RNA without 5' triphosphate. *Nucleic Acids Res* **39:** 1565-1575

Lua LHL, Connors NK, Sainsbury F, Chuan YP, Wibowo N, Middelberg APJ (2014) Bioengineering Virus-Like Particles as Vaccines. *Biotechnol Bioeng* **111:** 425-440

Luo D, Kohlway A, Pyle AM (2013) Duplex RNA activated ATPases (DRAs): platforms for RNA sensing, signaling and processing. *RNA biology* **10:** 111-120

Luo D, Xu T, Hunke C, Gruber G, Vasudevan SG, Lescar J (2008) Crystal structure of the NS3 protease-helicase from dengue virus. *Journal of virology* **82:** 173-183

Luo DH (2014) Toward a crystal-clear view of the viral RNA sensing and response by RIG-I-like receptors. *RNA biology* **11:** 25-32

Luo DH, Ding SC, Vela A, Kohlway A, Lindenbach BD, Pyle AM (2011) Structural Insights into RNA Recognition by RIG-I. *Cell* **147:** 409-422

Luthra P, Ramanan P, Mire CE, Weisend C, Tsuda Y, Yen BJM, Liu G, Leung DW, Geisbert TW, Ebihara H, Amarasinghe GK, Basler CF (2013) Mutual Antagonism between the Ebola Virus VP35 Protein and the RIG-I Activator PACT Determines Infection Outcome. *Cell Host Microbe* **14:** 74-84

Machida K, Imataka H (2015) Production methods for viral particles. *Biotechnol Lett* **37:** 753-760

Maharaj NP, Wies E, Stoll A, Gack MU (2012) Conventional protein kinase C-alpha (PKC-alpha) and PKC-beta negatively regulate RIG-I antiviral signal transduction. *J Virol* **86:** 1358-1371

Malathi K, Dong B, Gale M, Jr., Silverman RH (2007) Small self-RNA generated by RNase L amplifies antiviral innate immunity. *Nature* **448:** 816-819

Malathi K, Saito T, Crochet N, Barton DJ, Gale M, Silverman RH (2010) RNase L releases a small RNA from HCV RNA that refolds into a potent PAMP. *Rna-a Publication of the Rna Society* **16:** 2108-2119

Malur M, Gale M, Krug RM (2012) LGP2 Downregulates Interferon Production during Infection with Seasonal Human Influenza A Viruses That Activate Interferon Regulatory Factor 3. *J Virol* **86:** 10733-10738

Mancini RJ, Stutts L, Ryu KA, Tom JK, Esser-Kahn AP (2014) Directing the immune system with chemical compounds. *ACS chemical biology* **9:** 1075-1085

Mao AP, Li S, Zhong B, Li Y, Yan J, Li Q, Teng CW, Shu HB (2010) Virus-triggered Ubiquitination of TRAF3/6 by cIAP1/2 Is Essential for Induction of Interferon-beta (IFN-beta) and Cellular Antiviral Response. *Journal of Biological Chemistry* **285:** 9470-9476

Marais DJ, Sampson C, Jeftha A, Dhaya D, Passmore JAS, Denny L, Rybicki EP, Van der Walt E, Stephen LXG, Williamson AL (2006) More men than women make mucosal IgA antibodies to Human papillomavirus type 16 (HPV-16) and HPV-18: a study of oral HPV and oral HPV antibodies in a normal healthy population. *Bmc Infect Dis* **6**

Martinez-Gil L, Goff PH, Hai R, Garcia-Sastre A, Shaw ML, Palese P (2013) A Sendai virus-derived RNA agonist of RIG-I as a virus vaccine adjuvant. *J Virol* **87:** 1290-1300

Martinon F, Burns K, Tschopp J (2002) The inflammasome: a molecular platform triggering activation of inflammatory caspases and processing of proIL-beta. *Mol Cell* **10:** 417-426

Masson GR, Jenkins ML, Burke JE (2017) An overview of hydrogen deuterium exchange mass spectrometry (HDX-MS) in drug discovery. *Expert opinion on drug discovery* **12:** 981-994

Matei D, Fang F, Shen C, Schilder J, Arnold A, Zeng Y, Berry WA, Huang T, Nephew KP (2012) Epigenetic resensitization to platinum in ovarian cancer. *Cancer research* **72:** 2197-2205

McCoy AJ (2007) Solving structures of protein complexes by molecular replacement with Phaser. *Acta crystallographica Section D, Biological crystallography* **63:** 32-41

McCoy AJ, Grosse-Kunstleve RW, Adams PD, Winn MD, Storoni LC, Read RJ (2007) Phaser crystallographic software. *Journal of applied crystallography* **40:** 658-674

Mehrotra S, Britten CD, Chin S, Garrett-Mayer E, Cloud CA, Li ML, Scurti G, Salem ML, Nelson MH, Thomas MB, Paulos CM, Salazar AM, Nishimura MI, Rubinstein MP, Li ZH, Cole DJ (2017) Vaccination with poly (IC: LC) and peptide-pulsed autologous dendritic cells in patients with pancreatic cancer. *J Hematol Oncol* **10**

Meylan E, Curran J, Hofmann K, Moradpour D, Binder M, Bartenschlager R, Tschopp R (2005) Cardif is an adaptor protein in the RIG-I antiviral pathway and is targeted by hepatitis C virus. *Nature* **437:** 1167-1172

Mi ZQ, Fu JH, Xiong YB, Tang H (2010) SUMOylation of RIG-I positively regulates the type I interferon signaling. *Protein & cell* **1:** 275-283

Miao EA, Rajan JV, Aderem A (2011) Caspase-1-induced pyroptotic cell death. *Immunological reviews* **243:** 206-214

Mills DR, Priano C, Merz PA, Binderow BD (1990) Q-Beta Rna Bacteriophage - Mapping Cis-Acting Elements within an Rna Genome. *J Virol* **64:** 3872-3881

Minamitani T, Iwakiri D, Takada K (2011) Adenovirus Virus-Associated RNAs Induce Type I Interferon Expression through a RIG-I-Mediated Pathway. *J Virol* **85:** 4035-4040

Miyashita M, Oshiumi H, Matsumoto M, Seya T (2011) DDX60, a DEXD/H box helicase, is a novel antiviral factor promoting RIG-I-like receptor-mediated signaling. *Molecular and cellular biology* **31:** 3802-3819

Modis Y, Berke I (2012) MDA5 cooperatively forms dimers and ATP-sensitive filaments upon binding double-stranded RNA. *J Immunol* **188**

Moore CB, Bergstralh DT, Duncan JA, Lei Y, Morrison TE, Zimmermann AG, Accavitti-Loper MA, Madden VJ, Sun L, Ye Z, Lich JD, Heise MT, Chen Z, Ting JPY (2008) NLRX1 is a regulator of mitochondrial antiviral immunity. *Nature* **451:** 573

Morefield GL, Sokolovska A, Jiang D, HogenEsch H, Robinson JP, Hem SL (2005) Role of aluminum-containing adjuvants in antigen internalization by dendritic cells in vitro. *Vaccine* **23:** 1588-1595

Morita M, Stamp G, Robins P, Dulic A, Rosewell I, Hrivnak G, Daly G, Lindahl T, Barnes DE (2004) Gene-targeted mice lacking the Trex1 (DNase III) 3'-->5' DNA exonuclease develop inflammatory myocarditis. *Molecular and cellular biology* **24:** 6719-6727

Mosca F, Tritto E, Muzzi A, Monaci E, Bagnoli F, Iavarone C, O'Hagan D, Rappuoli R, De Gregorio E (2008) Molecular and cellular signatures of human vaccine adjuvants. *Proc Natl Acad Sci U S A* **105:** 10501-10506

Motz C, Schuhmann KM, Kirchhofer A, Moldt M, Witte G, Conzelmann KK, Hopfner KP (2013) Paramyxovirus V Proteins Disrupt the Fold of the RNA Sensor MDA5 to Inhibit Antiviral Signaling. *Science* **339:** 690-693

Moynihan KD, Irvine DJ (2017) Roles for Innate Immunity in Combination Immunotherapies. *Cancer research* **77:** 5215-5221

Mulder AM, Carragher B, Towne V, Meng Y, Wang Y, Dieter L, Potter CS, Washabaugh MW, Sitrin RD, Zhao QJ (2012) Toolbox for Non-Intrusive Structural and Functional Analysis of Recombinant VLP Based Vaccines: A Case Study with Hepatitis B Vaccine. *Plos One* **7**

Munir M, Berg M (2013) The multiple faces of proteinkinase R in antiviral defense. *Virulence* **4:** 85-89

Myong S, Cui S, Cornish PV, Kirchhofer A, Gack MU, Jung JU, Hopfner KP, Ha T (2009) Cytosolic Viral Sensor RIG-I Is a 5 '-Triphosphate-Dependent Translocase on Double-Stranded RNA. *Science* **323:** 1070-1074

Nasirudeen AMA, Wong HH, Thien PL, Xu SL, Lam KP, Liu DX (2011) RIG-I, MDA5 and TLR3 Synergistically Play an Important Role in Restriction of Dengue Virus Infection. *PLoS neglected tropical diseases* **5**

Naskalska A, Pyrc K (2015) Virus Like Particles as Immunogens and Universal Nanocarriers. *Pol J Microbiol* **64:** 3-13

Navabi H, Jasani B, Reece A, Clayton A, Tabi Z, Donninger C, Mason M, Adams M (2009) A clinical grade poly I:C-analogue (Ampligen (R)) promotes optimal DC maturation and Th1-type T cell responses of healthy donors and cancer patients in vitro. *Vaccine* **27:** 107-115

Nguyen NTH, Now H, Kim WJ, Kim N, Yoo JY (2016) Ubiquitin-like modifier FAT10 attenuates RIG-I mediated antiviral signaling by segregating activated RIG-I from its signaling platform. *Sci Rep-Uk* **6**

Now H, Yoo JY (2011) A protein-kinase, IFN-inducible double-stranded RNA dependent inhibitor and repressor of p58 (PRKRIR) enhances type I IFN-mediated antiviral response through the stability control of RIG-I protein. *Biochem Bioph Res Co* **413:** 487-493

O'Neal CM, Clements JD, Estes MK, Conner ME (1998) Rotavirus 2/6 viruslike particles administered intranasally with cholera toxin, Escherichia coli heat-labile toxin (LT), and LT-R192G induce protection from rotavirus challenge. *J Virol* **72:** 3390-3393

Oh YK, Sohn T, Park JS, Kang MJ, Choi HG, Kim JA, Kim WK, Ko JJ, Kim CK (2004) Enhanced mucosal and systemic immunogenicity of human papillomavirus-like particles encapsidating interleukin-2 gene adjuvant. *Virology* **328:** 266-273

Okada H, Butterfield LH, Hamilton RL, Hoji A, Sakaki M, Ahn BJ, Kohanbash G, Drappatz J, Engh J, Amankulor N, Lively MO, Chan MD, Salazar AM, Shaw EG, Potter DM, Lieberman FS (2015) Induction of Robust Type-I CD8(+) T-cell Responses in WHO Grade 2 Low-Grade Glioma Patients Receiving Peptide-Based Vaccines in Combination with Poly-ICLC. *Clin Cancer Res* **21:** 286-294

Okamoto M, Tsukamoto H, Kouwaki T, Seya T, Oshiumi H (2017) Recognition of Viral RNA by Pattern Recognition Receptors in the Induction of Innate Immunity and Excessive Inflammation During Respiratory Viral Infections. *Viral Immunol* **30:** 408-420

Olafsdottir TA, Lingnau K, Nagy E, Jonsdottir I (2009) IC31, a two-component novel adjuvant mixed with a conjugate vaccine enhances protective immunity against pneumococcal disease in neonatal mice. *Scandinavian journal of immunology* **69:** 194-202

Olagnier D, Scholte FEM, Chiang C, Albulescu IC, Nichols C, He Z, Lin RT, Snijder EJ, van Hemert MJ, Hiscott J (2014) Inhibition of Dengue and Chikungunya Virus Infections by RIG-I-Mediated Type I Interferon-Independent Stimulation of the Innate Antiviral Response. *J Virol* **88:** 4180-4194

Oshiumi H, Matsumoto M, Hatakeyama S, Seya T (2009) Riplet/RNF135, a RING Finger Protein, Ubiquitinates RIG-I to Promote Interferon-beta Induction during the Early Phase of Viral Infection. *J Biol Chem* **284:** 807-817

Oshiumi H, Matsumoto M, Seya T (2012) Ubiquitin-mediated modulation of the cytoplasmic viral RNA sensor RIG-I. *Journal of biochemistry* **151:** 5-11

Oshiumi H, Miyashita M, Inoue N, Okabe M, Matsumoto M, Seya T (2010a) The Ubiquitin Ligase Riplet Is Essential for RIG-I-Dependent Innate Immune Responses to RNA Virus Infection. *Cell Host Microbe* **8:** 496-509

Oshiumi H, Miyashita M, Matsumoto M, Seya T (2013) A distinct role of Riplet-mediated K63-Linked polyubiquitination of the RIG-I repressor domain in human antiviral innate immune responses. *Plos Pathog* **9:** e1003533

Oshiumi H, Sakai K, Matsumoto M, Seya T (2010b) DEAD/H BOX 3 (DDX3) helicase binds the RIG-I adaptor IPS-1 to up-regulate IFN-beta-inducing potential. *European journal of immunology* **40:** 940-948

Page R (2008) Strategies for improving crystallization success rates. *Methods in molecular biology* **426:** 345-362

Palmer CR, Jacobson ME, Fedorova O, Pyle AM, Wilson JT (2018) Environmentally Triggerable Retinoic Acid-Inducible Gene I Agonists Using Synthetic Polymer Overhangs. *Bioconjug Chem* **29:** 742-747

Panne D (2008) The enhanceosome. *Curr Opin Struct Biol* **18:** 236-242

Pasare C, Medzhitov R (2005) Toll-like receptors: Linking innate and adaptive immunity. *Adv Exp Med Biol* **560:** 11-18

Pascal BD, Willis S, Lauer JL, Landgraf RR, West GM, Marciano D, Novick S, Goswami D, Chalmers MJ, Griffin PR (2012) HDX workbench: software for the analysis of H/D exchange MS data. *Journal of the American Society for Mass Spectrometry* **23:** 1512-1521

Patel JR, Jain A, Chou YY, Baum A, Ha T, Garcia-Sastre A (2013) ATPase-driven oligomerization of RIG-I on RNA allows optimal activation of type-I interferon. *Embo Rep* **14:** 780-787

Patel KG, Swartz JR (2011) Surface functionalization of virus-like particles by direct conjugation using azide-alkyne click chemistry. *Bioconjug Chem* **22:** 376-387

Pattabhi S, Wilkins CR, Dong R, Knoll ML, Posakony J, Kaiser S, Mire CE, Wang ML, Ireton RC, Geisbert TW, Bedard KM, Iadonato SP, Loo YM, Gale M (2016) Targeting Innate Immunity for Antiviral Therapy through Small Molecule Agonists of the RLR Pathway. *J Virol* **90:** 2372-2387

Paz S, Vilasco M, Werden SJ, Arguello M, Joseph-Pillai D, Zhao T, Nguyen TL, Sun Q, Meurs EF, Lin R, Hiscott J (2011) A functional C-terminal TRAF3-binding site in MAVS participates in positive and negative regulation of the IFN antiviral response. *Cell research* **21:** 895-910

Peabody DS (1997) Role of the coat protein-RNA interaction in the life cycle of bacteriophage MS2. *Molecular & general genetics : MGG* **254:** 358-364

Peisley A, Jo MH, Lin C, Wu B, Orme-Johnson M, Walz T, Hohng S, Hur S (2012) Kinetic mechanism for viral dsRNA length discrimination by MDA5 filaments. *Proc Natl Acad Sci U S A* **109:** E3340-3349

Peisley A, Lin C, Wu B, Orme-Johnson M, Liu MY, Walz T, Hur S (2011) Cooperative assembly and dynamic disassembly of MDA5 filaments for viral dsRNA recognition. *P Natl Acad Sci USA* **108:** 21010-21015

Peisley A, Wu B, Xu H, Chen ZJJ, Hur S (2014) Structural basis for ubiquitin-mediated antiviral signal activation by RIG-I. *Nature* **509:** 110-+

Peisley A, Wu B, Yao H, Walz T, Hur S (2013) RIG-I Forms Signaling-Competent Filaments in an ATP-Dependent, Ubiquitin-Independent Manner. *Mol Cell* **51:** 573-583

Pichlmair A, Schulz O, Tan CP, Rehwinkel J, Kato H, Takeuchi O, Akira S, Way M, Schiavo G, Sousa CRE (2009) Activation of MDA5 Requires Higher-Order RNA Structures Generated during Virus Infection. *J Virol* **83:** 10761-10769

Pippig DA, Hellmuth JC, Cui S, Kirchhofer A, Lammens K, Lammens A, Schmidt A, Rothenfusser S, Hopfner KP (2009) The regulatory domain of the RIG-I family ATPase LGP2 senses double-stranded RNA. *Nucleic Acids Res* **37:** 2014-2025

Plumet S, Herschke F, Bourhis JM, Valentin H, Longhi S, Gerlier D (2007) Cytosolic 5 '-Triphosphate Ended Viral Leader Transcript of Measles Virus as Activator of the RIG I-Mediated Interferon Response. *Plos One* **2**

Pohar J, Lainscek D, Kunsek A, Cajnko MM, Jerala R, Bencina M (2018) Phosphodiester backbone of the CpG motif within immunostimulatory oligodeoxynucleotides augments activation of Toll-like receptor 9 (vol 7, 14598, 2017). *Sci Rep-Uk* **8**

Pokorski JK, Hovlid ML, Finn MG (2011) Cell targeting with hybrid Qbeta virus-like particles displaying epidermal growth factor. *Chembiochem : a European journal of chemical biology* **12:** 2441-2447

Poltorak A, Ricciardi-Castagnoli P, Citterio S, Beutler B (2000) Physical contact between lipopolysaccharide and Toll-like receptor 4 revealed by genetic complementation. *P Natl Acad Sci USA* **97:** 2163-2167

Powell HR, Kara T, Jones CL (2007) Early experience with conversion to sirolimus in a pediatric renal transplant population. *Pediatr Nephrol* **22:** 1773-1777

Prins KC, Cardenas WB, Basler CF (2009) Ebola virus protein VP35 impairs the function of interferon regulatory factor-activating kinases IKKepsilon and TBK-1. *J Virol* **83:** 3069-3077

Probst P, Grigg JB, Wang M, Munoz E, Loo YM, Ireton RC, Gale M, Jr., Iadonato SP, Bedard KM (2017) A small-molecule IRF3 agonist functions as an influenza vaccine adjuvant by modulating the antiviral immune response. *Vaccine* **35:** 1964-1971

Puerta-Fernandez E, Romero-Lopez C, Barroso-delJesus A, Berzal-Herranz A (2003) Ribozymes: recent advances in the development of RNA tools. *FEMS microbiology reviews* **27:** 75-97

Pushko P, Tumpey TM, Bu F, Knell J, Robinson R, Smith G (2005) Influenza virus-like particles comprised of the HA, NA, and M1 proteins of H9N2 influenza virus induce protective immune responses in BALB/c mice. *Vaccine* **23:** 5751-5759

Rajsbaum R, Albrecht RA, Wang MK, Maharaj NP, Versteeg GA, Nistal-Villan E, Garcia-Sastre A, Gack MU (2012) Species-Specific Inhibition of RIG-I Ubiquitination and IFN Induction by the Influenza A Virus NS1 Protein. *Plos Pathog* **8**

Ramanathan A, Devarkar SC, Jiang F, Miller MT, Khan AG, Marcotrigiano J, Patel SS (2016) The autoinhibitory CARD2-Hel2i Interface of RIG-I governs RNA selection. *Nucleic Acids Res* **44:** 896-909

Ramos HJ, Gale M (2011) RIG-I like receptors and their signaling crosstalk in the regulation of antiviral immunity. *Current opinion in virology* **1:** 167-176

Ranjan P, Singh N, Kumar A, Neerincx A, Kremmer E, Cao W, Davis WG, Katz JM, Gangappa S, Lin R, Kufer TA, Sambhara S (2015) NLRC5 interacts with RIG-I to induce a robust antiviral response against influenza virus infection. *European journal of immunology* **45:** 758-772

Rawling DC, Fitzgerald ME, Pyle AM (2015) Establishing the role of ATP for the function of the RIG-I innate immune sensor. *eLife* **4**

Rawling DC, Kohlway AS, Luo DH, Ding SC, Pyle AM (2014) The RIG-I ATPase core has evolved a functional requirement for allosteric stabilization by the Pincer domain. *Nucleic Acids Res* **42:** 11601-11611

Rawling DC, Pyle AM (2014) Parts, assembly and operation of the RIG-I family of motors. *Current opinion in structural biology* **25:** 25-33

Rice G, Newman WG, Dean J, Patrick T, Parmar R, Flintoff K, Robins P, Harvey S, Hollis T, O'Hara A, Herrick AL, Bowden AP, Perrino FW, Lindahl T, Barnes DE, Crow YJ (2007) Heterozygous mutations in TREX1 cause familial chilblain lupus and dominant Aicardi-Goutieres syndrome. *American journal of human genetics* **80:** 811-815

Roby JA, Pijlman GP, Wilusz J, Khromykh AA (2014) Noncoding subgenomic flavivirus RNA: multiple functions in West Nile virus pathogenesis and modulation of host responses. *Viruses* **6:** 404-427

Rodriguez KR, Bruns AM, Horvath CM (2014a) MDA5 and LGP2: Accomplices and Antagonists of Antiviral Signal Transduction. *Journal of virology* **88:** 8194-8200

Rodriguez KR, Bruns AM, Horvath CM (2014b) MDA5 and LGP2: accomplices and antagonists of antiviral signal transduction. *Journal of virology* **88:** 8194-8200

Roers A, Hiller B, Hornung V (2016) Recognition of Endogenous Nucleic Acids by the Innate Immune System. *Immunity* **44:** 739-754

Rohovie MJ, Nagasawa M, Swartz JR (2017) Virus-like particles: Next-generation nanoparticles for targeted therapeutic delivery. *Bioengineering & translational medicine* **2:** 43-57

Roldao A, Mellado MCM, Castilho LR, Carrondo MJT, Alves PM (2010) Virus-like particles in vaccine development. *Expert Rev Vaccines* **9:** 1149-1176

Rolfsson O, Toropova K, Morton V, Francese S, Basnak G, Thompson GS, Homans SW, Ashcroft AE, Stonehouse NJ, Ranson NA, Stockley PG (2008) RNA packing specificity and folding during assembly of the bacteriophage MS2. *Comput Math Method M* **9:** 339-349

Rothenfusser S, Goutagny N, DiPerna G, Gong M, Monks BG, Schoenemeyer A, Yamamoto M, Akira S, Fitzgerald KA (2005) The RNA Helicase Lgp2 Inhibits TLR-Independent Sensing of Viral Replication by Retinoic Acid-Inducible Gene-I. *The Journal of Immunology* **175:** 5260-5268

Rumnieks J, Tars K (2014) Crystal Structure of the Bacteriophage Q beta Coat Protein in Complex with the RNA Operator of the Replicase Gene. *J Mol Biol* **426:** 1039-1049

Runge S, Sparrer KM, Lassig C, Hembach K, Baum A, Garcia-Sastre A, Soding J, Conzelmann KK, Hopfner KP (2014) In vivo ligands of MDA5 and RIG-I in measles virus-infected cells. *Plos Pathog* **10:** e1004081

Ryu KA, McGonnigal B, Moore T, Kargupta T, Mancini RJ, Esser-Kahn AP (2017) Light Guided In-vivo Activation of Innate Immune Cells with Photocaged TLR 2/6 Agonist. *Sci Rep* **7:** 8074

Sabbatini P, Tsuji T, Ferran L, Ritter E, Sedrak C, Tuballes K, Jungbluth AA, Ritter G, Aghajanian C, Bell-McGuinn K, Hensley ML, Konner J, Tew W, Spriggs DR, Hoffman EW, Venhaus R, Pan LD, Salazar AM, Diefenbach CM, Old LJ, Gnjatic S (2012) Phase I Trial of Overlapping Long Peptides from a Tumor Self-Antigen and Poly-ICLC Shows Rapid Induction of Integrated Immune Response in Ovarian Cancer Patients. *Clin Cancer Res* **18:** 6497-6508

Saito T, Hirai R, Loo Y-M, Owen D, Johnson CL, Sinha SC, Akira S, Fujita T, Gale M (2007a) Regulation of innate antiviral defenses through a shared repressor domain in RIG-I and LGP2. *Proceedings of the National Academy of Sciences of the United States of America* **104:** 582-587

Saito T, Hirai R, Loo YM, Owen D, Johnson CL, Sinha SC, Akira S, Fujita T, Gale M (2007b) Regulation of innate antiviral defenses through a shared repressor domain in RIG-I and LGP2. *P Natl Acad Sci USA* **104:** 582-587

Saito T, Owen DM, Jiang F, Marcotrigiano J, Gale M, Jr. (2008) Innate immunity induced by composition-dependent RIG-I recognition of hepatitis C virus RNA. *Nature* **454:** 523-527

Salazar AM, Levy HB, Ondra S, Kende M, Scherokman B, Brown D, Mena H, Martin N, Schwab K, Donovan D, Dougherty D, Pulliam M, Ippolito M, Graves M, Brown H, Ommaya A (1996) Long-term treatment of malignant gliomas with intramuscularly administered polyinosinic-polycytidylic acid stabilized with polylysine and carboxymethylcellulose: an open pilot study. *Neurosurgery* **38:** 1096-1103; discussion 1103-1094

Sanchez JG, Chiang JJ, Sparrer KMJ, Alam SL, Chi M, Roganowicz MD, Sankaran B, Gack MU, Pornillos O (2016) Mechanism of TRIM25 Catalytic Activation in the Antiviral RIG-I Pathway. *Cell reports* **16:** 1315-1325

Sato K, Yang XL, Yudate T, Chung JS, Wu J, Luby-Phelps K, Kimberly RP, Underhill D, Cruz PD, Jr., Ariizumi K (2006) Dectin-2 is a pattern recognition receptor for fungi that couples with the

Fc receptor gamma chain to induce innate immune responses. *The Journal of biological chemistry* **281:** 38854-38866

Sato S, Li K, Kameyama T, Hayashi T, Ishida Y, Murakami S, Watanabe T, Iijima S, Sakurai Y, Watashi K, Tsutsumi S, Sato Y, Akita H, Wakita T, Rice CM, Harashima H, Kohara M, Tanaka Y, Takaoka A (2015) The RNA sensor RIG-I dually functions as an innate sensor and direct antiviral factor for hepatitis B virus. *Immunity* **42:** 123-132

Satoh T, Kato H, Kumagai Y, Yoneyama M, Sato S, Matsushita K, Tsujimura T, Fujita T, Akira S, Takeuchi O (2010) LGP2 is a positive regulator of RIG-I– and MDA5-mediated antiviral responses. *Proceedings of the National Academy of Sciences* **107:** 1512-1517

Scheiermann J, Klinman DM (2014) Clinical evaluation of CpG oligonucleotides as adjuvants for vaccines targeting infectious diseases and cancer. *Vaccine* **32:** 6377-6389

Schlee M (2013) Master sensors of pathogenic RNA - RIG-I like receptors. *Immunobiology* **218:** 1322-1335

Schlee M, Roth A, Hornung V, Hagmann CA, Wimmenauer V, Barchet W, Coch C, Janke M, Mihailovic A, Wardle G, Juranek S, Kato H, Kawai T, Poeck H, Fitzgerald KA, Takeuchi O, Akira S, Tuschl T, Latz E, Ludwig J, Hartmann G (2009) Recognition of 5' triphosphate by RIG-I helicase requires short blunt double-stranded RNA as contained in panhandle of negative-strand virus. *Immunity* **31:** 25-34

Schmidt A, Schwerd T, Hamm W, Hellmuth JC, Cui S, Wenzel M, Hoffmann FS, Michallet MC, Besch R, Hopfner KP, Endres S, Rothenfusser S (2009) 5'-triphosphate RNA requires base-paired structures to activate antiviral signaling via RIG-I. *Proc Natl Acad Sci U S A* **106:** 12067-12072

Schmolke M, Garcia-Sastre A (2010) Evasion of innate and adaptive immune responses by influenza A virus. *Cell Microbiol* **12:** 873-880

Schneider WM, Chevillotte MD, Rice CM (2014) Interferon-stimulated genes: a complex web of host defenses. *Annual review of immunology* **32:** 513-545

Schnell G, Loo YM, Marcotrigiano J, Gale M, Jr. (2012) Uridine composition of the poly-U/UC tract of HCV RNA defines non-self recognition by RIG-I. *Plos Pathog* **8:** e1002839

Schoggins JW, Rice CM (2011) Interferon-stimulated genes and their antiviral effector functions. *Current opinion in virology* **1:** 519-525

Schoggins JW, Wilson SJ, Panis M, Murphy MY, Jones CT, Bieniasz P, Rice CM (2011) A diverse range of gene products are effectors of the type I interferon antiviral response. *Nature* **472:** 481-485

Schroder K, Tschopp J (2010) The Inflammasomes. *Cell* **140:** 821-832

Schuberth-Wagner C, Ludwig J, Bruder AK, Herzner AM, Zillinger T, Goldeck M, Schmidt T, Schmid-Burgk JL, Kerber R, Wolter S, Stumpel JP, Roth A, Bartok E, Drosten C, Coch C, Hornung V, Barchet W, Kummerer BM, Hartmann G, Schlee M (2015) A Conserved Histidine in the RNA Sensor RIG-I Controls Immune Tolerance to N-1-2 ' O-Methylated Self RNA. *Immunity* **43:** 41-51

Seth RB, Sun LJ, Ea CK, Chen ZJJ (2005) Identification and characterization of MAVS, a mitochondrial antiviral signaling protein that activates NF-kappa B and IRF3. *Cell* **122:** 669-682

Shu HB, Takeuchi M, Goeddel DV (1996) The tumor necrosis factor receptor 2 signal transducers TRAF2 and c-IAP1 are components of the tumor necrosis factor receptor 1 signaling complex. *Proc Natl Acad Sci U S A* **93:** 13973-13978

Siu KL, Chan CP, Kok KH, Chiu-Yat Woo P, Jin DY (2014) Suppression of innate antiviral response by severe acute respiratory syndrome coronavirus M protein is mediated through the first transmembrane domain. *Cellular & molecular immunology* **11:** 141-149

Spiropoulou CF, Ranjan P, Pearce MB, Sealy TK, Albarino CG, Gangappa S, Fujita T, Rollin PE, Nichol ST, Ksiazek TG, Sambhara S (2009) RIG-I activation inhibits ebolavirus replication. *Virology* **392:** 11-15

Stockley PG, White SJ, Dykeman E, Manfield I, Rolfsson O, Patel N, Bingham R, Barker A, Wroblewski E, Chandler-Bostock R, Weiss EU, Ranson NA, Tuma R, Twarock R (2016) Bacteriophage MS2 genomic RNA encodes an assembly instruction manual for its capsid. *Bacteriophage* **6:** e1157666

Stonehouse NJ, Stockley PG (1993) Effects of amino acid substitution on the thermal stability of MS2 capsids lacking genomic RNA. *FEBS letters* **334:** 355-359

Sun L, Xing Y, Chen X, Zheng Y, Yang Y, Nichols DB, Clementz MA, Banach BS, Li K, Baker SC, Chen Z (2012) Coronavirus papain-like proteases negatively regulate antiviral innate immune response through disruption of STING-mediated signaling. *Plos One* **7:** e30802

Sun ZG, Ren HW, Liu Y, Teeling JL, Gu J (2011) Phosphorylation of RIG-I by Casein Kinase II Inhibits Its Antiviral Response. *J Virol* **85:** 1036-1047

Suraj S, Dhar C, Srivastava S (2017) Circulating nucleic acids: An analysis of their occurrence in malignancies. *Biomed Rep* **6:** 8-14

Suresh M, Korolowicz KE, Balarezo M, Iyer RP, Padmanabhan S, Cleary D, Gimi R, Sheri A, Yon C, Kallakury BV, Tucker RD, Afdhal N, Menne S (2017) Antiviral Efficacy and Host Immune Response Induction during Sequential Treatment with SB 9200 Followed by Entecavir in Woodchucks. *Plos One* **12**

Tacket CO, Sztein MB, Losonsky GA, Wasserman SS, Estes MK (2003) Humoral, mucosal, and cellular immune responses to oral Norwalk virus-like particles in volunteers. *Clin Immunol* **108:** 241-247

Takahasi K, Kumeta H, Tsuduki N, Narita R, Shigemoto T, Hirai R, Yoneyama M, Horiuchi M, Ogura K, Fujita T, Inagaki F (2009) Solution Structures of Cytosolic RNA Sensor MDA5 and LGP2 C-terminal Domains IDENTIFICATION OF THE RNA RECOGNITION LOOP IN RIG-I-LIKE RECEPTORS. *J Biol Chem* **284:** 17465-17474

Takashima K, Oshiumi H, Takaki H, Matsumoto M, Seya T (2015) RIOK3-Mediated Phosphorylation of MDA5 Interferes with Its Assembly and Attenuates the Innate Immune Response. *Cell reports* **11:** 192-200

Talreja J, Stechschulte DJ, Dileepan KN (2003) Synergistic activation of endothelial cells by histamine and bacterial cell wall components involves histamine receptor-1 and toll-like receptors 2 and 4. *Faseb J* **17:** C45-C45

Tanemura A, Kiyohara E, Katayama I, Kaneda Y (2013) Recent advances and developments in the antitumor effect of the HVJ envelope vector on malignant melanoma: from the bench to clinical application. *Cancer gene therapy* **20:** 599-605

Tang D, Kang R, Coyne CB, Zeh HJ, Lotze MT (2012) PAMPs and DAMPs: signal 0s that spur autophagy and immunity. *Immunol Rev* **249:** 158-175

Tang ED, Wang CY (2009) MAVS Self-Association Mediates Antiviral Innate Immune Signaling. *J Virol* **83:** 3420-3428

Tanji H, Ohto U, Shibata T, Miyake K, Shimizu T (2013) Structural Reorganization of the Toll-Like Receptor 8 Dimer Induced by Agonistic Ligands. *Science* **339:** 1426-1429

Thomas SN, Vokali E, Lund AW, Hubbell JA, Swartz MA (2014) Targeting the tumor-draining lymph node with adjuvanted nanoparticles reshapes the anti-tumor immune response. *Biomaterials* **35:** 814-824

Ting JPY, Lovering RC, Alnemri ES, Bertin J, Boss JM, Davis BK, Flavell RA, Girardin SE, Godzik A, Harton JA, Hoffman HM, Hugot JP, Inohara N, MacKenzie A, Maltais LJ, Nunez G, Ogura Y, Otten LA, Philpott D, Reed JC, Reith W, Schreiber S, Steimle V, Ward PA (2008) The NLR gene family: A standard nomenclature. *Immunity* **28:** 285-287

Travassos LH, Carneiro LAM, Ramjeet M, Hussey S, Kim YG, Magalhaes JG, Yuan L, Soares F, Chea E, Le Bourhis L, Boneca IG, Allaoui A, Jones NL, Nunez G, Girardin SE, Philpott DJ (2010) Nod1 and Nod2 direct autophagy by recruiting ATG16L1 to the plasma membrane at the site of bacterial entry. *Nat Immunol* **11:** 55-U67

Trinchieri G (2010) Type I interferon: friend or foe? *Journal of Experimental Medicine* **207:** 2053-2063

Trollfors B, Bergfors E, Inerot A (2005) Vaccine related itching nodules and hypersensitivity to aluminium. *Vaccine* **23:** 975-976

Tsuji T, Sabbatini P, Jungbluth AA, Ritter E, Pan L, Ritter G, Ferran L, Spriggs D, Salazar AM, Gnjatic S (2013) Effect of Montanide and Poly-ICLC Adjuvant on Human Self/Tumor Antigen-Specific CD4(+) T Cells in Phase I Overlapping Long Peptide Vaccine Trial. *Cancer Immunol Res* **1:** 340-350

Uchikawa E, Lethier M, Malet H, Brunel J, Gerlier D, Cusack S (2016) Structural Analysis of dsRNA Binding to Anti-viral Pattern Recognition Receptors LGP2 and MDA5. *Mol Cell* **62:** 586-602

Vallabhapurapu S, Karin M (2009) Regulation and function of NF-kappaB transcription factors in the immune system. *Annual review of immunology* **27:** 693-733

Ve T, Williams SJ, Kobe B (2015) Structure and function of Toll/interleukin-1 receptor/resistance protein (TIR) domains. *Apoptosis* **20:** 250-261

Vela A, Fedorova O, Ding SC, Pyle AM (2012) The Thermodynamic Basis for Viral RNA Detection by the RIG-I Innate Immune Sensor. *J Biol Chem* **287:** 42564-42573

Walker JE, Saraste M, Runswick MJ, Gay NJ (1982) Distantly Related Sequences in the Alpha-Subunits and Beta-Subunits of Atp Synthase, Myosin, Kinases and Other Atp-Requiring Enzymes and a Common Nucleotide Binding Fold. *Embo Journal* **1:** 945-951

Wang LJ, Zhao W, Zhang M, Wang P, Zhao K, Zhao XY, Yang SR, Gao CJ (2013) USP4 Positively Regulates RIG-I-Mediated Antiviral Response through Deubiquitination and Stabilization of RIG-I. *J Virol* **87:** 4507-4515

Wang M, Yu F, Wu W, Zhang Y, Chang WG, Ponnusamy M, Wang K, Li PF (2017) Circular RNAs: A novel type of non-coding RNA and their potential implications in antiviral immunity. *Int J Biol Sci* **13:** 1497-1506

Wang Y, Tong X, Li G, Li J, Deng M, Ye X (2012a) Ankrd17 positively regulates RIG-I-like receptor (RLR)-mediated immune signaling. *European journal of immunology* **42:** 1304-1315

Wang YL, Ludwig J, Schuberth C, Goldeck M, Schlee M, Li HT, Juranek S, Sheng G, Micura R, Tuschl T, Hartmann G, Patel DJ (2010) Structural and functional insights into 5 '-ppp RNA pattern recognition by the innate immune receptor RIG-I. *Nat Struct Mol Biol* **17:** 781-U719

Wang YT, Tong XM, Omoregie ES, Liu WJ, Meng SD, Ye X (2012b) Tetraspanin 6 (TSPAN6) Negatively Regulates Retinoic Acid-inducible Gene I-like Receptor-mediated Immune Signaling in a Ubiquitination-dependent Manner. *J Biol Chem* **287:** 34626-34634

Waters JA, Pignatelli M, Brown D, Orourke S, Lever A, Thomas HC (1987) The Immune-Response to Hepatitis-B Virus. *Postgrad Med J* **63:** 51-56

Weber M, Gawanbacht A, Habjan M, Rang A, Borner C, Schmidt AM, Veitinger S, Jacob R, Devignot S, Kochs G, Garcia-Sastre A, Weber F (2013) Incoming RNA virus nucleocapsids containing a 5'-triphosphorylated genome activate RIG-I and antiviral signaling. *Cell Host Microbe* **13:** 336-346

Wei MX, Zhang X, Yu H, Tang ZM, Wang KH, Li ZY, Zheng ZZ, Li SW, Zhang J, Xia NS, Zhao QJ (2014) Bacteria expressed hepatitis E virus capsid proteins maintain virion-like epitopes. *Vaccine* **32:** 2859-2865

Wies E, Wang MK, Maharaj NP, Chen K, Zhou S, Finberg RW, Gack MU (2013) Dephosphorylation of the RNA Sensors RIG-I and MDA5 by the Phosphatase PP1 Is Essential for Innate Immune Signaling. *Immunity* **38:** 437-449

Winn MD, Ballard CC, Cowtan KD, Dodson EJ, Emsley P, Evans PR, Keegan RM, Krissinel EB, Leslie AG, McCoy A, McNicholas SJ, Murshudov GN, Pannu NS, Potterton EA, Powell HR, Read RJ, Vagin A, Wilson KS (2011) Overview of the CCP4 suite and current developments. *Acta crystallographica Section D, Biological crystallography* **67:** 235-242

Witherell GW, Uhlenbeck OC (1989) Specific Rna-Binding by Q-Beta Coat Protein. *Biochemistry-Us* **28:** 71-76

Woo SR, Fuertes MB, Corrales L, Spranger S, Furdyna MJ, Leung MYK, Duggan R, Wang Y, Barber GN, Fitzgerald KA, Alegre ML, Gajewski TF (2014) STING-Dependent Cytosolic DNA Sensing Mediates Innate Immune Recognition of Immunogenic Tumors. *Immunity* **41:** 830-842

Wrangle J, Wang W, Koch A, Easwaran H, Mohammad HP, Vendetti F, VanCriekinge W, De Meyer T, Du ZZ, Parsana P, Rodgers K, Yen RW, Zahnow CA, Taube JM, Brahmer JR, Tykodi SS, Easton K, Carvajal RD, Jones PA, Laird PW, Weisenberger DJ, Tsai S, Juergens RA, Topalian SL, Rudin CM, Brock MV, Pardoll D, Baylin SB (2013) Alterations of immune response of non-small cell lung cancer with Azacytidine. *Oncotarget* **4:** 2067-2079

Wu B, Peisley A, Richards C, Yao H, Zeng XH, Lin C, Chu FX, Walz T, Hur S (2013) Structural Basis for dsRNA Recognition, Filament Formation, and Antiviral Signal Activation by MDA5. *Cell* **152:** 276-289

Wu B, Peisley A, Tetrault D, Li ZL, Egelman EH, Magor KE, Walz T, Penczek PA, Hur S (2014) Molecular Imprinting as a Signal-Activation Mechanism of the Viral RNA Sensor RIG-I. *Mol Cell* **55:** 511-523

Wu M, Brown WL, Stockley PG (1995) Cell-Specific Delivery of Bacteriophage-Encapsidated Ricin-a Chain. *Bioconjugate Chem* **6:** 587-595

Xu H, He XJ, Zheng H, Huang LJ, Hou FJ, Yu ZH, de la Cruz MJ, Borkowski B, Zhang XW, Chen ZJJ, Jiang QX (2014) Structural basis for the prion-like MAVS filaments in antiviral innate immunity. *eLife* **3**

Xu J, Mercado-Lopez X, Grier JT, Kim WK, Chun LF, Irvine EB, Del Toro Duany Y, Kell A, Hur S, Gale M, Jr., Raj A, Lopez CB (2015) Identification of a Natural Viral RNA Motif That Optimizes Sensing of Viral RNA by RIG-I. *mBio* **6:** e01265-01215

Xu L, Xiao N, Liu F, Ren H, Gu J (2009) Inhibition of RIG-I and MDA5-dependent antiviral response by gC1qR at mitochondria. *Proc Natl Acad Sci U S A* **106:** 1530-1535

Xu LG, Wang YY, Han KJ, Li LY, Zhai ZH, Shu HB (2005) VISA is an adapter protein required for virus-triggered IFN-beta signaling. *Mol Cell* **19:** 727-740

Yamasaki S, Ishikawa E, Sakuma M, Hara H, Ogata K, Saito T (2008) Mincle is an ITAM-coupled activating receptor that senses damaged cells. *Nature immunology* **9:** 1179-1188

Yan J, Li Q, Mao AP, Hu MM, Shu HB (2014a) TRIM4 modulates type I interferon induction and cellular antiviral response by targeting RIG-I for K63-linked ubiquitination. *J Mol Cell Biol* **6:** 154-163

Yan R, Hallam A, Stockley PG, Boyes J (2014b) Oncogene dependency and the potential of targeted RNAi-based anti-cancer therapy. *The Biochemical journal* **461:** 1-13

Yang YK, Qu H, Gao D, Di W, Chen HW, Guo X, Zhai ZH, Chen DY (2011) ARF-like protein 16 (ARL16) inhibits RIG-I by binding with its C-terminal domain in a GTP-dependent manner. *J Biol Chem* **286:** 10568-10580

Yasukawa K, Oshiumi H, Takeda M, Ishihara N, Yanagi Y, Seya T, Kawabata S, Koshiba T (2009) Mitofusin 2 inhibits mitochondrial antiviral signaling. *Science signaling* **2:** ra47

Yoneyama M, Fujita T (2004) [RIG-I: critical regulator for virus-induced innate immunity]. *Tanpakushitsu kakusan koso Protein, nucleic acid, enzyme* **49:** 2571-2578

Yoneyama M, Kikuchi M, Matsumoto K, Imaizumi T, Miyagishi M, Taira K, Foy E, Loo YM, Gale M, Akira S, Yonehara S, Kato A, Fujita T (2005a) Shared and Unique Functions of the DExD/H-Box Helicases RIG-I, MDA5, and LGP2 in Antiviral Innate Immunity. *The Journal of Immunology* **175:** 2851-2858

Yoneyama M, Kikuchi M, Matsumoto K, Imaizumi T, Miyagishi M, Taira K, Foy E, Loo YM, Gale M, Jr., Akira S, Yonehara S, Kato A, Fujita T (2005b) Shared and unique functions of the DExD/H-box helicases RIG-I, MDA5, and LGP2 in antiviral innate immunity. *J Immunol* **175:** 2851-2858

Yoneyama M, Kikuchi M, Natsukawa T, Shinobu N, Imaizumi T, Miyagishi M, Taira K, Akira S, Fujita T (2004) The RNA helicase RIG-I has an essential function in double-stranded RNA-induced innate antiviral responses. *Nat Immunol* **5:** 730-737

Yoneyama M, Suhara W, Fukuhara Y, Fukuda M, Nishida E, Fujita T (1998) Direct triggering of the type I interferon system by virus infection: activation of a transcription factor complex containing IRF-3 and CBP/p300. *The EMBO journal* **17:** 1087-1095

Yong HY, Luo D (2018) RIG-I-Like Receptors as Novel Targets for Pan-Antivirals and Vaccine Adjuvants Against Emerging and Re-Emerging Viral Infections. *Front Immunol* **9:** 1379

Zabel F, Mohanan D, Bessa J, Link A, Fettelschoss A, Saudan P, Kundig TM, Bachmann MF (2014) Viral Particles Drive Rapid Differentiation of Memory B Cells into Secondary Plasma Cells Producing Increased Levels of Antibodies. *Scand J Immunol* **80:** 239-239

Zdanowicz M, Chroboczek J (2016) Virus-like particles as drug delivery vectors. *Acta Biochim Pol* **63:** 469-473

Zelensky AN, Gready JE (2005) The C-type lectin-like domain superfamily. *The FEBS journal* **272:** 6179-6217

Zhang D, Lin J, Han J (2010) Receptor-interacting protein (RIP) kinase family. *Cellular & molecular immunology* **7:** 243-249

Zhang HX, Liu ZX, Sun YP, Zhu J, Lu SY, Liu XS, Huang QH, Xie YY, Zhu HB, Dang SY, Chen HF, Zheng GY, Li YX, Kuang Y, Fei J, Chen SJ, Chen Z, Wang ZG (2013) Rig-I regulates NF-kappa B activity through binding to Nf-kappa b1 3 '-UTR mRNA. *P Natl Acad Sci USA* **110:** 6459-6464

Zhang L, Lua LH, Middelberg AP, Sun Y, Connors NK (2015) Biomolecular engineering of virus-like particles aided by computational chemistry methods. *Chemical Society reviews* **44:** 8608-8618

Zhang R, Li M, Chen C, Yao Q (2004) SHIV virus-like particles bind and activate human dendritic cells. *Vaccine* **23:** 139-147

Zhang XO, Wei MX, Pan HR, Lin ZJ, Wang KH, Weng ZS, Zhu YB, Xin L, Zhang J, Li SW, Xia NS, Zhao QJ (2014) Robust manufacturing and comprehensive characterization of recombinant hepatitis E virus-like particles in Hecolin (R). *Vaccine* **32:** 4039-4050

Zhang Z, Yuan B, Lu N, Facchinetti V, Liu YJ (2011) DHX9 pairs with IPS-1 to sense double-stranded RNA in myeloid dendritic cells. *J Immunol* **187:** 4501-4508

Zhao GN, Jiang DS, Li H (2015) Interferon regulatory factors: at the crossroads of immunity, metabolism, and disease. *Biochimica et biophysica acta* **1852:** 365-378

Zhao J, Zeng Y, Xu SM, Chen J, Shen GB, Yu CQ, Knipe D, Yuan WM, Peng J, Xu WQ, Zhang C, Xia ZX, Feng PH (2016a) A Viral Deamidase Targets the Helicase Domain of RIG-I to Block RNA-Induced Activation. *Cell host & microbe* **20:** 770-784

Zhao K, Zhang Q, Li X, Zhao DZ, Liu YQ, Shen QC, Yang MJ, Wang CM, Li N, Cao XT (2016b) Cytoplasmic STAT4 Promotes Antiviral Type I IFN Production by Blocking CHIP-Mediated Degradation of RIG-I. *J Immunol* **196:** 1209-1217

Zhao QH, Chen WH, Chen YD, Zhang LM, Zhang JP, Zhang ZJ (2011) Self-Assembled Virus-Like Particles from Rotavirus Structural Protein VP6 for Targeted Drug Delivery. *Bioconjugate Chem* **22:** 346-352

Zheng J, Chang MR, Stites RE, Wang Y, Bruning JB, Pascal BD, Novick SJ, Garcia-Ordonez RD, Stayrook KR, Chalmers MJ, Dodge JA, Griffin PR (2017) HDX reveals the conformational dynamics of DNA sequence specific VDR co-activator interactions. *Nat Commun* **8**

Zheng J, Yong HY, Panutdaporn N, Liu CF, Tang K, Luo DH (2015) High-resolution HDX-MS reveals distinct mechanisms of RNA recognition and activation by RIG-I and MDA5. *Nucleic Acids Res* **43:** 1216-1230

Zhu J, Zhang Y, Ghosh A, Cuevas RA, Forero A, Dhar J, Ibsen MS, Schmid-Burgk JL, Schmidt T, Ganapathiraju MK, Fujita T, Hartmann R, Barik S, Hornung V, Coyne CB, Sarkar SN (2014) Antiviral activity of human OASL protein is mediated by enhancing signaling of the RIG-I RNA sensor. *Immunity* **40:** 936-948